Iron Nitrosyl Complexes

by

Carol F. Fortney

B. S., University of Pittsburgh, 1998

M. S., University of Pittsburgh, 2002

Submitted to the Graduate Faculty of

Arts and Sciences in partial fulfillment

of the requirements for the degree of

Master of Science

University of Pittsburgh

2002

UNIVERSITY OF PITTSBURGH

FACULTY OF ARTS AND SCIENCES

This thesis was presented

by

Carol F.Fortney

It was defended on

December 19, 2002

and approved by

Professor Rex E. Shepherd

Professor David H. Waldeck

Professor Stéphane Petoud

ACKNOWLEDGEMENTS

I would like to express my sincere gratitude to my committee members, Professors David H. Waldeck and Stéphane Petoud, and to my advisor for this project, the late Professor Rex E. Shepherd.

Iron Nitrosyl Complexes

Carol F. Fortney, M. S.

University of Pittsburgh, 2002

Nitric oxide (NO) is an endogenously produced bioregulatory agent that also is toxic. Disturbances in NO production and regulation are known to cause central nervous system disorders and asthma among many other diseases. Iron nitrosyl complexes help to balance the beneficial effects of NO against its potentially fatal effects. This document reviews the literature devoted to structural and chemical characteristics of iron nitrosyl porphyrin complexes, bimetallic iron containing nitrosyl complexes, dinitrosyl complexes, iron nitrosyl cluster complexes, and non-heme nitrosyl complexes prepared between 1992 and 2002.

TABLE OF CONTENTS

LIST OF TABLES

LIST OF FIGURES

LIST OF ABBREVIATIONS

18C6	1, 4, 7, 10, 13, 16-hexaoxacyclooctadecane
1-MeIm	1-methylimidazole
2, 4-DMOEiBC	2, 4-dimethyloctaethylisobacteriochlorin
ABT	2-aminobenzylthiolato anion
acac	acetoacetonato
ARDS	adult respiratory distress syndrome
ATR-IR	attenuated total reflectance infrared spectroscopy
BM	benzyl mercapto anion
bpy	2, 2′-bipyridine
CV	cyclic voltammetry
cy	cyclohexane
cyclam	1, 4, 8, 11-tetraazacyclotetradecane
DFT	density functional theory
dien	*N*-(2-aminoethyl)ethane-1, 2-diamine
dioxo-OEiBC	dianion of dioxooctaethylisobacteriochlorin
dmen	2-dimethylaminoethylamine
dmpn	1-dimethylamino-2-propylamine
DPP	differential pulse polarography
dppe	1, 1′-bis(diphenylphosphino)ethane
dppf	1, 1′-bis(diphenylphosphino)ferrocene
edampda^{2-}	*N*, *N*′-bis(pyridylmethyl)ethylenediamine- *N*,*N*′-diacetate
EDRF	endothelium-derived relaxing factor

EDTA	ethylenediamine tetraacetate
en	ethylenediamine
EPR	electron paramagnetic resonance
Et-HPTB	*N*, *N*, *N*′, *N*′-tetrakis(*N*-ethyl-2-benzimidazoly-methyl)-2-hydroxy-1, 3,-diaminopropane
FAD	flavin adenine dinucleotide
FMN	flavin mononucleotide
GSH	glutathione
HOMO	highest occupied molecular orbital
IR	infra-red
Iz	imidazole
K(222)	4, 7, 13, 16, 21, 24-hexaoxa-1, 10-diazabicyclo[8.8.8]hexacosane
LUMO	lowest occupied molecular orbital
ME	mercapto ethanoate anion
medpt	*N*-(3-aminopropyl)-*N*-methylpropane-1, 3-diamine
MIDA	methyliminodiacetic acid
MOEC	methyloctaethylchlorin
NACysMe-S	*N*-acetyl-L-cysteinate methyl ester
NADPH	nicotinamide adenine dinucleotide phosphate
NHA	*N*-hydroxylarginine
NHE	normal hydrogen electrode
NMR	nuclear magnetic resonance
NO	nitric oxide
NOS	nitric oxide synthase

NSAIDS	non-steroidal anti-inflammatory drugs
nta^{3-}	nitrilotriacetate
OEP	octaethylporphyrinato anion
OETAP	octaethyltetraazaporphyrin
ORTEP	Oak Ridge thermal ellipsoid plot
oxoOEC	3, 3, 7, 8, 12, 13, 17, 18-octaethyl-3*H*-porphin-2-onato(2^-) dianion
oxpn	dianion of *N, N*′-bis(3-aminopropyl)oxamide
PEt_3	triethylphosphine
$pida^{2-}$	2-pyridylmethyliminodiacetate
por	porphyrin
PPDME	protoporphyrin IX dimethyl ester
PPh_3	triphenylphosphine
py	pyridine
RONO	isoamylnitrite
RSNO	thionitrite
shf	super hyperfine
SNO	thionitrite
TBA	tetra-*n*-butylammoniumhydroxide
TCNE	tetracyanoethane
THF	tetrahydrofuran
TIM	2, 3, 9, 10-tetramethyl-1, 4, 9, 11-tetraazacyclodeca-1, 3, 8, 10-tetraene
tmen	*N*, *N*, *N*′, *N*′-tetramethylethane-1, 2-diamine
TMPyP	*meso*-tetra(*N*-methyl-4-pyridyl)porphyrin

tpa	tris(2-pyridylmethyl)amine
tpen	*N, N′, N ,N*′-tetrakis(2-pyridylmethyl)ethylenediamine
TpivPP	tetrakis(*o*-pivalamidophenyl)-porphinato
TPP	tetraphenyl porphyrin
TPP-$(OMe)_3$	tetra-*p*-methoxyphenyl porphyrin
$TPPBr_4$	2, 3, 12, 13-tetrabromo-5, 10, 15, 20-tetraphenylporphyrin dianion
Trimeen	*N*, *N*, *N*′-trimethylethane-1,2-diamine
TTP	tetratolyporphyrinato dianon
$uedda^{2-}$	*N*, *N*′-ethylenediaminediacetate

1. IRON NITROSYL COMPLEXES

1.1. INTRODUCTION

Nitric oxide (NO) is an endogenously produced bioregulatory agent that also is toxic. Being a small, uncharged molecule, NO can diffuse freely across cell membranes. However, because of its multiple and sometimes paradoxical roles as a neurotransmitter, autacoid, constitutive mediator, inducible mediator, cytoprotective molecule, and as a cytotoxic molecule, nitric oxide's release and action must be well regulated. Disturbances in NO regulatory pathways are known to cause central nervous system disorders, diabetes mellitus, asthma, gastrointestinal disorders, and atherosclerosis.[1] In particular, the pathophysiological effects of vascular nitric oxide are well known and have been reviewed.[2] Nitric oxide release is also related to hypotension characteristic of septic shock that is induced by group B streptococcus, the leading cause of sepsis in neonates.[3] Yet, nitric oxide has been incorporated into non-steroidal and anti-inflammatory drugs (NSAIDs) to inhibit gastrointestinal side effects.[4] This subject has also been reviewed. Figure 1.1[5] summarizes many of the other physiological benefits and pathological effects elicited by NO. As will be discussed in this document, iron nitrosyl complexes play a major role in balancing the beneficial effects of NO against its potentially fatal effects.

Given the myriad bioregulatory and pathophysiological roles of NO, most pharmaceutical companies have devoted some of their research efforts to the discovery of NO based therapeutic drugs.[1] Therefore, elucidation of the mechanisms by which NO is produced and regulated in the body is a goal which has been pursued by chemists, biochemists, and biologists. Because scientists initially studied nitric oxide within their respective fields, nitric oxide reviews have emphasized either chemistry[6-15] or biology[2,4,16-23] with nomenclature specific to each.[24] More recent reviews have been written from a combined perspective.[1]

The divergent routes scientists have taken to understand nitric oxide's origin and function have lead to the common conclusion that heme and non-heme iron nitrosyl complexes are involved in many aspects of nitric oxide regulation, transport, pathophysiology, and function. This review is limited to the iron nitrosyl complexes that have been prepared between 1992 (when Richter-Addo and Legzdins published their book, Metal Nitrosyls.[25]) and 2002. Physiological roles, synthetic methods and chemical characteristics of iron nitrosyls are discussed.

Figure 1.1 – Physiological and Pathophysiological Roles of Nitric Oxide
(Reproduced from *Cell*, *78*, 919-925, "NO at Work", H. W. Schmidt and Walter Ulrich, Copyright 1994, with permission from Elsevier. 4)

Tissue	Messenger	Toxin
Blood Vessels	EDRF, antithrombotic, ischemic protection, antiatherosclerotic, inhibition of smooth muscle migration and proliferation, antiadhesive	Septic Shock, inflammation, reperfusion injury, microvascular leakage, atherosclerosis
Heart	Coronary perfusion, negative inotropic ischemia	Myocardial "stunning," septic shock, reperfusion
Lung	Ventilation-perfusion matching, bronchiociliar motility, mucus secretion, immune defense	Immune complex-induced alveolitis, silo filler's disease, asthma? ARDS?
Kidney	Tubuloglomerular feedback, glomerular perfusion, renin secretion	Acute kidney failure, glomerulonephritis
CNS	Synaptogenesis, synaptic plasticity, memory formation, cerebral blood flow and ischemia, neuroendocrine secretion, visual transduction, olfaction	Neurotoxic, proconvulsive, migraine, hyperalgesia, reperfusion
Pancreas	Endocrine/exocrine secretion	β cell destruction
Gut	Blood flow, peristalsis, exocrine secretion, mucosal protection, antimicrobial	Mutagenesis, mucosal damage
Immune System	Antimicrobial, antitumor	Antiallograft, graft versus host disease, inflammation, septic shock, tissue damage

1.2. NITRIC OXIDE SYNTHASE

Nitric oxide is produced in the body by nitric oxide synthase (NOS). The subject has been reviewed.[5,16,18-20,22] NOS has several isoforms (distinct forms).[26,27] Appendix A describes the different isoforms, their structural features, characterization, and activation. This section describes the proposed mechanism by which nitric oxide synthase oxidizes *N*-hydroxyl-L-arginine to citrulline to produce NO.

NOS enzymes have a heme domain that consumes five electrons to produce nitric oxide directly from the guanidine nitrogen of L-arginine. The mechanism of electron transfer has been proposed to be similar to that of cytochrome p-450 in which NADPH (nicotinamide adenine dinucleotide phosphate) reduces FAD (flavin adenine dinucleotide) which in turn reduces FMN (flavin mononucleotide; for structure see Appendix A). FMN ultimately transfers electrons to ferric heme to promote the interaction with molecular oxygen shown in Figure 1.2.[26] In the first step, L-arginine binds close to the ferric heme. As an electron is transferred to the heme, oxygen binds to the iron center. After a second electron from NADPH promotes cleavage of the oxygen-oxygen bond, the remaining oxygen atom inserts into a terminal guanidino N-H bond to form N-hydroxyl arginine as an enzyme bound intermediate. In the second step, as another electron is transferred from NADPH to ferric heme, another oxygen molecule bonds with the iron center. The resulting ferrous oxyheme may oxidize bound N-hydroxyl arginine to form a peroxide iron species. The peroxide iron species may then attack the guanidine carbon to yield citrulline, NO, H_2O and ferric heme. There is evidence for heme participation in both oxidation steps from carbon monoxide inhibition studies[28,29] and from optical difference binding studies.[29,30]

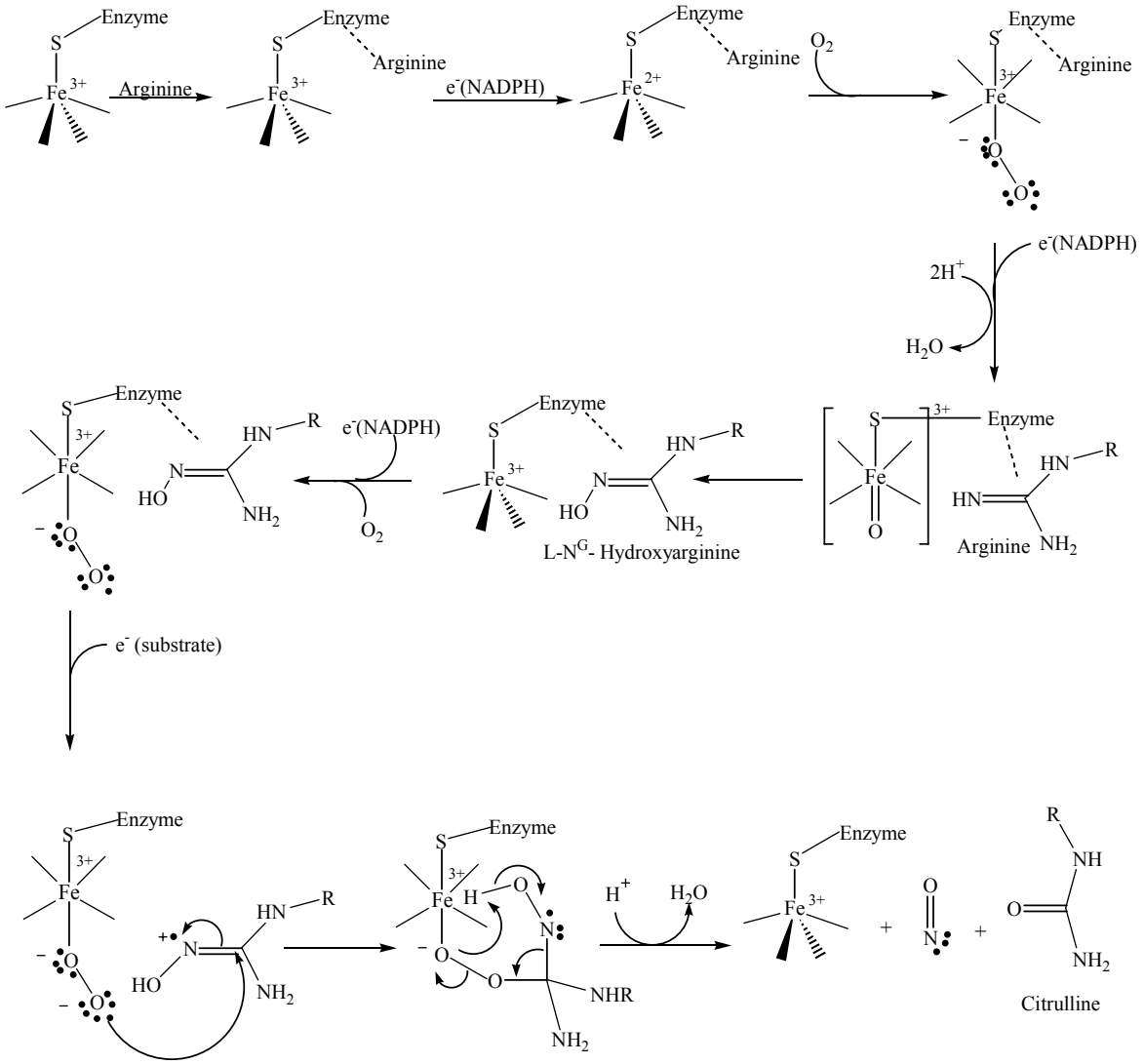

Figure 1.2 – Nitric Oxide Synthesis
(Reprinted from *Nitric Oxide Principles and Actions*, "The Intracellular Reactions of Nitric oxide in the Immune System and Its Enzymatic Synthesis", Jack Lancaster, Jr. and Dennis J. Stuehr, p. 154, Copyright 1996, with permission from Elsevier.)

1.3. BIOLOGICAL ROLES OF IRON NITROSYL COMPLEXES

From the discussion of nitric oxide synthesis it is clear that iron heme complexes are important in NO synthesis. Iron heme complexes, as well as many other iron complexes, have a propensity to bind with nitric oxide to form iron nitrosyl complexes. In general, a physiological response is elicited upon formation of an iron nitrosyl complex in a target heme protein. Non-heme and cluster[31] iron nitrosyl complexes are also involved in biological chemistry.

Crane[32] and co-workers have determined the structure of an NOS heme protein from *Bacillus subtillus*. While the structure suggests that this NOS produces NO from L-arginine and NHA (*N*-hydroxy-L-Arginine) in a pterin dependent manner (Appendix A), the regulation and purpose of its production may be very different from that in mammals. Human pathogens such as *Staphylococcus aureus* and *Bacillus anthracis* (Anthrax) have proteins very similar to *Bacillus subtillus*. If the *Staphylococcus aureus* and *Bacillus anthracis* NOS proteins are found to be crucial for viability or pathogenicity, much that is known about NOS regulation in mammalian cells can be applied to fight these pathogens in humans. As noted by Crane and co-workers, structural differences in the heme pocket, pterin site, and substrate access channels of the *Bacillus subtillus* NOS could allow inhibitors to discriminate between bacterial and mammalian NOS proteins.

Nitric oxide forms heme and sulfur containing iron nitrosyl complexes with targets in murine (mouse) tumor cells.[33] EPR (electron paramagnetic resonance) signals of nitrosylated heme and non-heme iron containing dinitrosyls were also observed from tissues after rat heart allograft rejection.[34] The most notable target for NO in the natural function of cells is guanylate cyclase, another iron heme involved in vasodilation. Evidence for a five-coordinated [Fe^{II}(heme)(NO)] complex that catalyzes formation of the muscle relaxer, cGMP, has been detected by Raman spectroscopy.[5,20]

NO binds to reduced cobalamin as a $Co^{II}(NO)$ complex.[35-37] There have been numerous claims and counterclaims about NO coordination with aquacobalamin (Co^{III}). Early reports claimed NO would not coordinate.[38] Later, evidence suggested that aquacobalamin does bind NO.[39-45] But recent studies of Van Eldik show that vitamin B_{12} and cobalamin coordinate with NO_2^- impurities rather than NO itself. The Co^{II} form of cobalamin reacts much faster with $NO^\bullet$ than with NO_2^-, [46] a feature also observed with iron hemes.[47]

The action of NO on suppressing or promoting cellular redox events is quite controversial. There are reports that NO complexes sacrificially reduce cytotoxicity in cells by removing organic peroxides, H_2O_2, and high valent iron species.[48,49] Another mode of control upon cellular redox events is through coordination to metal sites in a fashion that prevents Fenton-type catalysis.[50-52] A discussion of this work is provided in Appendix B for those who wish additional details.

A major aspect of NO storage is illustrated by the discovery that NO is transported in the bloodstream as an S-nitrosylated thiol, predominantly with glutathione (GSH) as the carrier, but also directly attached to a cysteine functionality of hemoglobin, and not at the heme site.[53] Details of these types of NO carriers as well as of other physiological implications of NO appear in Appendix B. These examples show that metal nitrosyl complexes represent both active molecules and inhibited molecules, in the diverse chemistry that has been, and continues to be, uncovered for physiological NO.

1.4. COMMON IRON NITROSYL SYNTHETIC METHODS

Since iron nitrosyl complexes and iron complexes that bind nitric oxide have important physiological and industrial applications, several synthetic methods have been developed. Some of the common methods for preparing transition metal nitrosyl complexes are summarized in this section. These representative cases serve as examples of synthetic strategies that have been used to prepare the iron nitrosyl complexes that appear in the main body of this review. In the later sections, attention will be given to the structure and reactivity, rather than to the synthesis as long as one of the standard preparative routes has been followed. Extensive collections of preparatory methods have been given by Mingos and Sherman,[8] Richter-Addo et al.,[17] Greenwood and Earnshaw,[54] and Caulton[55,56] more recently in reviews by Legzdins et al.,[9] and Ford and Lorkovic.[6]

1.4.1. NITROSYLATION BY NO^+ DONORS

Ligand displacement by NO^+ delivery agents such as $[NO^+]BF_4$ is the most common method, after addition of NO gas, to displace a solvent molecule. Treating metal carbonyl complexes with $(NO)PF_6$ or $(NO)BF_4$, allows for substitution of CO by the isoelectronic NO^+ ligand. For example, Simpson and King prepared $[(\eta^5\text{-}C_5H_5)Fe(P\{OMe\}_3)(NO)(I)]BF_4$ from its CO analogue[57,58] and $(NO)BF_4$.[59] X-ray and ^{31}P NMR evidence showed that the better π-accepting ability of the cationic NO ligand reduces the degree of iron to phosphorous back-donation such that $[(\eta^5\text{-}C_5H_5)Fe(P\{OMe\}_3)(NO)(I)]BF_4$ exhibits a longer Fe-P bond and shorter P-OCH_3 bonds than its CO precursor.

PF_6^- and BF_4^- salts of NO^+ also serve as a source of NO^+ for the direct addition to coordinatively unsaturated transition metal complexes. Sellman and co-workers used this direct addition pathway to prepare a series of 18- and 19-electron iron nitrosyls of the pentadentate

ligand, 2,6-bis(2-mercaptophenylthiomethyl)pyridine^{2-} as presented in Figure 1.3.[60] Reaction path **a** of Scheme 1.2 illustrates the direct addition reaction, while path **b** is another example of the CO displacement route using NO^+ as the entering ligand. Both routes form the same nitrosyl product, but path **b** has a lower yield and requires additional purification from the precursor complex.

1.4.2. DIRECT ADDITION OF NO GAS

While direct addition of nitric oxide gas is a convenient method of preparing transition metal nitrosyl complexes, nitric oxide gas degrades to N_2O and NO_2 under pressure and must be purified prior to use under an inert atmosphere.[46,61,62]

Reaction path **c** in Figure 1.3 of Sellman et al.[60] illustrates a reaction in which a coordinatively unsaturated complex is exposed to NO gas. Stoichiometric addition yields the mono nitrosyl via path **c**. But excess NO affords a dinitrosyl product (path **f**). Two iron nitrosyls that differ by one electron (central complex shown in Figure 1.3) were prepared by this method. These two complexes have been compared by X-ray crystallography, DFT calculations, cyclic voltammetry and IR methods which reveal that the site of the extra electron is largely localized on the NO ligand and an Fe^{II} center in both species.[60]

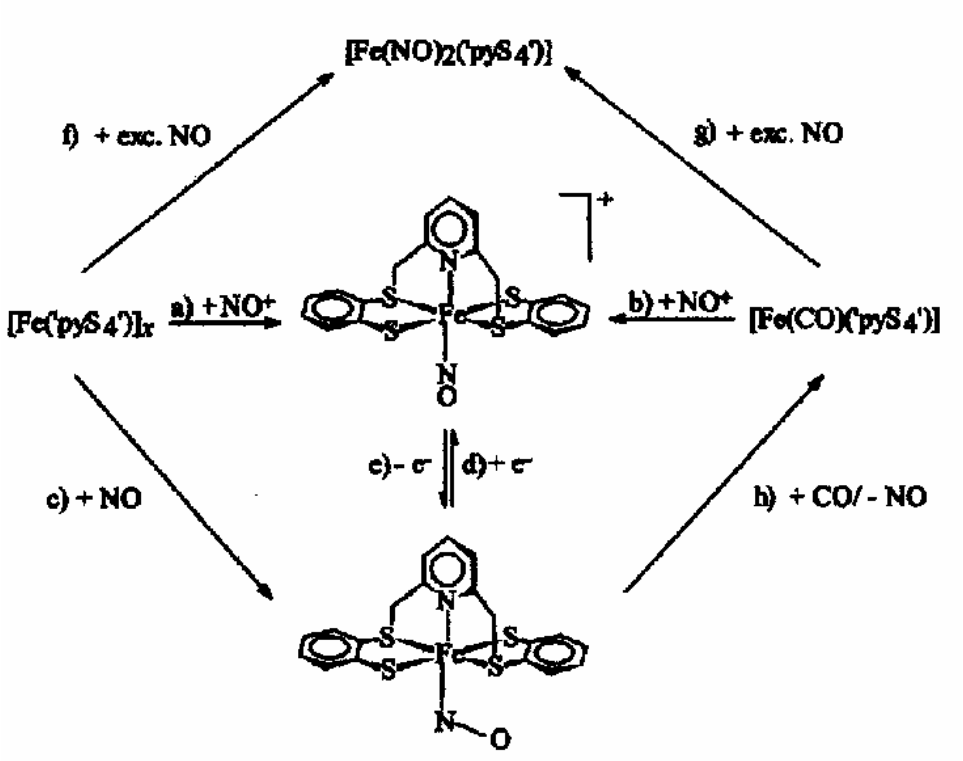

Figure 1.3 – Nitrosylation by NO Donors and Direct Addition of NO Gas
a) CH_2Cl_2, $NOBF_4$, 25 ºC; **b**) CH_2Cl_2, $NOBF_4$, 0 ºC; **c**) CH_2Cl_2, 1 equiv of NO(g), 25 ºC; **d**) CH_2Cl_2, N_2H_4, NH_3, $NaNH_2$, NEt_4N_3, $BuNH_2$, MeOH, or DMF, 25 ºC; **e**) CH_2Cl_2, $[Cp_2Fe]PF_6$, 78 ºC; **f**) CH_2Cl_2, excess NO (g), 25 ºC; **g**) CH_2Cl_2, excess NO (g), 25 ºC; **h**) CH_2Cl_2, excess NO (g), 25 ºC. (Reprinted from *Chem. Eur. J.*, **2001**, *7*, 1874, "Synthesis, Reactivity, and Structure of Strictly Homologous 18 and 19 Valence Electron Iron Nitrosyl Complexes", Dieter Sellmann, Nicole Blum, Frank W. Heinemann, and Bernd A. Hess, Copyright 2001, with permission from Wiley-VHC. 60)

1.4.3. SODIUM NITRITE AS AN NO^+ SOURCE

NO^+ may be generated from $NaNO_2$ and a mineral acid in organic or aqueous media.[63] Bhattacharya and co-workers prepared two thiolato-bridged Roussin's esters, $[(NO)_2Fe(BM)_2Fe(NO)_2]$ (BM = benzyl mercapto anion) and $[(NO)_2Fe(ME)Fe(NO)_2]$ (ME = 2–mercaptoethanoate anion). They also prepared a monomeric, paramagnetic dinitrosyl, $[Fe(NO)_2(ABT)]$ (ABT = 2-aminobenzylthiolato anion) which is reported to be stable under aerobic conditions in aqueous solution. All three species were characterized by IR, EPR and electrochemical methods.[64]

1.4.4. HYDROXYLAMINE AS AN NO SOURCE

Reductive nitrosylation, in which a coordinated hydroxylamine (NH_2OH) is oxidized to NO, at the expense of an additional molecule of NH_2OH being reduced to NH_3, is a convenient way to introduce coordinated NO, particularly ^{15}NO, via $^{15}NH_2OH$. Ryan and co-workers have utilized this route to prepare various nitrosyl porphyrin complexes of formulation Fe(P)(NO) (P = tetraphenylporphyrin (TPP), octaethyl porphyrin (OEP), or tetrachlorin (TPC)) in quantitative yields in a 1:1 methanol/chloroform solution at room temperature. The desired product precipitates at room temperature.[65] The protoporphyrin IX dimethyl ester complex, Fe(PPDME)(NO) was obtained from a 4:1 methanol/chloroform solution. Co, Mn, and Cr porphyrins were also prepared by this method.

1.4.5. NITROSAMIDES

Nitrosamides such as Diazald™ (*N*-methyl-*N*-nitroso-*p*-toluenesulfonamide) and Piltoy's acid (*N*-hydroxybenzenesulfonamide) are convenient alternative nitrosating agents, especially when over exposure to NO gas may lead to multiple products. For example, Hughes and co-workers[66] reported the synthesis of mononuclear, and polynuclear iron nitrosyl complexes with the tripodal tetradentate $[N(CH_2CH_2S)_3]^{3-}$ ligand. They found that NO gas reacted rapidly with $(NEt_4)[Fe(NS_3)(CO)]$ to form $(NEt_4)[Fe(NS_3)(NO)]$. However, exposing the reaction mixture to NO gas for more than a few minutes led to insoluble products with multiple NO groups as indicated by several IR bands between 1600 and 1800 cm^{-1}. Preparation with Piloty's acid in the presence of lithium methoxide or with Diazald™ produced the desired products without overnitrosation.

2. REVIEW OF IRON NITROSYL COMPLEXES

2.1. ENEMARK-FELTHAM NOTATION

The remainder of this document utilizes the Enemark–Feltham notation[11-13] to describe the MNO moiety in transition metal nitrosyl complexes. The Enemark–Feltham notation, $\{MNO\}^n$, will be explained after a brief introduction to its inception.

In the 1930's Sidgwick recognized that, in bonding interactions with transition metals, nitric oxide, $NO^{\bullet}$, could lose an electron to form NO^+ or gain an electron to form NO^-.[12,13,67] The valence bond structure for NO^+ is has triple bond character (*sp* hybridized, linear), so Sidgwick proposed that NO^+ complexes would exhibit a linear MNO group. The valence bond structure for NO^- has double bond character (sp^2 hybridized, 120° bond angle), thus it was assumed that NO^- complexes would exhibit a bent MNO bond. In fact, the first linear MNO complexes characterized in the 1930's were NO^+; later, in the 1960's, bent MNO NO^- groups were also characterized.[68] The available experimental evidence seemed to indicate that the charge on the NO group directed the MNO bond angle. But, after more transition metal nitrosyl complexes were characterized, it became clear that something other than the charge on NO was directing the MNO bond angle. Recognizing that metal nitrosyl complexes are highly covalent, Enemark and Feltham[11-13] developed a system that accounts for the MNO angle based upon molecular orbital correlation diagrams. The Enemark–Feltham approach treats each MNO group as a covalently bound entity which is sensitive to ligand field effects. The method correlates molecular orbital orderings in various geometries, and considers how the character of the HOMO affects the geometry of the MNO group.[11] The MNO moiety is bent when the HOMO is antibonding and linear when the HOMO is bonding. In the Enemark–Feltham notation, $\{MNO\}^n$, *n* represents

the total number of metal d and NO π* electrons when NO is arbitrarily assigned as NO^+. The notation, which reflects the fact that there is significant mixing of metal d and π* NO orbitals, allows for some generalizations. For example, according to the Enemark–Feltham notation, six coordinate octahedral complexes with $\{MNO\}^6$ are expected to be linear based upon molecular orbital correlation diagrams. Exceptions occur and are understood by considering factors that influence the molecular orbital ordering, hence influence the MNO bond angle. The following sections describe factors influencing the MNO bond angles in iron nitrosyl porphyrins, porphyrin related complexes, dinitrosyl complexes, bimetallic nitrosyl complexes, cluster complexes and non-heme complexes.

2.2. PORPHYRIN COMPLEXES

Elucidation of the chemistry, structure and function of iron porphyrin nitrosyl complexes offers the promise of advances in medicine and a display of intriguing chemistry. This section reviews some of the model complexes synthesized to study the chemistry and structural features exhibited exhibited by iron nitrosyl porphyrins.[10,69,70]

Thiolates react with bis(nitro)[α,α,α,α-*meso*-tetrakis(*o*-pivalamidophenyl)-porphinato] Fe^{III} ([$Fe(NO_2)_2$(TpivPP)]) and 2,3,5,6-tetrafluorothiophenolate to produce the mixed ligand (thiolate/nitrite) Fe^{III} complex [$Fe(NO_2)(SC_6HF_4)$(TpivPP)]$^-$. [71] On the other hand, 2,3,5,6-tetrafluorothiophenol reacts with [$Fe(NO_2)_2$(TpivPP)] to yield the reduced ($Fe^{II}(NO^{\bullet})$) product, [Fe(NO)(TpivPP)], which exhibits a bent nitrosyl group, typical of $\{FeNO\}^7$ complexes. [Fe(NO)(TpivPP)] was later converted, with exposure to air, to the nitrite complex, [Fe^{III}(TpivPP)(NO_2)(py)] in $CHCl_3$ in the presence of pyridine.[72] In the absence of pyridine, [Fe(NO)(TpivPP)] oxidizes with air to the ferric chloro complex, [Fe(Cl)(TpivPP)]. Richter-Addo and co-workers propose that pyridine assists stabilization of the nitrite product. This result has implications for iron nitrosyl reactivity in heme proteins bearing trans axial nitrogen bases. Iron-bound nitrite may be an intermediate or a product in some heme-NO ligand oxidations;[72] thus, release of coordinated NO may not be required for formation of NO_2^-, or NO_3^-.

Whereas [M(OEP)(CO)] and [M(TTP)(CO)] (M = Ru, Os; OEP = octaethylporphyrinato anion; TTP = tetratolylporphyrinato dianion) form the corresponding [(por)M(NO)(SR)] and [(por)M(NO)(OR)] addition products, upon reaction with thionitrites (RSNO) and isoamyl nitrite (RONO), $[(TPP)Fe(THF)_2]^+$ reacts with isoamyl nitrate to produce the air sensitive and thermally unstable nitrosyl alcohol product $[(TPP)Fe(NO)(HO\text{-}i\text{-}C_5H_{11})]^+$ formally $[Fe^{II}NO^+]$. Consistent with coordinated NO^+, the X-ray crystal structure reveals a linear Fe-N-O linkage. The

thionitrite NO donor, *S*-nitroso-*N*-acetyl-L-cysteine methyl ester, reacts with $[(TPP)Fe(THF)_2]^+$ to form [(TPP)Fe(NO)] in high yield, yet reacts with (OEP)Ru(CO) to form the trans addition product, (OEP)Ru(NO)(NACysMe-S), (NACysMe-S = *N*-acetyl-L-cysteinate methyl ester) coordinated as a thiolate.[73]

In related work, Ford and Lorkovic[74] found that, upon exposure to NO gas, [Ru(P)(CO)] (P = various porphyrins), forms $[Ru(P)(NO)_2]$. The dinitrosyl then reacts with two equivalents of NO to give [Ru(P)(NO)(ONO)] and N_2O.[75-77] In contrast, [Fe(TPP)(NO)], formally $\{Fe^{II}NO^{\bullet}\}$ is unreactive with NO in toluene and in chloroform at room temperature. Instead, [Fe(TPP)(NO)] reacts with NO_2 (N_2O_3) impurities in the NO gas stream to form $[Fe(TTP)(NO)(NO_2)]$. This finding highlights the complications introduced by NO*x* impurities in NO gas and the fact that there are substantial kinetic differences between the reactivities of Fe and Ru porphyrins.

In the same study, it was also observed that NO dissociates more readily from $[Fe(TTP)(NO)(NO_2)]$, formally an $\{Fe^{III}(NO^{\bullet})(NO_2^{-})\}$ species, than does NO_2. Treatment of $[K(222)][Fe(TpivPP)(NO_2)]$ (formed *in situ* from the reaction between $[Fe^{II}(TpivPP)]$ and an excess of Kryptofix-222-solubilized KNO_2; K(222) = potassium complex of 4,7,13,16,21,24 hexaoxa–1,10-diazabicyclo[8.8.8]hexacosane) with gaseous NO yielded two crystalline forms of the Fe^{II} $\{FeNO\}^7$ complex, $[Fe(TpivPP)(NO_2)(NO)]^-$.[78] The first form exists as two independent anion complexes. One, shown in Figure 2.1, has ordered axial ligands. The other, shown in Figure 2.2 has disordered axial ligands. In each anion, the plane of the nitro group is almost perpendicular to the plane of the nitrosyl group. Figure 2.3 shows form 2 in which the plane of the nitro group is nearly parallel to the plane of the nitrosyl. The perpendicular orientation in the two complexes of form 1 allows each ligand to interact with distinct dπ orbitals, thus to bond

more strongly to iron than does the parallel orientation of form 2 in which the ligands compete for π-bonding. The nitrosyl group is bent in all three cases indicative of an [$Fe^{II}NO^{\bullet}$] assignment. These observations contrast with those for the nearly linear nitrosyl ligand of the diamagnetic Fe^{III}, $\{FeNO\}^6$ derivative of [Fe(TpivPP)(NO_2)(NO)].[69] Here, the formal assignment is Fe^{III} $NO^{\bullet}$, but a large Fe^{II} NO^+ resonance contributor must also exist. Two new synthetic methods were developed to prepare the Fe^{III} derivative of [Fe(TpivPP)(NO_2)(NO)]. In the same study tetraphenyl porphyrin (TPP), octaethyl porphyrin (OEP), tetra-*p*-methoxyphenyl porphyrin (TPP-$(OMe)_3$) complexes were also synthesized and studied by Mossbauer and IR spectroscopies as well as by X-ray crystallography.

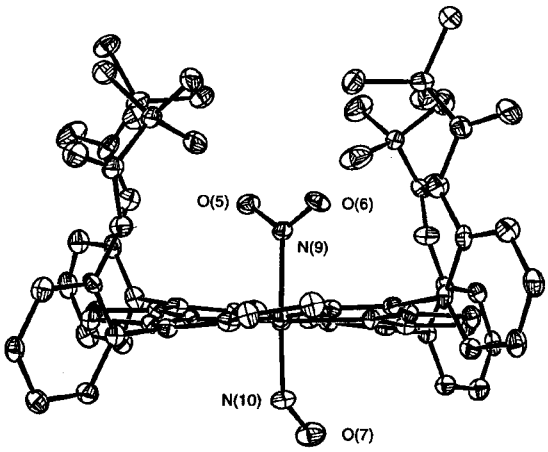

Figure 2.1 – ORTEP Diagram of [Fe(TpivPP)(NO_2)(NO)]$^-$ Form 1 Anion 1
(30% probability ellipsoids) The two ordered axial ligands have been labeled. The angle between the NO_2 and the FeNO planes is 85.4º. (Reprinted with permission from *J. Am. Chem. Soc*., **1997**, *119*, 6274-6283. Copyright 1997 American Chemical Society. 76)

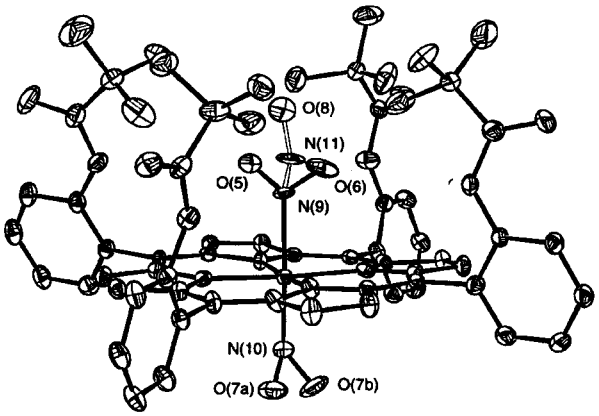

Figure 2.2 – ORTEP Diagram of [Fe(TpivPP)(NO_2)(NO)]$^-$ Form 1 Anion 2
(30% probability ellipsoids) The disorder in the axial ligands is shown. (Reprinted with permission from *J. Am. Chem. Soc*., **1997**, *119*, 6274-6283. Copyright **1997** American Chemical Society. 76)

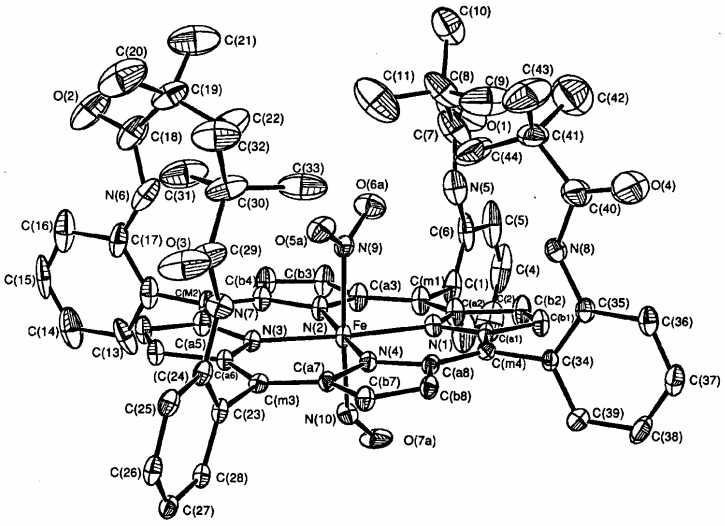

Figure 2.3 – ORTEP Diagram of [Fe(Tpivpp)(NO_2)(NO)]$^-$ Form 2
(30% probability ellipsoids). The labels of the crystallographically unique atoms are shown along with the values of the bond distances in the coordination group. The near parallel orientation of the nitrite ion plane and the iron-nitrosyl plane is evident (the dihedral angle is 20.9º). (Reprinted with permission from *J. Am. Chem. Soc*., *119*, 6274-6283. **1997**, Copyright 1997, American Chemical Society. 76)

The related Fe^{II} complex, $[Fe^{II}(TpivPP)(NO)]$, also forms along with $[Fe^{III}(TpivPP)(NO_3)]$, in the reaction between $BF_3{\bullet}OEt_2$ and the bis(nitro) complex of Fe^{III} picket-fence porphyrin $[K(18C6)(OH_2)][Fe(TpivPP)(NO_2)_2]$ (18C6 = 1,4,7,10,13,16-hexaoxacyclooctadecane).[79] A possible pathway to the products is depicted in Figure 2.4. Initially, $BF_3{\bullet}OEt_2$ acts as a Lewis acid to compete for one of the nitrite ligands of $[Fe(TpivPP)(NO_2)_2]^-$ and forms the mono(nitro)iron(III) complex along with a BF_3-nitrite adduct. The reactive mono(nitro)iron(III) complex, $[Fe^{III}(TpivPP)(NO_2)]$ then disproportionates via oxygen atom transfer to $[Fe^{III}(TpivPP)(NO_3)]$ and $[Fe^{II}(TpivPP)(NO)]$. Formation of crystals of $[K(18C6)][BF_3{\bullet}NO_3]$ suggests that $[BF_3NO_2]^-$ acts as a competitive O-atom acceptor.[79]

$$[Fe^{III}(TpivPP)(NO_2)_2]^- + BF_3{\bullet}OEt_2 \longrightarrow [Fe^{III}(TpivPP)(NO_2)] + [BF_3NO_2]^- \quad (1)$$

$$2[Fe^{III}(TpivPP)(NO_2)] \longrightarrow [Fe^{III}(TpivPP)(NO_3)] + [Fe^{II}(TpivPP)(NO)] \quad (2)$$

Figure 2.4 – Formation of $[Fe^{III}(TpivPP)(NO_3)]$ and $[Fe^{II}(TpivPP)(NO)]$
(Reprinted with permission from *Inorg. Chem.*, **1998** *37*, 2308-2316. Copyright 1998 American Chemical Society.77)

A group of $\{FeNO\}^6$ complexes, of formulation $[Fe(NO)(OEP)L]^+$, was prepared by adding excess NO to solutions of $[Fe(OEP)(OClO_3)]$ and one of the neutral trans ligands illustrated in Figure 2.5.[80] These are linear nitrosyl complexes, formally $[Fe^{II}(NO)^+]$. The reaction was carried out under an NO atmosphere due to the extreme lability of the NO ligand. Crystals were also cultivated under an NO atmosphere using special techniques. Scheidt and co-workers had previously prepared the five-coordinate square-pyramidal $\{FeNO\}^7$ complex, [Fe(OEP)(NO)] that exhibited a well ordered, bent nitrosyl in two forms. Figures 2.6 and 2.7 display the crystal structures of forms one and two, respectively. Each form shows an off axis

Fe-N_{NO} vector that is proposed to induce differences in the Fe-N_p bond distances in both complexes. An off axis tilt is suggested to be inherent to $\{FeNO\}^7$ nitrosyl hemes. Scheidt proposes that the structural distortions that result from the off axis tilts may be responsible for the difference in dissociation rates observed for the two forms of [Fe(NO)(OEP)].[81]

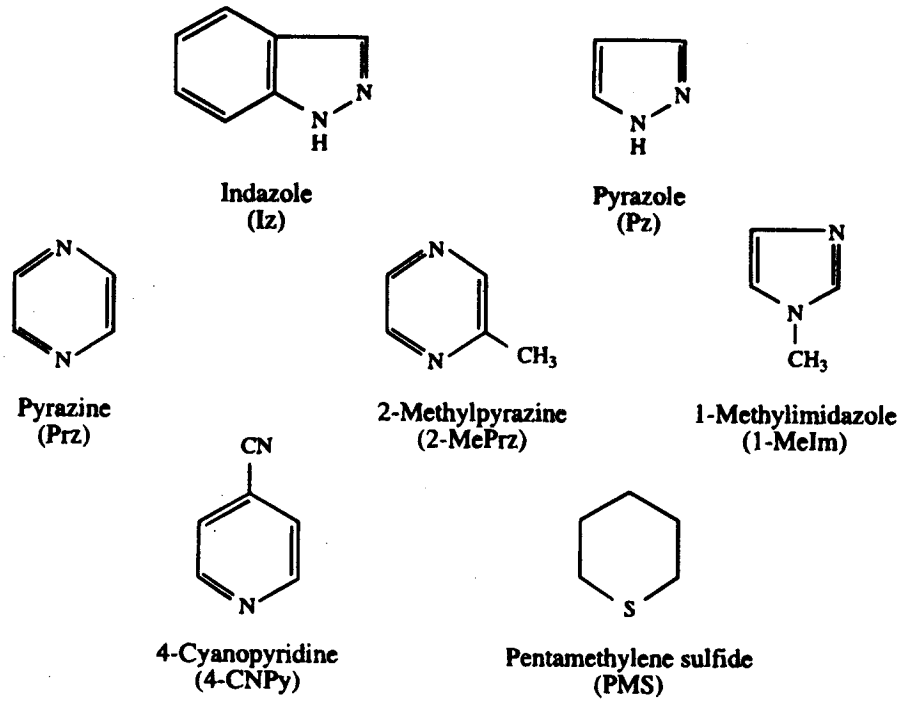

Figure 2.5 – Neutral Trans Ligands for [Fe(NO)(OEP)L] Complexes
(Reprinted with permission from *J. Am. Chem. Soc*. **1999**, *121*, 5210-5219. Copyright 1999 American Chemical Society. 78)

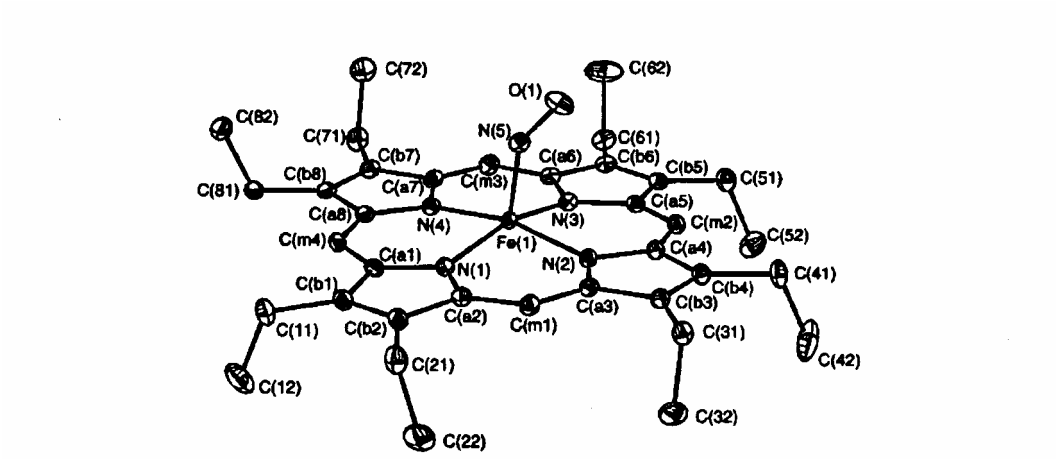

Figure 2.6 – ORTEP Diagram of [Fe(OEP)(NO)] Form 1
(50% probability ellipsoids) (Reprinted with permission from *J. Am. Chem. Soc*. **1997**, *119*, 7404-7405. Copyright 1997 American Chemical Society.79)

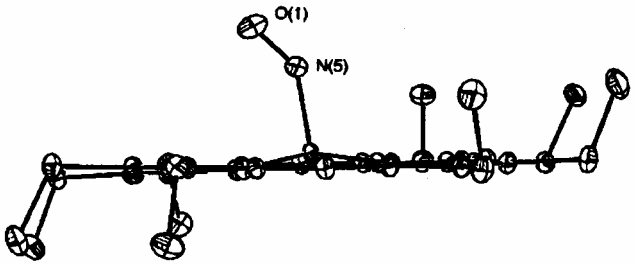

Figure 2.7 – Edge-on View of [Fe(OEP)(NO)] Form 2
(Reprinted with permission from *J. Am. Chem. Soc*. **1997**, *119*, 7404-7405. Copyright 1997 American Chemical Society. 79)

Bohle et al. characterized octaethyltetraazaporphyrin complex [Fe(OETAP)(NO)] (OETAP = octaethyltetraazaporphyrin), which is isostructural to [Fe(NO)(OEP)]), by X-ray crystallography, IR, EPR, Mossbauer spectroscopies, electrochemistry and elemental analysis.[82] Physical and kinetic data can be seen in Table 2.1. The increased reduction potential of the first oxidation couple, $\{FeNO\}^6$-$\{FeNO\}^7$ is a result of the electron withdrawing nature of the nitrogen atoms of the tetraaza derivative.

Table 2.1 – Physical and Kinetic Data for [Fe(OEP)(NO)] and [Fe(OETAP)(NO)]
(*Chem. Commun*., **1997**, 91-92 - reproduced by permission of the Royal Society of Chemistry. 80)

Compound	ν(NO)[a]/cm^{-1}	$E_{\frac{1}{2}}$[b]/mV	g_{iso}	a(^{14}N)/G	Mössbauer data[d]/mm s^{-1} Δ	δ	Added ligand L	[L]/M	k_{obs}[e]/s^{-1}
[Fe(oep)(NO)]	1672	390	2.05	18.0	1.258(1)	0.348(1)	*N*-mim	6.3	3.8(1) × 10^{-5}
							py	6.0	2.2(1) × 10^{-5}
[Fe(oetap)(NO)]	1666	733	1.99	17.0	1.951(1)	0.209(1)	*N*-mim	6.3	0.148(2)
							py	6.0	0.072(1)

[a] KBr pellet. [b] Potentials in mV *vs.* Ag^+/Ag in dichloromethane solution with 0.1 M NBu_4PF_6 as supporting electrolyte on a platinum-button working electrode. [c] Room-temp. EPR spectra measured in toluene solution. [d] At 100 K. [e] Pseudo-first-order rate constants for the rate of denitrosylation in 1 : 1 toluene–ligand solution at 25 °C.

The X-ray crystal structure of [Fe(OETAP)NO], shown in Figure 2.8, reveals a bent nitrosyl, characteristic of $\{Fe^{II}NO^{\bullet}\}^7$ complexes, which is oriented away from the ethyl groups on the same face of the complex. In spite of almost identical steric constraints on axial ligand binding as compared to [Fe(OEP)(NO)], [Fe(OETAP)(NO)] dissociates NO four times faster upon treatment with pyridine or *N*-methylimidazole. Differences in electronic character, as illustrated by the different Mossbauer and EPR spectra, are considered to be responsible for the different reactivities.

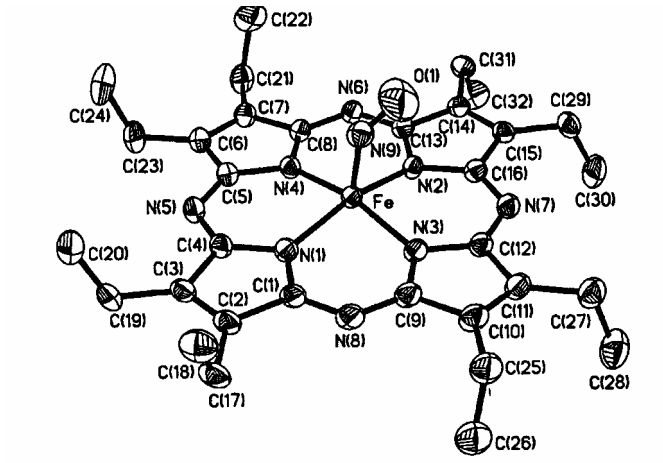

Figure 2.8 – Molecular Structure of [Fe(OETAP)(NO)]
Shown with hydrogen atoms omitted for clarity. Important bond lengths (Å) and angles (º): Fe(1)-N(1-4) 1.922-1.941(3), Fe(1)-N(9), 1.721(4), N(9)-O(1) 1.155(5); Fe(1)-N(9)-O(1) 143.7(4). (*Chem. Commun*., **1997**, 91-92 - reproduced by permission of the Royal Society of Chemistry 80)

Scheidt[83] and co-workers also compared the newly synthesized $[Fe(OEP)(NO)]ClO_4$, formally an $[Fe^{II}(NO^+)]$ or $\{FeNO\}^6$ linear nitrosyl, with that of a previously reported solvated form, $[Fe(OEP)(NO)]ClO_4 \bullet CHCl_3$. The data displayed in Table 2.2 highlights some important differences in bond angles, distances and stretching frequencies between $[Fe(OEP)(NO)]ClO_4$ and $[Fe(OEP)(NO)]ClO_4 \bullet CHCl_3$ as well as differences relevant to the cofacial dimers formed by both forms in the crystalline state. One important difference is the 30 cm^{-1} difference in the IR stretching frequency with $\bar{\nu}_{NO}$ at 1868 cm^{-1} for $[Fe(OEP)(NO)]ClO_4 \bullet CHCl_3$ and $\bar{\nu}_{NO}$ at 1838 cm^{-1} for $[Fe(OEP)(NO)]ClO_4$. The origin of this difference was investigated by X-ray crystallography, Mossbauer spectroscopy and electrochemical methods. The ORTEP diagram of $[Fe(OEP)(NO)]ClO_4$ in Figure 2.9 reveals a nearly linear Fe-N-O (173.19(13)°) group which is consistent with that determined for $[Fe(OEP)(NO)]ClO_4 \bullet CHCl_3$ (176.9(3)°).

Table 2.2 – Selected Comparisons for $[Fe(OEP)(NO)]^+$
(Reprinted with permission from *Inorg. Chem.*, *39*, **2000**, 5102-5110. Copyright 2000, American Chemical Society. 81)

	$[Fe(OEP)(NO)]ClO_4 \cdot CHCl_3$ [10]	$[Fe(OEP)(NO)]ClO_4$
	IR Data	
ν (NO)[a]	1868	1838
	Coordination Group Distances and Angles	
$Fe-N_{NO}$ [b]	1.644(3)	1.6528(13)
$N-O$ [b]	1.112(4)	1.140(2)
$Fe-N_P$ [b]	1.994(1)	1.994(5)
$Fe-N-O$ [c]	176.9(3)	173.19(13)
ΔFe [b,d]	0.29	0.32
tilt[c]	0.6	4.6
	Intermolecular Distances	
$Fe\cdots Fe$ [b]	4.24	4.26
MPS [b,e]	3.36	3.41
$Ct\cdots Ct$ [b,f]	3.65	3.65
LS [b,g]	1.43	1.32

[a] Nujol or KBr (cm^{-1}). [b] Values in angstroms. [c] Values in degrees. [d] Displacement from the 24-atom mean porphyrin plane. [e] Mean separation between the two planes. [f] Distance between two porphyrin centers. [g] Lateral shift.

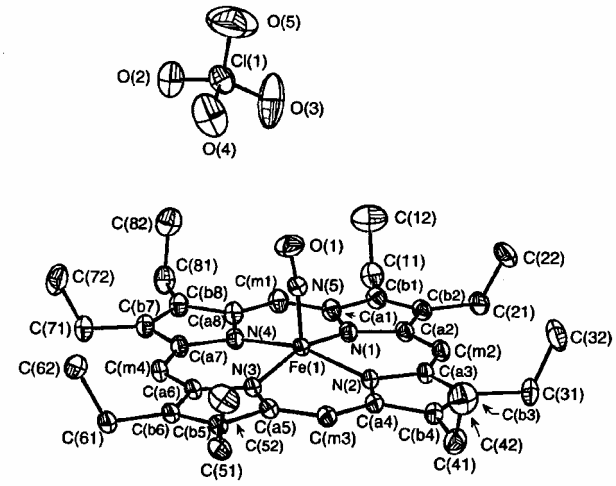

Figure 2.9 – Crystal Structure of $[Fe(OEP)(NO)]ClO_4$
The closest perchlorate anion is shown. Thermal ellipsoids are contoured at the 50% probability level. The labeling scheme is also shown. (Reprinted with permission from *Inorg. Chem.*, *39*, **2000**, 5102-5110. Copyright 2000, American Chemical Society. 81)

The ORTEP diagrams of the cofacial dimers of each complex (Figure 2.10) show that, while the nitrosyl group in [Fe(OEP)(NO)]ClO_4 **(B)** tilts 4.6° from the heme normal, essentially no tilt is observed for the solvated form [Fe(OEP)(NO)]ClO_4•$CHCl_3$ **(D)**. The slight difference in the tilting of the nitrosyl is group is the most glaring reason for the difference in stretching frequency**.** The off axis tilt in the direction of the bend is consistent with the conclusions of Ghosh and Bocian[84] who have illustrated that CO tilting is strongly coupled with CO bending in monoxyheme. In fact, all well characterized $\{FeNO\}^7$ porphyrin species exhibit such tilting and bending; it has been suggested that tilting allows better overlap between the π^* orbital of NO and the dz^2 orbital of the metal.[81,85] Figure 2.12[85] illustrates the greater π^*_{NO} - dz^2 orbital overlap achieved by tilting of dz^2 orbital. The existence of both forms of these $\{FeNO\}^6$ porphyrin complexes suggests that the stabilization gained by tilting and bending is insufficient to cause titling in all cases. The difference in $\bar{\nu}_{NO}$ may also arise from differences in how the cations interact to form crystalline dimers. Figure 2.10 reveals that the porphyrinato nitrogen of [Fe(OEP)(NO)]ClO_4•$CHCl_3$ is located almost directly above the iron atom of the closest molecule. For the $CHCl_3$ solvated complex, the iron center may adopt this extra interaction from the next plane as a sixth ligand. A sixth ligand would reduce tilting and as a result, increase stretching frequency. This contact is lacking in the unsolvated [Fe(OEP)(NO)]ClO_4 which has no pseudo sixth ligand. Another interesting feature of these two different crystalline forms is asymmetric Fe-N_p bonds which seem to correlate with the off axis tilt of the nitrosyl. Figure 2.11[85] shows how the two equatorial bonds in the direction of the tilt shorten while those in the opposite direction lengthen. Scheidt and co-workers explain the correlation of tilting with bond shortening based upon an observation first noted by Hoffman. Hoffman suggested that the tilting observed in some square pyramidal $\{MNO\}^8$ complexes could be caused by the increased

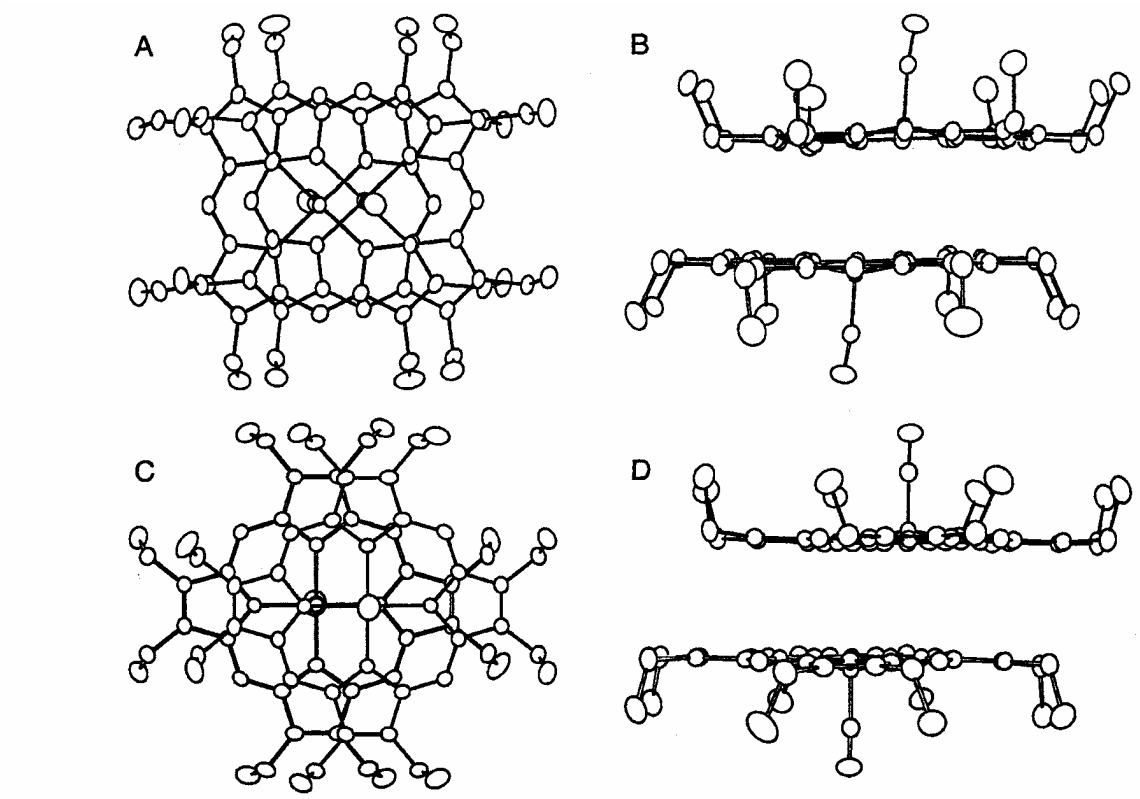

Figure 2.10 – ORTEP Diagrams of the Two Cations in [Fe(OEP)(NO)]ClO_4
(A) view perpendicular to the mean porphyrin plane and (B) view parallel to the mean porphyrin plane. ORTEP diagrams of the two closely interacting cations of the solvated form [Fe(OEP)(NO)]ClO_4•CH_3Cl; (C) view perpendicular to the mean porphyrin plane and (D) view parallel to the mean porphyrin plane. The differences in the bendings and tiltings of the nitrosyl groups are readily seen in views B and D. (Reprinted with permission from *Inorg. Chem*., *39*, **2000**, 5102-5110. Copyright 2000 American Chemical Society. 81)

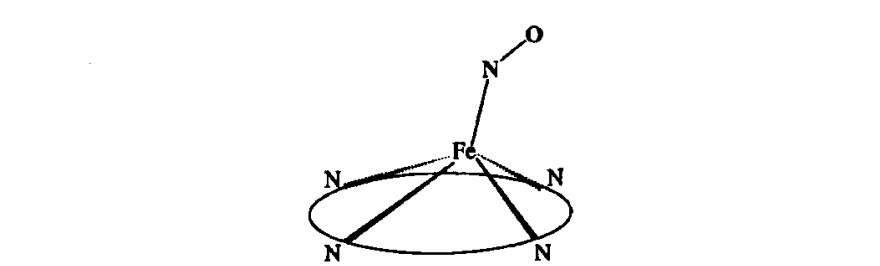

Figure 2.11 – Correlated Tilt/Asymmetry in Five-coordinated [Fe(Porph)(NO)] Derivatives
Correlated tilt/asymmetry in five-coordinated [Fe(Porph)(NO)] derivatives. The two equatorial Fe-Np bonds to the right (in the direction of the tilt) are shortened, while the Fe-Np bonds to the left are lengthened. The magnitudes of the distortion have been exaggerated for clarity. (Reprinted with permission from *J. Am. Chem. Soc*. **2000**, *122*, 4651-4659. Copyright 2000, American Chemical Society.[83])

overlap between the metal d_z^2 and one π^*_{NO} orbital that is achieved upon NO bending concomitant with sideways motion of the nitrosyl as depicted in Figure 2.12.[85,86] The tilting observed by Hoffman, however, is in the direction opposite that observed for $[Fe(OEP)(NO)]ClO_4 \bullet CHCl_3$ and $[Fe(OEP)(NO)]ClO_4$. The model suggested by Scheidt and co-workers involves an alternative way to increase d_z^2 and π^*_{NO} overlap. This model, also depicted in Figure 2.12, allows a rotation of the metal d_z^2 orbital which leads to a tilt in the direction opposite of that observed by Hoffman. In addition, rotation of the metal d_z^2 orbital with respect to the porphyrin plane changes the σ interactions of the metal d_z^2 orbital with the porphyrin when the metal ion is out of the porphyrin plane, as it is in these complexes. The σ interactions in the direction of the tilt will be enhanced, whereas those in the opposite direction will be weakened. Mossbauer measurements confirm a diamagnetic ground state.

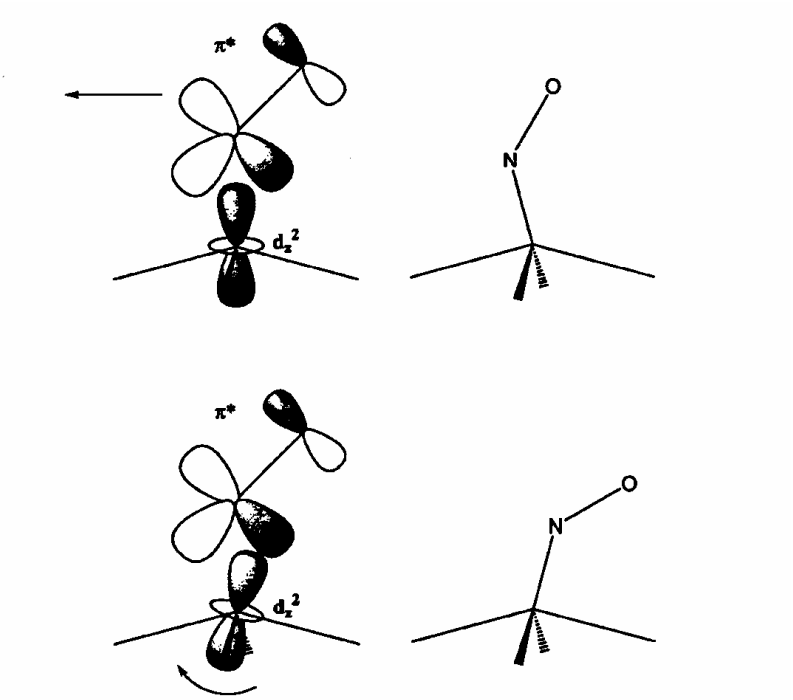

Figure 2.12 – Possible Distortions Leading to Greater Overlap of π^*_{NO} with Iron d_z^2
Possible distortions lead to two different tilt directions. (Reprinted with permission from *J. Am. Chem. Soc*. **2000**, *122*, 4651-4659. Copyright 2000, American Chemical Society. 83)

Unusual quadrupole splitting and isomer shifts (for low spin Fe^{III}) porphyrins are observed for $[Fe(OEP)(NO)]ClO_4 \bullet CHCl_3$, $[Fe(OEP)(NO)]ClO_4$, and $[Fe(OEP)(Iz)(NO)]ClO_4$ (Iz = imidazole).[83] Scheidt and co-workers view these species as low spin $[Fe^{III}NO\cdot]$ and argue this case from Mossbauer data. Similar complexes studied by Scheidt are $[Fe(TPPBr_4)(NO)]$ ($TPPBr_4$ = 2,3,12,13-tetrabromo-5,10,15,20-tetraphenylporphyrin dianion) and [Fe(oxoOEC)(NO)] (oxoOEC = 3,3,7,8,12,13,17,18-octaethyl-3*H*-porphin-2-onato(2^-) dianion).[85] Related iron and ruthenium porphyrin complexes, (OEP)Fe(NO)(*p*-C_6H_4F) and (OEP)Ru(NO)(*p*-C_6H_4F) exhibit strongly bent and tilted M-N-O units as well as elongated M-

N(NO) bonds.[87] The authors view these species as $\{M^{III}NO^{\bullet}\}^6$ (M^{III} = Fe^{III} and Ru^{III}) that yield bent nitrosyls due to very strongly σ donating ligands trans to NO·. In this case the trans ligands are strong carbon donors. Figures 2.13 and 2.14[87] illustrate the bent and tilted nitrosyl group in both complexes; Table 2.3[87] displays selected bond angles and bond distances for each complex. Richter-Addo and co-workers suggest that bending of the M-N-O group is inherent to (por)M(NO)(*p*-C_4H_4F) when X is a strong σ donor. Hybrid Hartee-Fock/density functional calculations reveal that a minimum energy structure exists with a bent NO group and with both the NO and the p-C_6H_4 ligands tilted off axis. The calculated values approximate the observed N-O, Fe-NO, and Fe-N_p bond distances as well as the observed tilt angles and the extent of NO bending. Theoretical values are compared with experimental values in Figure 2.15.

Extended Huckel calculations suggest that bending of the FeNO moiety to bisect an N_p-Fe-N_p angle provides a lower energy barrier than bending in a direction that eclipses an equatorial Fe-N_p bond. This is because bending that bisects an N_p-Fe-N_p angle avoids interaction between the NO π* orbital and the metal $d_{x^2-y^2}$ orbital. Figure 2.16 displays the molecular orbital energy level diagram of (porph)Fe(NO)(*p*-C_6H_4F) as well as the B_2 symmetry LUMO and the A_2 symmetry HOMO. Figure 2.17 illustrates how the $2A_1$ and $1B_1$ orbitals mix upon bending to hybridize the metal contribution such that it maintains a strong bonding interaction with the NO π* orbital. Figure 2.18 depicts the way nitrosyl bending causes mixing of nitrogen and oxygen p_z character to enhance the bonding interaction of the metal and the nitrosyl. In addition, upon tilting the d_{xz} component maintains a favorable interaction with the porphyrin π system. Richter-Addo and coworkers have provided tables of selected comparisons for axial bonding parameters for several $\{MNO\}^6$ and $\{MNO\}^7$ metalloporphyrins as well as for IR stretching frequencies for $\{FeNO\}^6$ and $\{RuNO\}^6$ complexes. Results of Mossbauer spectroscopic investigations suggest

that bending can be expected when strong σ donors are trans to the nitrosyl group. Stong σ donors trans to the nitrosyl group automatically stabilize the M^{III} state, hence the assignment $[M^{III}NO^{\bullet}]$. Extended Huckel calculations show that bending to bisect an N_p-Fe-N_p angle is energetically favorable to eclipse an Fe-N_p bond. These results suggest that the convention that assumes a linear MNO linkage for ferric nitrosyl hemes needs to be changed to account for the low energy bending and axial tilting exhibited by these unprecedented strongly bent $\{FeNO\}^6$ complexes.

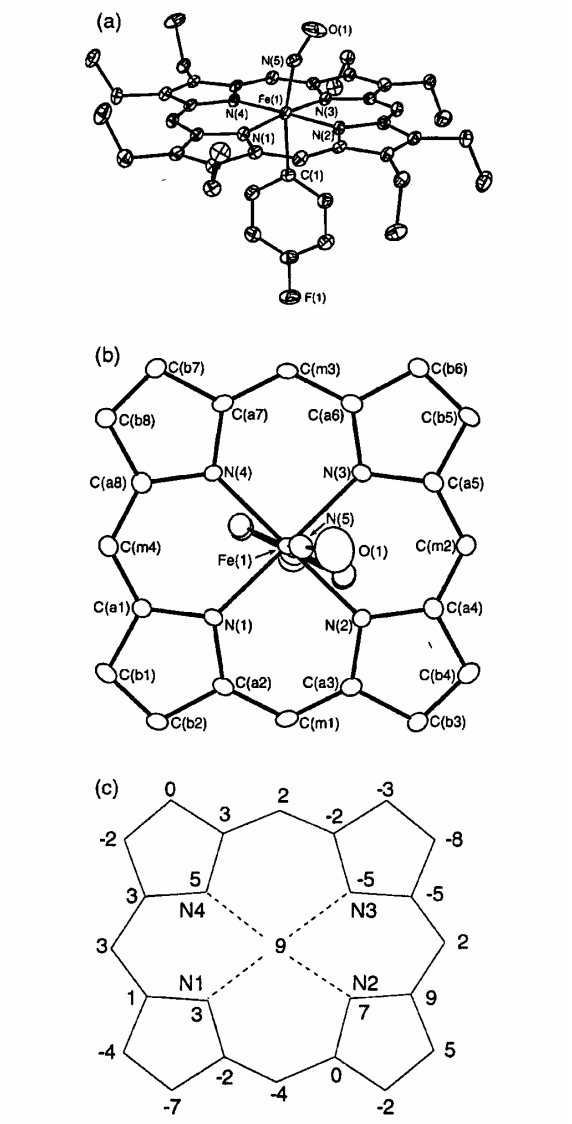

Figure 2.13 – Molecular Structure of (OEP)Fe(NO)(*p*-C_6H_4F)
(a) Molecular structure of (OEP)Fe(NO)(*p*-C_6H_4F). Hydrogen atoms have been omitted for clarity. (b) Top view (perpendicular to the porphyrin plane) showing the orientation of the axial groups with respect to the porphyrin skeleton. (c) Perpendicular atom displacements from the 24-atom porphyrin plane (in 0.01 Å units). (Reprinted with permission from *J. Am. Chem. Soc*. **2001**, *123*, 6314-6326. Copyright 2001, American Chemical Society. 85)

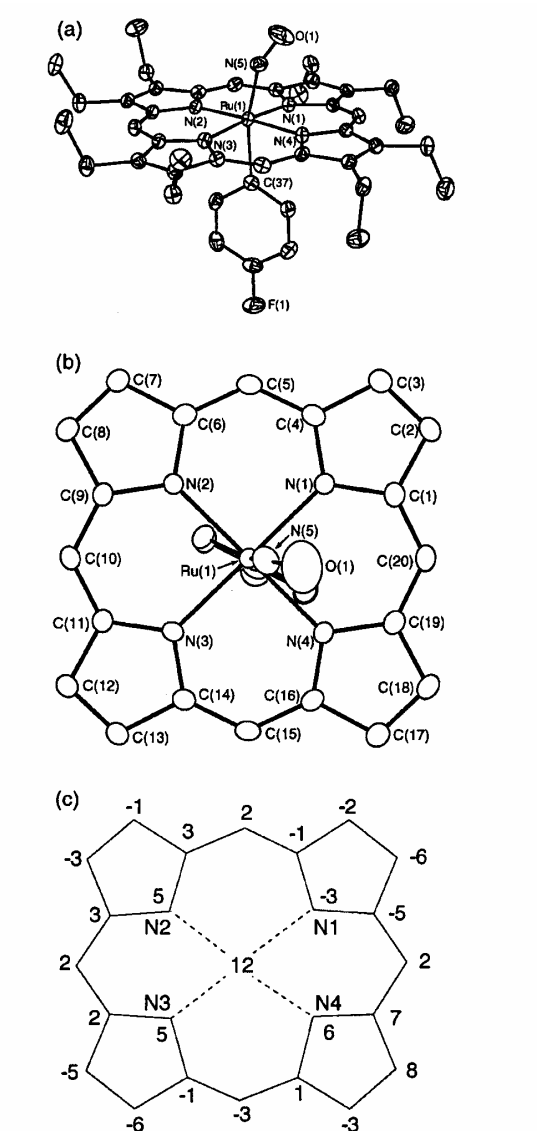

Figure 2.14 – Molecular Structure of (OEP)Ru(NO)(*p*-C_6H_4F)
(a) Molecular structure of (OEP)Ru(NO)(*p*-C_6H_4F). Hydrogen atoms have been omitted for clarity. (b) Top view (perpendicular to the porphyrin plane) showing the orientation of the axial groups with respect to the porphyrin skeleton. (c) Perpendicular atom displacements from the 24-atom porphyrin plane (in 0.01 Å units). (Reprinted with permission *J. Am. Chem. Soc*. **2001**, *123*, 6314-6326. Copyright 2001 American Chemical Society. 85)

Table 2.3 – Selected Bond Lengths and Angles for (OEP)M(p-C_6H_4F) M = Ru, Fe
(Reprinted with permission from *J. Am. Chem. Soc.* **2001**, *123*, 6314-6326, Copyright 2001, American Chemical Society. 85)

Bond Lengths (Å)

(OEP)Fe(NO)(p-C_6H_4F)		(OEP)Ru(NO)(p-C_6H_4F)	
Fe(1)−N(1)	2.001(2)	Ru(1)−N(3)	2.052(3)
Fe(1)−N(2)	2.024(2)	Ru(1)−N(4)	2.059(3)
Fe(1)−N(3)	2.023(2)	Ru(1)−N(1)	2.068(3)
Fe(1)−N(4)	2.015(2)	Ru(1)−N(2)	2.056(3)
Fe(1)−N(5)	1.728(2)	Ru(1)−N(5)	1.807(3)
N(5)−O(1)	1.153(3)	N(5)−O(1)	1.146(4)
Fe(1)−C(1)	2.040(3)	Ru(1)−C(37)	2.111(3)

Bond Angles (deg)

(OEP)Fe(NO)(p-C_6H_4F)		(OEP)Ru(NO)(p-C_6H_4F)	
Fe(1)−N(5)−O(1)	157.4(2)	Ru(1)−N(5)−O(1)	154.9(3)
C(1)−Fe(1)−N(5)	168.85(11)	C(37)−Ru(1)−N(5)	166.59(13)
N(5)−Fe(1)−N(1)	98.56(10)	N(5)−Ru(1)−N(3)	99.07(12)
N(5)−Fe(1)−N(2)	84.43(10)	N(5)−Ru(1)−N(4)	83.47(13)
N(5)−Fe(1)−N(3)	87.09(10)	N(5)−Ru(1)−N(1)	86.67(12)
N(5)−Fe(1)−N(4)	97.24(10)	N(5)−Ru(1)−N(2)	99.74(13)
C(1)−Fe(1)−N(1)	87.83(10)	C(37)−Ru(1)−N(3)	87.92(11)
C(1)−Fe(1)−N(2)	86.43(10)	C(37)−Ru(1)−N(4)	85.09(12)
C(1)−Fe(1)−N(3)	86.51(9)	C(37)−Ru(1)−N(1)	86.35(11)
C(1)−Fe(1)−N(4)	91.89(10)	C(37)−Ru(1)−N(2)	91.70(12)

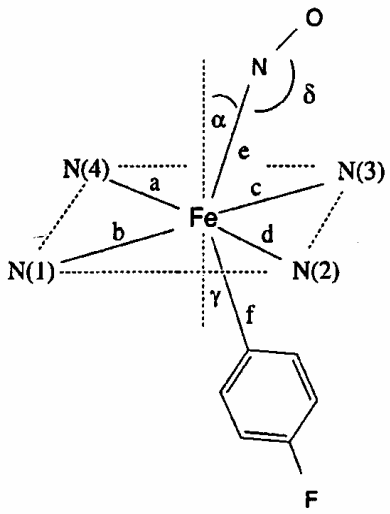

a = 1.964 (2.015)	α = 11.3 (8.6)
b = 1.964 (2.001)	δ = 150.4 (157.4)
c = 2.002 (2.023)	γ = 4.4 (2.8)
d = 2.002 (2.024)	Δ = 0.08 (0.065)
e = 1.666 (1.728)	
f = 1.968 (2.040)	

Figure 2.15 – Selected Geometrical Parameters for (porph)Fe(NO)(*p*-C_6H_4F)
Selected geometrical parameters (in Å and °) calculated by using the B3LYP hybrid Hartree-Fock/density functional method, compared with corresponding parameters for (OEP)Fe(NO)(*p*-C_6H_4F), determined by X-ray diffraction (in parentheses). The tilting angles and atom displacement (Δ) are with respect to the four nitrogen porphyrin plane. (Reprinted with permission from *J. Am. Chem. Soc*. **2001**, *123*, 6314-6326. Copyright 2001, American Chemical Society. 85)

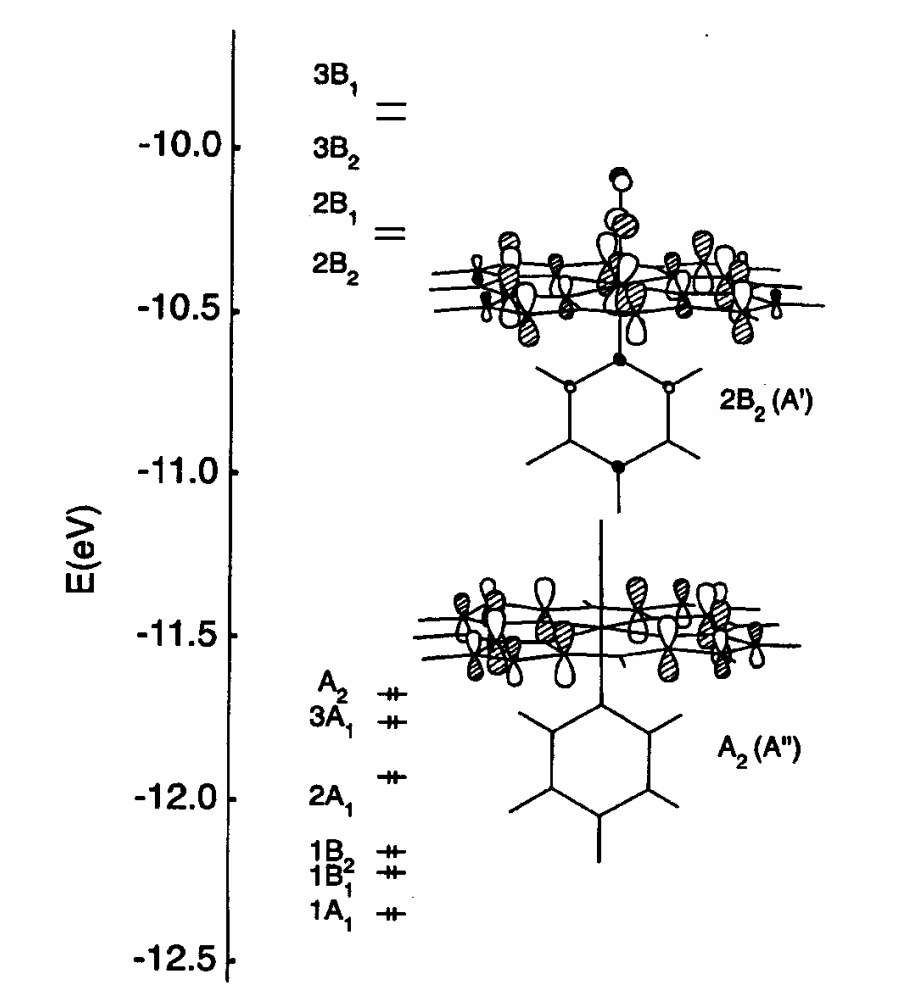

Figure 2.16 – Molecular Orbital Diagram of (porph)Fe(NO)(*p*-C_6H_4F)
Molecular orbital energy level diagram of (porph)Fe(NO)(*p*-C_6H_4F) The B_2 symmetry LUMO and the A_2 symmetry HOMO are also shown. (Reprinted with permission from *J. Am. Chem. Soc*. **2001**, *123*, 6314-6326. Copyright 2001, American Chemical Society. 85)

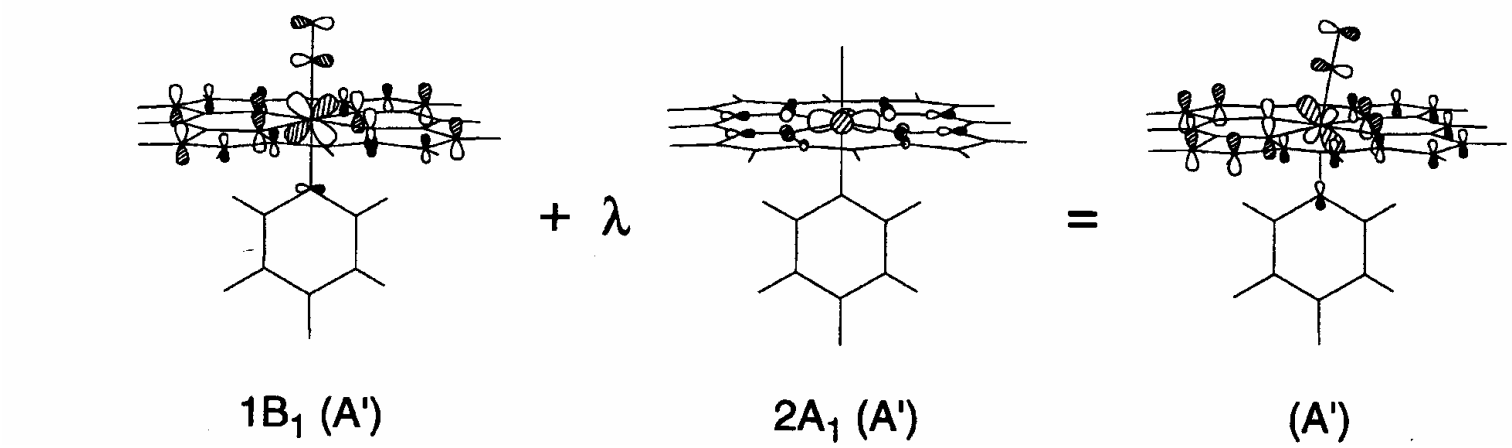

Figure 2.17 – Orbitals $1B_1$ and $2A_1$
Orbitals $1B_1$ and $2A_1$ mix upon tilting axial ligands to give the orbital shown on the right. (Reprinted with permission from *J. Am. Chem. Soc*. **2001**, *123*, 6314-6326. Copyright 2001, American Chemical Society. 85)

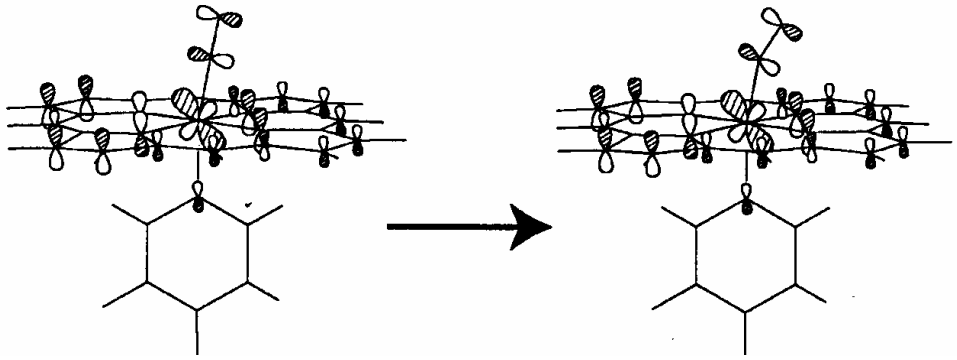

Figure 2.18 – Bending of the Nitrosyl Ligand
Bending the nitrosyl ligand mixes nitrogen (and oxygen) P_z character into the orbital shown on the left to better aligns the nodes on the NO π* and metal d orbitals, as shown on the right. (Reprinted with permission from *J. Am. Chem. Soc.* **2001**, *123*, 6314-6326. Copyright 2001 American Chemical Society. 85)

Metalloporphyrin nitrosyl complexes also exhibit linkage isomerization. While the nitrosyl group usually binds η^1 through the nitrogen atom, it has been observed to bind via the oxygen atom. The first low temperature infrared spectroscopic evidence for photo-induced metastable η^1-O and η^2-NO linkage isomers of the group 8 $\{MNO\}^6$ (linear) nitrosyl metalloporphyrins, [(OEP)Ru(NO)(L)], (L = O-iC_5H_{11}, SCH_2CF_3, Cl) and $[(OEP)Ru(NO)(py)]^+$ was reported by Coppens, et al.[88] Coppens and co-workers later reported the first spectroscopic and theoretical evidence of linkage isomerism for bent MNO. The five coordinate $\{MNO\}^7$ iron nitrosyl porphyrins, [Fe(OEP)(NO)] and [Fe(TPP)NO] produce [Fe(OEP)(η^1-ON)] and [Fe(TTP)(η^1-ON)] as low-temperature photoproducts[89] Ground state optimization of [Fe(OEP)NO] by Bagley et al.[89] reproduced the structural distortions reported by Scheidt and co-workers[81,85] and previously discussed in this thesis.

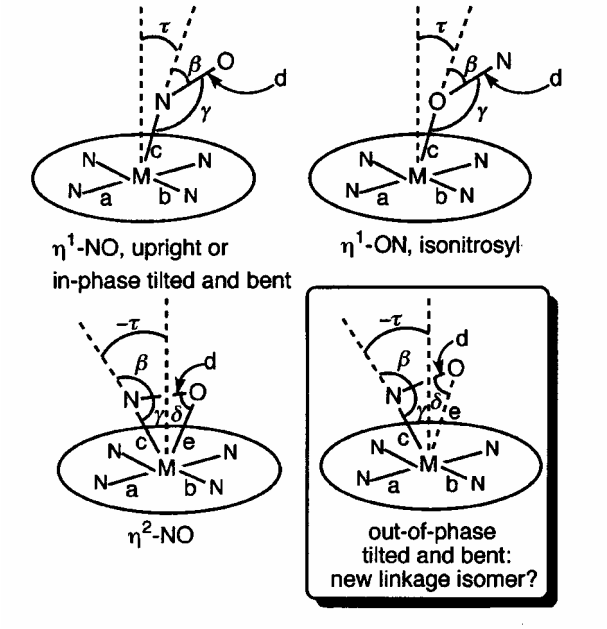

Figure 2.19 – NO Linkage Isomers
(Reprinted with permission from *J. Am. Chem. Soc.* **2001**, *123*, 5680-5683. Copyright 2001 American Chemical Society. 88)

Wondimagegn and Ghosh[90] completed a quantum chemical survey of the η^1-ON, η^1-NO, η^2-NO linkage isomers as well as of the structural distortions induced by tilting of the MNO bond in conjunction with bending of the MNO group observed by Scheidt. Figure 2.19[90] illustrates the various linkage isomers and the out of phase tilted and bent isomer observed by Scheidt and co-workers.[85] Density functional theory (DFT) calculations were completed for [M(P)(NO)] (M = Mn, Fe, Ru, Co, Rh), $[M(P)(NO)]^+$ (M = Fe, Ru), $[M(P)(N)(imidazole)]^+$ (M = Fe, Ru) and [M(P)(NO)(L)] (M = Fe, Ru; L = Cl, Ph, SCH_3).[90] Table 2.4 shows the relative energies of the η^1-ON, η^1-NO, η^2-NO linkage isomers. The global minimum for each complex was calculated to be the η^1-NO isomer. The η^1-ON isomer exists at 1.06-1.47 eV higher in energy than the η^1-NO isomer, therefore, η^1-ON isomer, formed by photoexcitation processes, is expected to be metastable at 77 K or lower, and to return to the η^1-NO form upon warming. Isonitrosyl complexes Fe(TTP)(η^1-ON) and Fe(OEP)(η^1-ON) were also observed as low temperature photoproducts.[89] While optimized η^1-ON isomers were obtained for all complexes by Wondimagegn and Ghosh (Table 2.4[90]), the η^2 linkage isomers were theoretically established only for Mn(P)(NO), $[Fe(P)(NO)]^+$, Ru((P)(NO)Cl, $[Ru(P)(NO)(L)]^+$ (L = no ligand, imidazole, and pyridine). These calculated results are consistent with the experimental observations of Coppens and co-workers.[88] The implication is that an $\{MNO\}^6$ electron count contributes to the stabilization of η^2 coordinated nitrosyl groups. This same conclusion has been drawn by Coppens et al. with respect to photo-induced metastable linkage isomers of nonporphyrin transition metal complexes.[91] Wondimagegn and Ghosh explain, that the LUMO of $[Fe(P)(NO)]^+$, depicted in Figure 2.20,[90] is both bonding and antibonding with respect to the metal d_z^2-NO(π^*) interaction. Upon addition of an electron to this molecular orbital, as in

Table 2.4 – Energetics (eV) of Different Metalloporphyrin-NO Linkage Isomers
Energetics (eV) of Different Metalloporphyrin-NO Linkage Isomers[a,b] (Reprinted with permission from *J. Am. Chem. Soc.* **2001**, *123*, 5680-5683. Copyright 2001 American Chemical Society. 88)

Energetics (eV) of Different Metalloporphyrin−NO Linkage Isomers[a,b]

formula	M(η^1-NO) in-phase/upright	M(η^1-NO) out-of-phase[c]	M(η^1-ON)	M(η^2-NO)
{MNO}^{6}				
Mn(P)(NO)	0.0000	NI	1.9016	1.6698
[Fe^{III}(P)(NO)]$^+$	0.0000	NI	1.7505	1.4609
[Fe^{III}(P)(NO)(Cl)]	0.0000	1.1998	NI	OU
[Fe^{III}(P)(NO)(SCH$_3$)]	0.0000	1.0560	NI	OU
[Fe^{III}(P)(NO)(Im)]$^+$	0.0000	1.3364	NI	OU
[Fe^{III}(P)(NO)(Ph)]	0.0000	0.9049	NI	OU
[Ru^{III}(P)(NO)]$^+$	0.0000	NI	2.0168	1.4989
[Ru^{III}(P)(NO)(Cl)]	0.0000	NI	NI	1.2343
[Ru^{III}(P)(NO)(SCH$_3$)]	0.0000	1.0756	NI	OU
[Ru^{III}(P)(NO)(Im)]$^+$	0.0000	NI	NI	1.5453
[Ru^{III}(P)(NO)(Ph)]	0.0000	0.8191	NI	OU
{MNO}^{7}				
Fe(P)(NO)	0.0000	–	1.5070	OU
Ru(P)(NO)	0.0000	–	1.3062	OU
{MNO}^{8}				
Co(P)(NO)	0.0000	–	1.1980	OU
Rh(P)(NO)	0.0000	–	1.6708	OU

[a] OU = opened up. [b] NI = not investigated. [c] The out-of-phase tilted and bent forms were not specifically searched for. They are reported only when approximate M(η^2-NO) starting geometries partially opened up to the out-of-phase tilted and bent forms.

[Fe(P)(NO)]^0 the MNO unit will open to maintain only the bonding dz^2 – NO(π^*) interaction. Hence, attempts to optimize [Fe(P)(η^2-NO)(L)]^0 (L = Cl, Ph, SCH_3), [Fe(P)(η^2-NO)(imidazole)]$^+$, and [Ru(P)(η^2-NO)(L)] (L = Ph, SCH_3) yielded partially ring-opened MNO geometries with MN(O) and NO vectors oriented in opposite directions with respect to the heme normal. This result is pertinent to results obtained from a high resolution X-ray crystallographic analysis[92] of nitrophorin 4, a nitric oxide binding heme protein discovered in the blood sucking insect *Rhodnius prolixus*. Montfort and co-workers observed two distinct NO conformations, one with a relatively upright orientation and another in which the FeN(O) and NO vectors were tilted in opposite directions with respect to the heme normal. The authors suggest that this unusual out-of phase tilted and bent orientation, shown in Figure 2.20[90,93] may correspond

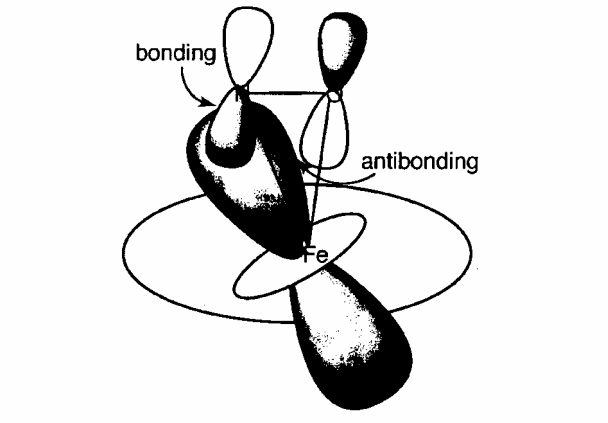

Figure 2.20 – The $[Fe(P)(NO)]^+$ LUMO is Bonding and Antibonding
(Reprinted with permission from *J. Am. Chem. Soc*., **2001**, *123*, 5680-5683. Copyright 2001 American Chemical Society. 88)

to a loosely bound or to an η^2-NO. The theoretical calculations and experimental evidence indicate that the "out of phase titled and bent FeNO geometries do correspond to true local minima on the potential energy surfaces of these molecules."[90] Thus, the in phase titled and bent geometries and the out-of-phase tilted and bent geometries may represent examples of "bond angle isomerism."[90] The $\{MNO\}^7$ and $\{MNO\}^8$ η^2-NO complexes open upon optimization to give only in phase titled and bent η^1 geometries.

Morishima et al.[94] have conducted model studies of dissimilatory nitrite reductase, which catalyzes single-electron reduction of nitrite, mostly to nitric oxide, and under appropriate conditions to nitrous oxide. There have been attempts, some successful, to mimic the function of metalloenzymes, such as nitrate reductase, by incorporating iron porphyrins into polymeric films.[95-98] The ultimate goal is to utilize electropolymerized metalloporphyrins as electrode materials for chemical and biological sensors. Nitrite reductase comprises two subunits which contain hemes *c* and d_1. Heme d_1 is the preferential binding and catalytic site of nitrite

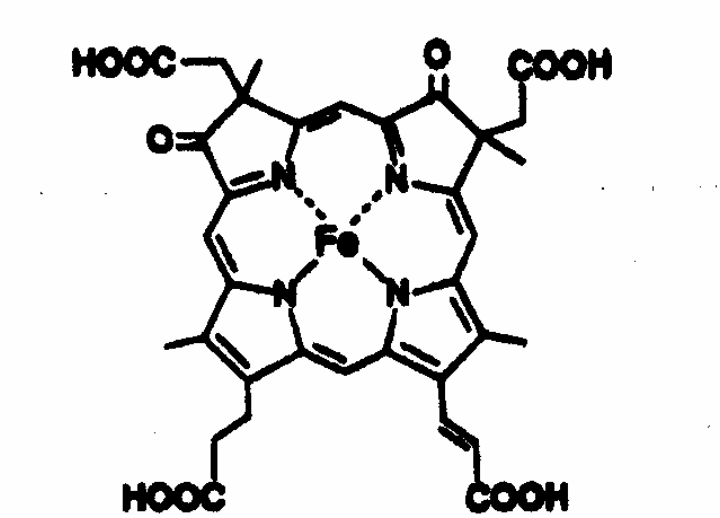

Figure 2.21 – Proposed Structure for Dioxobacteriochlorin (heme d_1)
(Reprinted with permission from *Inorg. Chem*., 1995, 34, 6362-6370. Copyright 1995 American Chemical Society. 92)

reductase. A proposed structure for Heme d_1 is that of iron dioxoisobacteriochlorin, illustrated in Figure 2.21.[94]

An $[Fe(NO)]^+$ nitrosyl complex has been proposed by Kim and Hollocher [99]to form as an intermediate via dehydration of NO_2^- to NO during the reduction cycle (Figure 2.22) by dissimilatory nitrite reductase. The $[Fe(NO)]^+$, produced in the proposed catalytic cycle, has three possible valence isomers, the paramagnetic [Fe^{II}(NO) π-cation radical], and the diamagnetic isomers, [Fe^{III}(NO)], and [$Fe^{II}(NO^+)$]. Clearly, the electronic configuration of $[Fe(NO)]^+$ plays a crucial role in the reduction of NO_2^- to NO. Morishima et al.[100] initially prepared Fe^{II}(NO) cation radical complexes via oxidation of oxooctaethylchlorin (oxo-OEC) and 2,3,7,8-dioxooctaethylisobacteriochlorin (dioxo-OEiBC) in order to learn more about the

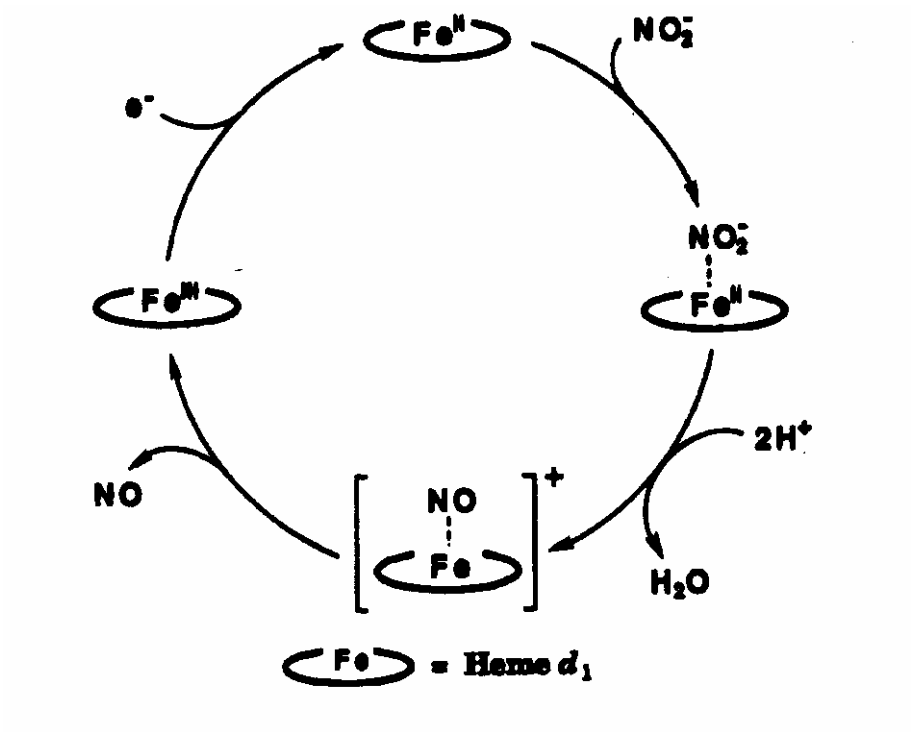

Figure 2.22 – Proposed Dissimilatory Nitrite Reductase Catalytic Cycle
(Reprinted with permission from *Inorg. Chem*., 1995, 34, 6362-6370. Copyright 1995 American Chemical Society. 92)

character of $[Fe(NO)]^{+}$. In a follow-up study, Morishima and co-workers[94] reported that the one-electron oxidation of $(OEP)Fe^{II}(NO)$, $(oxo\text{-}OEC)Fe^{II}(NO)$ and $(dioxo\text{-}OeiBC)Fe^{II}$ (NO), illustrated in Figure 2.23[94] form formally $[Fe(NO)]^{+}$ oxidation products. Electronic absorption, ESR, NMR and IR spectroscopies reveal that the one-electron oxidation product of $(oxo\text{-}OEC)Fe^{II}(NO)$ and $(dioxo\text{-}OeiBC)Fe^{II}(NO)$ is the π–cation radical, which exhibits a bent FeNO moiety, while the one-electron oxidation product of $(OEP)Fe^{II}(NO)$ is an $Fe^{III}(NO)$ complex with a nearly linear Fe-NO unit. In the same investigation, it was found that valence isomerization which occurs upon ligation of *N*-methyl imidazole to the cation radicals, $[(oxo\text{-}OEC^{+})Fe^{II}(NO)]$

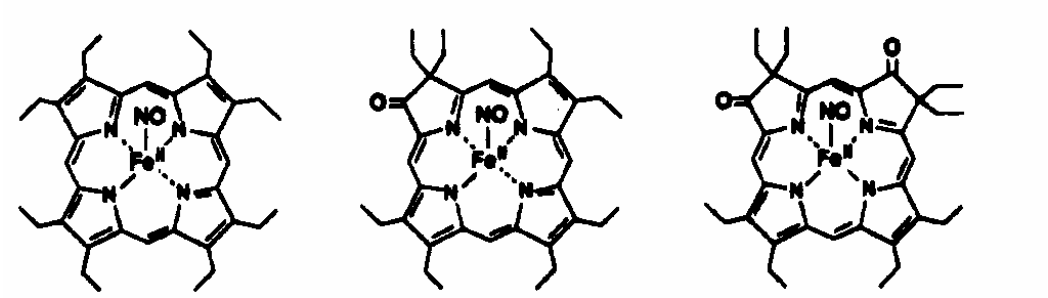

Figure 2.23 – [(OEP)Fe^{II}(NO)]$^+$, [(oxo-OEC)Fe^{II}(NO)]$^+$, [(dioxo-OeiBC)Fe^{II}(NO)]$^+$
(Reprinted with permission from *Inorg. Chem*., **1995**, *34*, 6362-6370. Copyright 1995 American Chemical Society. 92)

and [(dioxo-OeiBC$^+$)Fe^{II}(NO)], yields the respective Fe^{II}(NO^+)(*N*-MeIm) complexes which readily release NO in the presence of additional *N*-MeIm. The possible structures for the valence isomers are illustrated in Figure 2.24. Morishima et al.[94] link the facile release of NO from (oxo-OEC)Fe^{II}(NO^+) and (dioxo-OeiBC) Fe^{II} (NO^+) in the presence of *N*-MeIm to the presence of oxo groups, on the porphyrin ring, which increase the positive charge on iron and deplete the extent of Fe(dπ)-NO(π*) backbonding. The (OEP)Fe^{II}(NO) derivative lacks oxo groups, thus requires almost four moles of *N*-MeIm for complete formation of the

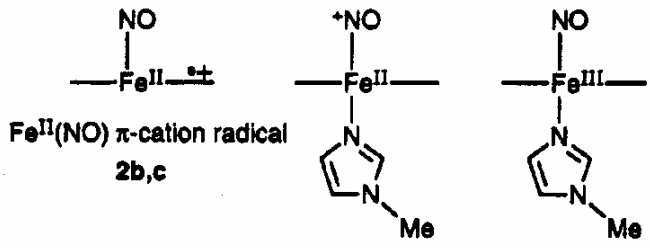

Figure 2.24 – Valence Isomerization Upon Addition of N-Methyl Imidazole
(Reprinted with permission from *Inorg. Chem.*, **1995**, *34*, 6362-6370. Copyright 1995 American Chemical Society. 92)

corresponding iron(III)bis(imidazole) complex. Morishima et al. suggest that the NO bound heme d_1 in nitrite reductase forms the intermediate $Fe^{II}(NO^+)(L)$. The ready release of NO in the reaction with *N*-MeIm suggests ligation of a distal histidine or a nucleophilic amino acid residue to initiate NO release in the enzyme. In fact tyrosine in the distal pocket has been shown to ligate to heme d_1.[101] Morishima et al. also conclude that it is likely that the presence of the oxo groups on heme d_1 influence NO release from the $[Fe^{II}NO^+]$ intermediate and influence the redox properties of the metal center thus facilitate use of heme d_1 in dissimilatory nitrite reductases.

Ryan and Liu[102] used pulse polarography and cyclic voltammetry[103] to investigate the kinetics for the reduction of iron porphyrin nitrosyls to ammonia by assimilatory nitrite reductases using the following model complexes: Fe(TTP)(NO), Fe(OEP)(NO), Fe(2,4-DMOEiBC)(NO), (2,4-DMOEiBC=2,4-methyloctaethylisobacteriochlorin), Fe(oxo-OEC)(NO) and Fe(MOEC)(NO) (MOEC = methyloctaethylchlorin). The siroheme model complex Fe(2,4-DMOEiBC)(NO) exhibited the most facile formation of $Fe(P)(NH_2O^+)$; the dissimilatory nitrate reductase model complex Fe(2,4-dioxo-OEiBC)(NO) formed the intermediate $Fe(P)(NH_2O^+)$ least readily. In non-aqueous solvents and in the presence of weak acids NH_2O^+ is released as NH_2OH. NH_2OH is reduced to NH_3 is the presence of iron porphyrins. The authors conclude that the macrocycle influences the rate at which NO is reduced to NH_3.

Chen and Ikeda[104] reported that $[Fe^{III}(TMPyP)]^{5+}$ (TMPyP = *meso*-tetra(*N*-methyl-4-pyridyl) porphyrin) catalyzes the oxidation of NO to NO_2^- in a phosphate buffer solution at pH = 7.4 at a current that is ten times higher than that for Fe^{III} phosphate in solution without the porphyrin. This current is large enough to be useful in a chemical sensor that can be used in oxygen containing physiological environments because oxygen is electroinactive at positive potentials. The oxidation-reduction mechanism in Figure 2.25[104] was proposed.

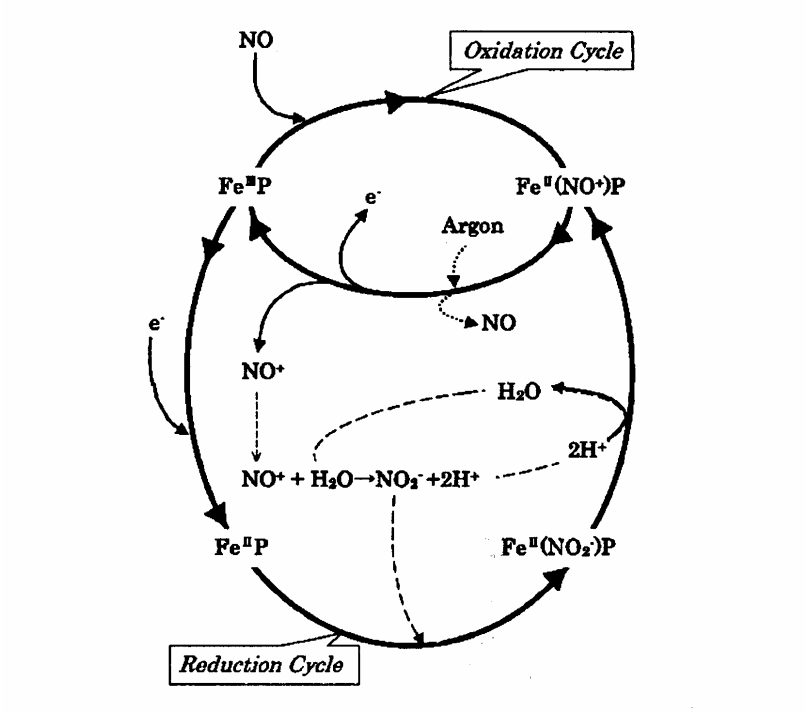

Figure 2.25 – The Oxidation-Reduction Mechanism of NO with [Fe(TMPyP)]$^{5+}$
The oxidation-reduction mechanism of NO with water soluble iron porphyrin, [Fe(TMPyP)]$^{5+}$ (Reprinted with permission from *Electroanalysis*, **2001**, *13*, 1076-1081. Copyright 2001 John H. Wiley and Sons, Inc. 102)

2.3. METALLOPORPHYRIN RELATED IRON NITROSYL COMPLEXES

Because NO binds Fe^{II} porphyrins for the activation of guanylate cyclase and in equilibria related to biological clearance pathways, it is important to understand how the bonding interaction between Fe(II) porphyrins and NO differs from that between Fe(II) porphyrins and CO or O_2. Since the unsaturated macrocyclic water soluble Fe^{II} complex , $[Fe(TIM)(CH_3CN)_2(PF_6)_2]$ (TIM = 2,3,9,10-tetramethyl-1,4,8,11-tetraazacyclodeca-1,3,8,10-tetraene) satisfies some of the criteria as a possible NO scavenger,[105] Shepherd and Chen[106] presented a comparison between how NO, CO and O_2 bind to the macrocyclic TIM complex and to a porphyrin complex**.** Their paper also reports the reversible coordination of NO to $[Fe(TIM)(CH_3CN)_2]$,$^{2+}$ its characterization as a six coordinate nitrosyl, similar to Fe^{II} porphyrin nitrosyls in its EPR behavior, and its differing stability in CH_3CN, CH_3CN/CH_3OH, CD_3OD and D_2O.

The equilibrium described in figure 2.26 was established by exposing a solution of $[Fe(TIM)(CH_3CN)_2(PF_6)_2]$ (ca. 3×10^{-3} M) in Ar purged CH_3CN, to nitric oxide gas for twenty minutes. Spectral data (λ = 390 nm, $\varepsilon = 1.59 \times 10^3$ M^{-1} cm^{-1}) reveal that 53 % of the initial $[Fe(TIM)(CH_3CN)_2(PF_6)_2]$ was converted to the nitrosyl adduct. Assuming a first order dissociation of NO, in CH_3CN $[Fe(TIM)(CH_3CN)(NO)]^{2+}$ exhibits a dissociation rate constant of $k_d = 3.85 \times 10^{-3}$ s^{-1} by N_2 purging. The EPR spectrum of $[Fe(TIM)(CH_3CN)_2(NO)]^{2+}$, obtained in 60 % CH_3OH/40 % CH_3CN at 77K, and shown in figure 2.27, exhibited three features with g = 2.01, 1.99 and 1.97, indicative of an S = ½ $\{FeNO\}^7$ complex. Only the center line near g = 2 exhibited N-*shf* (*shf* – super hyperfine) structure indicating the presence of only one coordinated NO ligand. This behavior is similar to that of the heme nitrosyl complexes in which the heme macrocycle produces strong field NO complexes of S = ½**.**[107-109] Hemoglobin and myoglobin nitrosyls exhibit splitting of the middle or third component of the g features near g = 2.[110,111]

Splitting of the middle feature by N-*shf* indicates a six-coordinate low-spin Fe^{II} nitrosyl;[107,109] splitting of the third component indicates a five-coordinate low-spin Fe^{II} nitrosyl. Thus, the Fe(TIM) complex must have either an axial CH_3CN or CH_3OH, since the middle line exhibits N-*shf* structure.

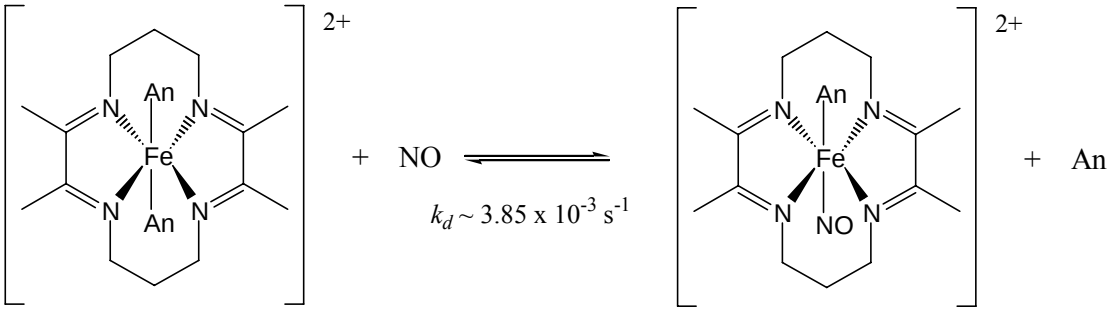

Figure 2.26 – $[Fe(TIM)(CH_3CN)_2]^{2+}$ and $[Fe(TIM)(CH_3CN)(NO)]^{2+}$
(Reprinted from *Inorg. Chim. Acta*, 260, Ya Chen, Michael A. Sweetland and Rex E. Shepherd*, "A reversible NO complex of Fe^{II}(TIM): an S = ½ $\{FeNO\}^7$ nitrosyl", 163-172, Copyright 1997, with permission from Elsevier. 104)

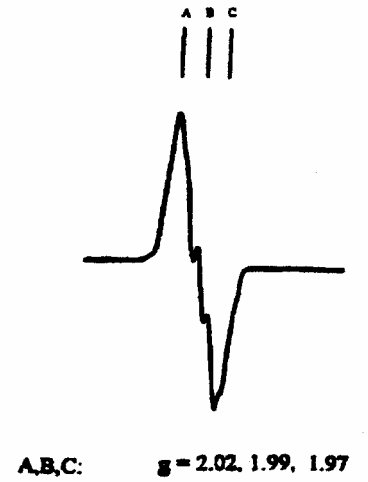

Figure 2.27 – EPR Spectrum of $[Fe(TIM)(CH_3CN)_2(NO)]^{2+}$
(Reprinted from *Inorg. Chim. Acta*, 260, Ya Chen, Michael A. Sweetland and Rex E. Shepherd*, "A reversible NO complex of Fe^{II}(TIM): an S = ½ $\{FeNO\}^7$ nitrosyl", 163-172, Copyright 1997, with permission from Elsevier. 104)

Previous studies[106] have shown that the use of mixed solvents lowers the activity of CH_3CN and favors the addition of nitrogen base donors. When a sample of $[Fe(TIM)(CH_3CN)_2(PF_6)_2]$ was prepared in 60% CH_3OH/40% CH_3CN (vol./vol.) the amount of coordinated NO increased from 53.1% (100% CH_3CN) to 80.7%. The band in the visible spectrum representing the nitrosyl complex occurred at 390 nm as it did in CH_3CN, this time with an extinction coefficient of 2.19×10^3 M^{-1} cm^{-1}.

The electronic spectrum changes when axial CH_3CN ligands are replaced with H_2O or CH_3OH. The extent of CH_3CN dissociation from $[Fe^{II}(TIM)]^{2+}$ in H_2O is concentration dependent as shown in Figure 2.28. At 3.06×10^{-4} M in a 1.00 cm cell Spectrum A in Figure 2.28 exhibits a major peak at 646 nm and a shoulder at 575 nm. Spectrum B in Figure 2.28 is that of more concentrated 3.06×10^{-3} M solution which shifts the equilibrium described in the equation below to the right in response to the higher concentration of liberated CH_3CN.

$$[Fe(TIM)(H_2O)_2]^{2+} + CH_3CN \overset{K_{CH_3CN}}{\rightleftharpoons} [Fe(TIM)(CH_3CN)(H_2O)]^{2+}$$

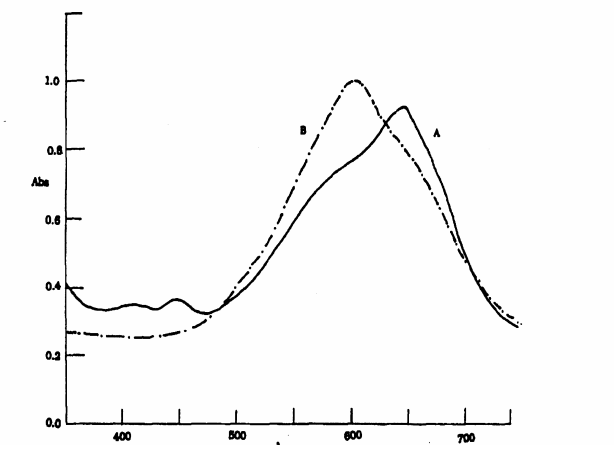

Figure 2.28 – Visible Spectrum of $[Fe(TIM)(CH_3CN)_2](PF_6)_2$ in H_2O
(Reprinted from Inorg. Chim. Acta, 260, Ya Chen, Michael A. Sweetland and Rex E. Shepherd*, "A reversible NO complex of Fe^{II}(TIM): an S = ½ $\{FeNO\}^7$ nitrosyl", 163-172, Copyright 1997, with permission from Elsevier. 104)

^{1}H NMR studies verified the existence of a stable $[Fe(TIM)(CH_3CN)(H_2O)]^{2+}$ complex in the presence of sufficient CH_3CN. If there is an insufficient concentration of CH_3CN to completely form the mono CH_3CN adduct, the $[Fe(TIM)(H_2O)_2]^{2+}$ complex slowly decomposes under Ar at room temperature as shown by Figure 2.29, as well as by ^{1}H NMR studies. ^{1}H NMR data also revealed that decomposition of the $[Fe(TIM)(H_2O)_2]^{2+}$ complex was strongly retarded by the presence of an axial π-acceptor ligand, such as NO, CO, or CH_3CN, trans to H_2O. That the $[Fe(TIM)(CH_3CN)(NO)]^{2+}$ complex forms more slowly than does $[Fe(TIM)(CH_3CN)(H_2O)]^{2+}$ complex, implies that NO adds on a displacement of H_2O in the mono acetonitrile product. Purging experiments to establish reversibility in H_2O were complicated by an O_2/NO reaction in which trace NO_2 forms and rapidly oxidizes $[Fe^{II}(TIM)]^{2+}$ thus rendering the starting spectrum A in figure 2.30 unrecoverable with N_2 purging. However, some of the $[Fe(TIM)(CH_3CN)(H_2O)]^{2+}$ regenerates in the presence of sufficient CH_3CN. Assuming a first-order dissociation of NO, a dissociation rate constant in CH_3CN, where reversibility occurs, was calculated from the time required for complete removal of NO from the $[Fe(TIM)(CH_3CN)(NO)]^{2+}$ by N_2 purging to be $k_d = 3.85 \times 10^{-3}\ s^{-1}$. NO dissociation from $[Fe(TIM)(H_2O)NO]^{2+}$ via Ar or N_2 purging was complicated by oxidation pathways previously described. In addition, the subsequent decomposition steps for $[Fe(TIM)(H_2O)_2]^{2+}$, shown in Figure 2.31, occur more rapidly than does NO dissociation; thus, decomposition products, rather than $[Fe(TIM)(H_2O)_2]^{2+}$ are observed. Solubility and side reactions in H_2O limit the viability of $[Fe(TIM)(CH_3CN)_2(PF_6)_2]$ as an NO scavenger for the treatment of sepsis.

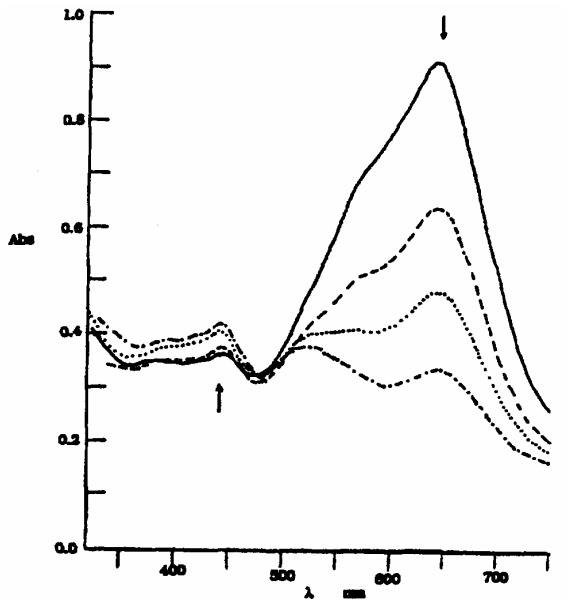

Figure 2.29 – $[Fe(TIM)(CH_3CN)_2](PF_6)_2$ Decomposition in H_2O
(Reprinted from *Inorg. Chim. Acta*, 260, Ya Chen, Michael A. Sweetland and Rex E. Shepherd*, "A reversible NO complex of Fe^{II}(TIM): an S = ½ $\{FeNO\}^7$ nitrosyl", 163-172, Copyright 1997, with permission from Elsevier. 104)

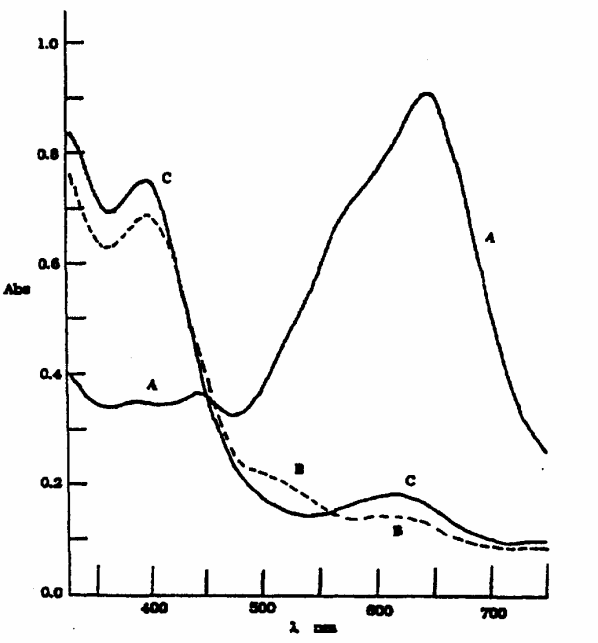

Figure 2.30 – Visible Spectrum of Reaction of $[Fe(TIM)(CH_3CN)_2](PF_6)_2$ with NO
(Reprinted from *Inorg. Chim. Acta*, 260, Ya Chen, Michael A. Sweetland and Rex E. Shepherd*, "A reversible NO complex of Fe^{II}(TIM): an S = ½ $\{FeNO\}^7$ nitrosyl", 163-172, Copyright 1997, with permission from Elsevier. 104)

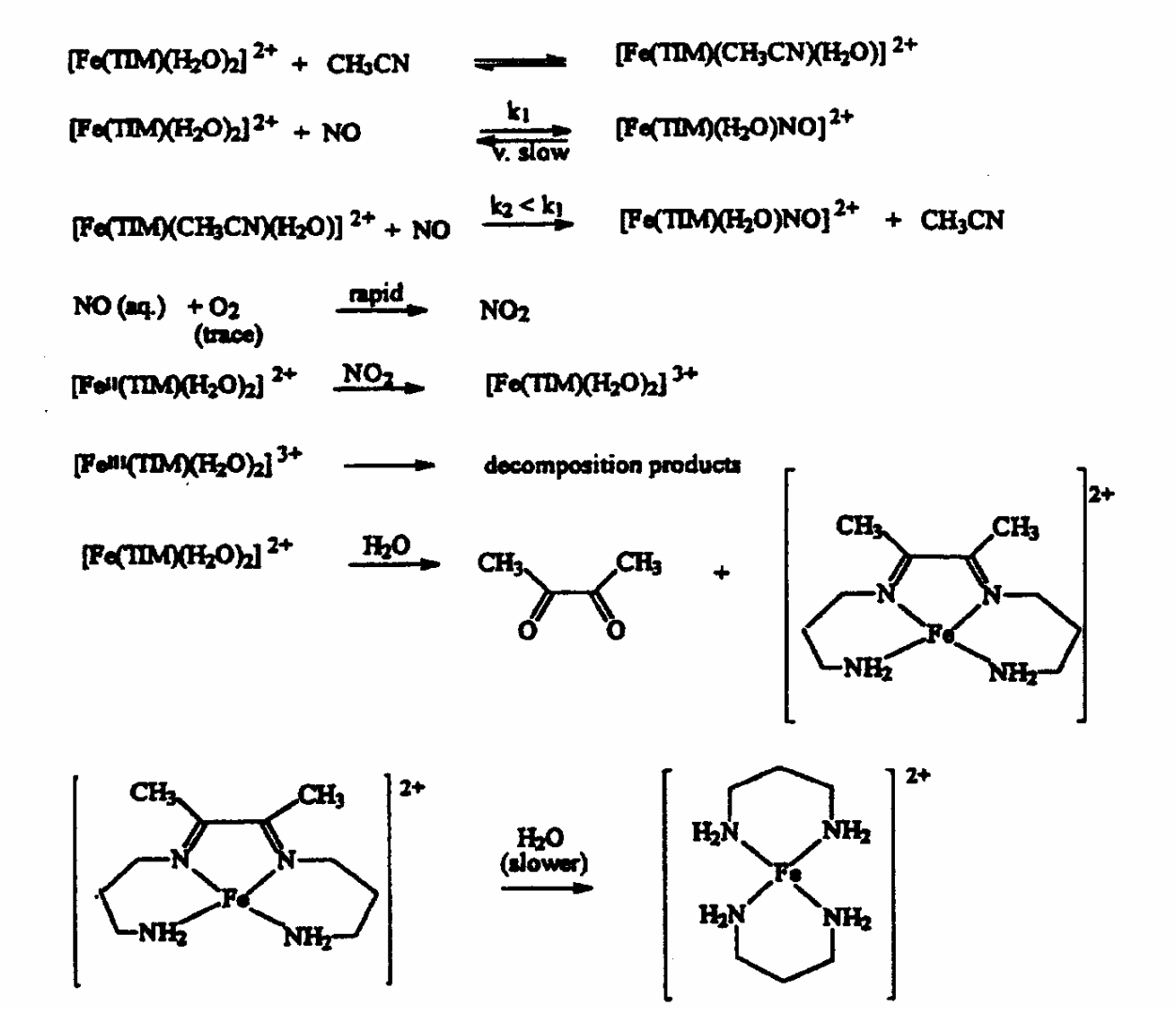

Figure 2.31 – Decompostion Pathways for $[Fe(TIM)CH_3CN)_2](PF_6)_2$ in H_2O
(Reprinted from *Inorg. Chim. Acta*, 260, Ya Chen, Michael A. Sweetland and Rex E. Shepherd*, "A reversible NO complex of Fe^{II}(TIM): an S = ½ $\{FeNO\}^7$ nitrosyl", 163-172, Copyright 1997, with permission from Elsevier. 104)

Table 2.5 – Estimated CO and NO Binding Constants
(Reprinted from *Inorg. Chim. Acta*, 260, Ya Chen, Michael A. Sweetland and Rex E. Shepherd*, "A reversible NO complex of Fe^{II}(TIM): an S = ½ $\{FeNO\}^7$ nitrosyl", 163-172, Copyright 1997, with permission from Elsevier. 104)

Estimates of binding constants for NO and CO with hemes, hemeproteins and $[Fe^{II}(TIM)]^{2+}$ [a]

Complex [b]	K_L (M^{-1})		K_{NO}/K_{CO}
	NO	CO	
Fe(PPIX)(MeIm)	5.8×10^{11}	7.8×10^{8}	740
Hb	2.5×10^{10}	2.3×10^{7}	1100
Mb	3.4×10^{11}	4.5×10^{7}	7500
$[Fe(TIM)(CH_3CN)]^{2+}$	80.1	1.73×10^{2}	0.46

[a] Hemes and hemoproteins in aqueous buffers, $[Fe(TIM)(CH_3CN)]^{2+}$ in CH_3CN.
[b] PPIX = protoporphyrin IX; Hb = hemoglobin; Mb = myoglobin.

The binding constants in Table 2.5[112-114] show that, in general, NO binds more strongly to Fe(II) porphyrins than does CO. Studies with model complexes have suggested that the linear Fe-CO bond causes peripheral globin and porphyrin interactions. Bent Fe-NO and Fe-O_2 moieties minimize these peripheral interactions. Therefore binding to NO or to O_2 is sterically favored over binding to CO for the porphyrins. Shepherd and Chen's[106] results reveal that, in contrast to Fe(II) porphyrin complexes, in CH_3CN, CO coordination is slightly favored over NO coordination to the Fe^{II} TIM macrocycle. The relative association constant K_{NO}/K_{CO} is ~ 0.46. As previously mentioned, peripheral interactions explain the K_{NO}/K_{CO} ratio (≥ 1100) for porphyrins in the presence of a trans axial base. For the TIM complex the absence of linear perturbations is expected to remove the hindrance component to CO coordination. Models reveal that the β-CH_2 units of the TIM ligand closely approach the axial position. Consequently, the bent S = ½ NO group, will interact more with the flexing CH_2 hydrogens than will a linear CO group. This idea is consistent with the observation that the $[Fe(TIM)(CH_3CN)NO]^{2+}$ complex will be relatively less stable than its CO analogue, opposite the case for the

[Fe^{II}(porphyrin)(base)NO] complexes compared to their CO analogues. With the $[Fe(TIM)]^{2+}$ system, removal of the hindrance to CO coordination along with incorporation of steric contacts for NO lowers K_{NO}/K_{CO} below one. It is reasonable that the formation constants K_{NO} and K_{CO} would be smaller for the $[Fe^{II}(TIM)(CH_3CN)]^{2+}$ species than for the related [Fe^{II}(heme)] as illustrated by the data in Table 2.5. Electrochemical data that show that $E'°$ for the methemoglobin/hemoglobin couple, at 0.17 V versus NHE,[115] is less than that for the $Fe^{II/III}$ couple for the $[Fe(TIM)(CH_3CN)_2]^{2+}$, at 0.83 V versus NHE; the Fe^{II} center is more stabilized by the TIM/CH_3CN environment than by the heme system. It follows that back donation from Fe^{II} to the TIM ligand in $[Fe(TIM)(CH_3CN)_2]^{2+}$ is greater than back donation from Fe^{II} to the anionic porphyrin in an [Fe^{II}(heme)] complex. The formation constants, K_{NO} and K_{CO}, are expected to be lower for the $[Fe^{II}(TIM)(CH_3CN)]^{2+}$ species than those for the related [Fe^{II}(heme)] species because stronger metal donation to the TIM ligand diminishes metal donation to the axial NO or CO ligand in the $[Fe^{II}(TIM)(CH_3CN)]^{2+}$ complex.

Given that, like the TIM ligand, quadridentate ligands based on thioalkylated isothiosemicarbazides also resemble biological complexes, Stavrov and Arion et al.[116] synthesized iron mononitrosyl complexes $[Fe(HL)NO]NO_3$ where H_3L = 2,4-pentanedione bis(*S*-methylisothiosemicarbazone) and $[Fe(R_2Q)NO]$, where R = CH_3, C_2H_5, *n*-C_3H_7, and *n*-C_4H_9. Figure 2.32 depicts $[Fe(HL)NO]NO_3$, while Figure 2.33 illustrates $[Fe(R_2Q)NO]$. The complexes were characterized by ^1H NMR, IR, Mossbauer, and electronic absorption spectroscopies. X-ray crystal structures, obtained for the square-pyramidal complexes $[Fe(HL)NO]NO_3$ and $[Fe(R_2Q)NO]$, where R = n-C_3H_7, are shown in Figures 2.34 and 2.35 respectively. Both complexes exhibit a nearly linear NO group, consistent with [$Fe^{II}NO^+$] formalisms.

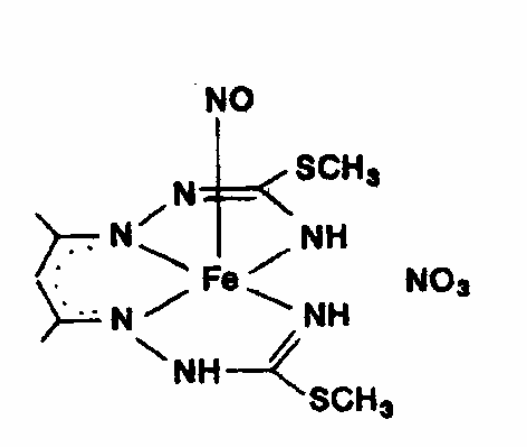

Figure 2.32 – [Fe(HL)(NO)]NO_3
HL_3 = 2,4-pentanedione bis(*S*-methylisothiosemicarbazone (Reprinted from *Inorg. Chim. Acta*, 202, Gerbeleu, N. V., Arion, V. B., Yu, A., Zavodnik, V. E., Stavrov, S. S., Turta, K. I., Gradinau, D. I., Birca, M. S., Pasynskii, A. A., Ellert, D., 173-181, Copyright 1992, with permission from Elsevier. 114)

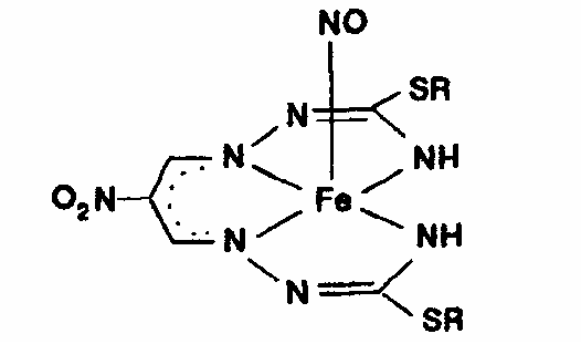

Figure 2.33 – [Fe(R_2Q)(NO)]
H_3R_2Q = nitromalondialdehyde bis(*S*-alkylisothiosemicarbazone (Reprinted from *Inorg. Chim. Acta*, 202, Gerbeleu, N. V., Arion, V. B., Yu, A., Zavodnik, V. E., Stavrov, S. S., Turta, K. I., Gradinau, D. I., Birca, M. S., Pasynskii, A. A., Ellert, D., 173-181, Copyright 1992, with permission from Elsevier. 114)

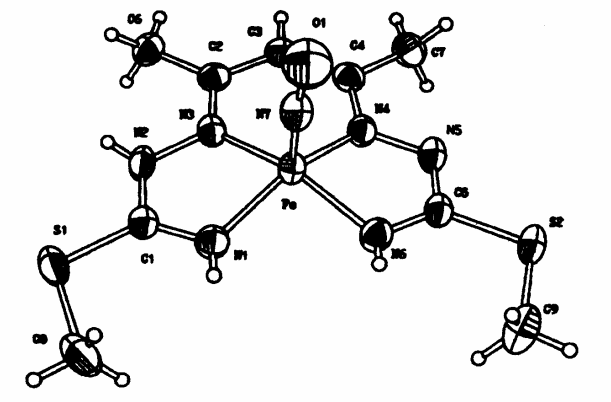

Figure 2.34 – $[Fe(HL)(NO)]^+$
HL_3 = pentandione bis(*S*-methylisothiosemicarbazone (Reprinted from *Inorg. Chim. Acta*, 202, Gerbeleu, N. V., Arion, V. B., Yu, A., Zavodnik, V. E., Stavrov, S. S., Turta, K. I., Gradinau, D. I., Birca, M. S., Pasynskii, A. A., Ellert, D., 173-181, Copyright 1992, with permission from Elsevier. 114)

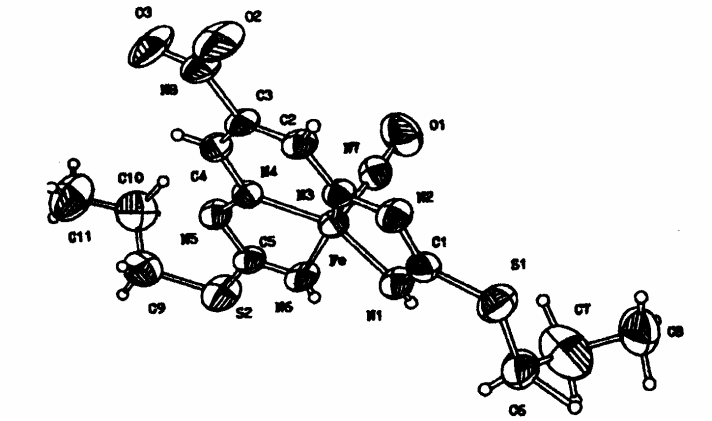

Figure 2.35 – $[Fe(R_2Q)(NO)]$
H_3R_2Q = nitromalondialdehyde bis(*S*-propyl-isothiosemicarbazone (Reprinted from *Inorg. Chim. Acta*, 202, Gerbeleu, N. V., Arion, V. B., Yu, A., Zavodnik, V. E., Stavrov, S. S., Turta, K. I., Gradinau, D. I., Birca, M. S., Pasynskii, A. A., Ellert, D., 173-181, Copyright 1992, with permission from Elsevier. 114)

Self-consistent charge molecular orbital calculations (SCC-MO) for the $\{FeNO\}^6$ complexes $[Fe(H_3L)NO]NO_3$ and $[Fe(R_2Q)NO]$ indicate that the geometry of NO coordination, along with $\bar{\nu}_{NO}$, is largely determined by the total number of metal ion d-electrons and the π-electrons of NO. When n < 6 the NO group should be linear with IR stretching frequencies similar to that of the neutral molecule. When n > 6 a bent nitrosyl is predicted. Infrared stretching frequencies, when n > 6, should be closer to the values expected for NO^-. Based upon their theoretical and experimental findings the authors conclude that the electronic structure of the quadridentate ligands (having more heteroatoms than TIM) approximates that observed in porphyrins.

2.4. DINITROSYL COMPLEXES

Equimolar amounts of $Fe(NO)_2(CO)PPh_3$ and tetracyanoethane (TCNE) in diethyl ether yield $Fe(NO)_2PPh_3(\eta^2\text{-TCNE})$[117] with loss of CO, within 1-2 h at ambient temperature. Figure 2.36 shows that $Fe(NO)_2PPh_3(\eta^2\text{-TCNE})$ exhibits two linear MNO groups. Upon coordination the olefinic carbon atoms of TCNE lose planarity as the π bond lengthens. The carbon atoms gain sp^3 character as the result of backdonation to the π∗ antibonding orbitals from the metal d orbitals. Accordingly the ^{13}C NMR signals for the olefinic carbons shift upfield upon coordination. Back-donation from filled metal d orbitals to vacant TCNE π* orbitals also decreases the TCNE CN stretching frequency and reduces back donation from the metal to NO. As a result IR signals for the nitrosyl groups in $Fe(NO)_2PPh_3(\eta^2\text{-TCNE})$ occur at higher frequency ($\bar{\nu}_{NO}$ = 1834 cm^{-1} and 1790 cm^{-1}) than those of the precursor, $Fe(NO)_2(CO)PPh_3$ ($\bar{\nu}_{NO}$ = 1766 cm^{-1} and 1718 cm^{-1}). The relatively rapid carbonyl replacement is explained by a free radical mechanism that invokes a 17 electron intermediate (Figure 2.37).

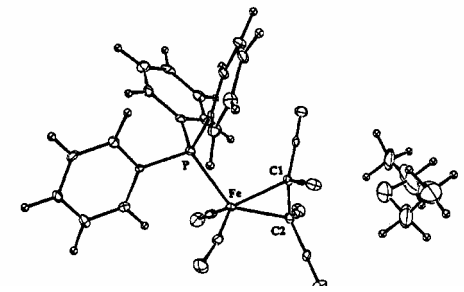

Figure 2.36 – ORTEP Diagram of $Fe(NO)_2PPh_3(\eta^2\text{-TCNE})$ and Solvent Molecule.
Selected bond lengths and bond angles: Re-P = 2.296(2) Å; Fe-N = 1.657(6) and 1.665(6) Å; Fe-C1/FeC2 = 2.029(7)/2.101(6) Å; C1-C2 = 1.473(9) Å; N1-Fe-N2 = 118.9º; Fe-N1-O1 = 178.0(5)º; Fe-N2-O2 = 165.8(5)º. (Reprinted with permission from *Organometallics*, **1994**, *13*, 4686-4688. Copyright 1994 American Chemical Society. 115)

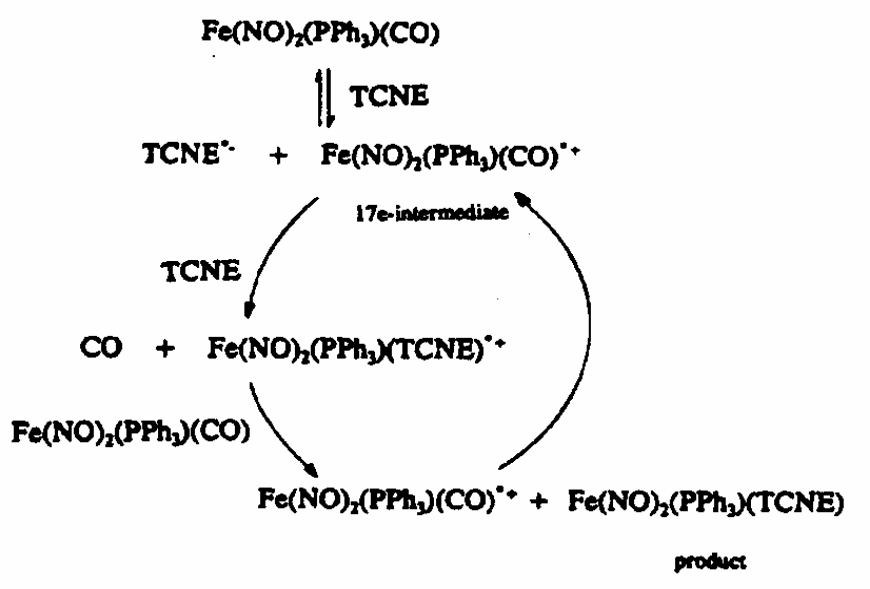

Figure 2.37 – Suggested Reaction Pathway

An Electron Transfer Autocatalysis Mechanism (Reprinted with permission from *Organometallics*, **1994**, *13*, 4686-4688. Copyright 1994 American Chemical Society. 115)

Blackwell[118] and co-workers reported the electrochemical and spectroscopic investigation of the interconversion of 18 electron $[FeXL(NO)_2]$ complexes and 17 electron $[FeL_2(NO)_2]$ complexes where L = PEt_3, PPh_3, or dppe and where X = Cl or I. These complexes provide the basis for a proposed redox-based scheme in which one electron reduction activates the 17 electron $[FeL_2(NO)_2]$ complexes toward substitution by better π acceptors while one electron oxidation activates 18 electron $[FeL_2(NO)_2]$ complexes toward substitution by σ donors (Figure 2.38).

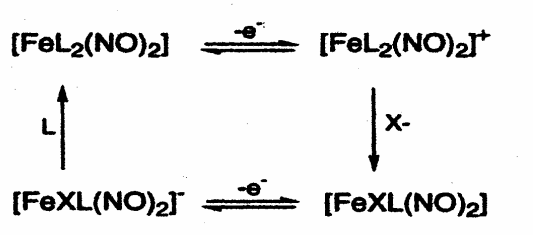

Figure 2.38 – Interconversion of 18 e- $[FeXL(NO)_2]$ and 17 e- $[FeL_2(NO)]$
(*J. Chem. Soc. Dalton Trans*., **1996**, 3491-3502 – Reproduced by permission of The Royal Society of Chemistry)

A series of iron dinitrosyl complexes of the form $Fe(NO_2)(PR_3)(\eta^2\text{-TCNE})$[119] where PR_3 = $P(OCH_3)$, $P(n\text{-Bu})_3$, PMe_2Ph, and PEt_2Ph forms within 3 hours upon reaction of the respective $Fe(NO_2)(PR_3)(CO)$ complex with TCNE in diethyl ether. The products, which are soluble in CH_2Cl_2, THF, $(CH_3)_2CO$, CH_3CN, and MeOH decompose in solution after a few days in a disproportionation reaction, similar to that shown in Figure 2.38, in which $Fe(NO)_2(PPh_3)_2^+$ converts to $Fe(NO)_2(PPh_3)_2$. The rapid formation of the TCNE product is believed to proceed through the same sort of 17 electron intermediate formed in the electron transfer autocatalysis which mechanism described Figure 2.37.

A decrease in NO stretching frequency upon addition of the phosphorus donor to $Fe(NO)_2(CO)_2$ arises from increased electron density at the iron center and subsequent increased backbonding to vacant $\pi*$ orbitals of the nitrosyl from filled iron d orbitals. This shift in ν_{NO} is reversed upon addition of TCNE as a result of efficient back donation from the iron d orbitals to the π^* orbitals of TCNE. The CN group of coordinated TCNE exhibits a corresponding decrease in stretching frequency as well. A positive shift in reduction potentials of the TCNE complexes compared to the carbonyl precursor supports the existence of strong metal backbonding to empty π^* orbitals of TCNE. The X-ray crystal structure of $Fe(NO)_2P(OMe)_3(\eta^2\text{-TCNE})$, shown in Figure 2.39, exhibits linear NO groups in an attracto conformation. NMR studies reveal restricted rotation about the Fe-TCNE π bond, which reflects enhanced back-donation from metal d orbitals to the π^* orbitals of the alkene. As illustrated in the second view of the x-ray crystal structure shown in Figure 2.40, there may be additional restrictive π orbital interactions between the NO and CN π systems due to alignment of the CN groups immediately above the NO groups.

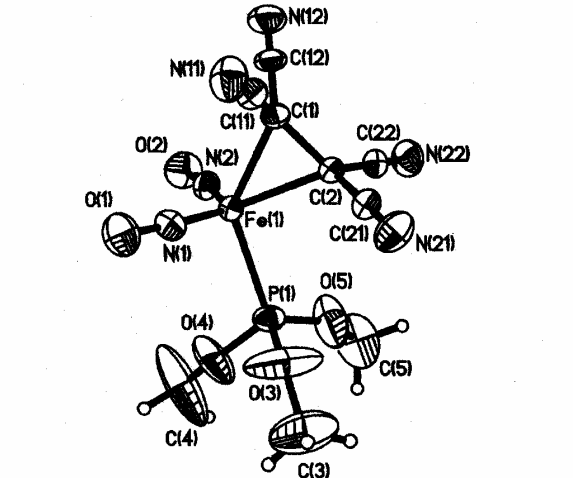

Figure 2.39 – The Molecular Structure of $Fe(NO)_2P(OMe)_3(\eta^2$-TCNE)
Anisotropic thermal ellipsoids are shown at 30%. (Reprinted from *J. Organomet. Chem*., 558, Hőrsken, Arne, Zheng, Guodong, Stradiotto, Mark., McCrory, Christopher. T. C., Lijuan, Li, 1-9, Copyright 1998, with permission from Elsevier. 117)

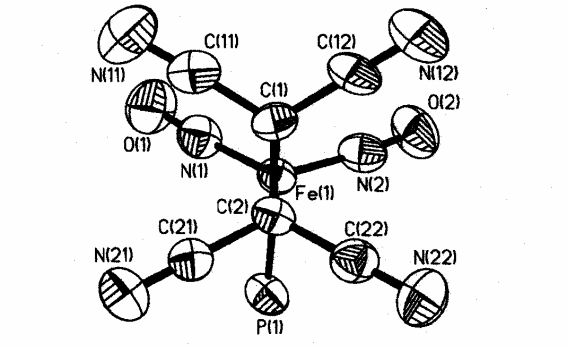

Figure 2.40 – The Molecular Structure of $Fe(NO)_2P(OMe)_3(\eta^2$-TCNE)
showing 50% thermal ellipsoids, viewed from the centroid of the C(1)-C(2) bond to the iron atom. The OCH_3 groups have been omitted for clarity. (Reprinted from *J. Organomet. Chem.*, 558, Hőrsken, Arne, Zheng, Guodong, Stradiotto, Mark., McCrory, Christopher. T. C., Lijuan, Li, 1-9, Copyright 1998, with permission from Elsevier. 117)

The first X-ray crystal structure of a non-heme-iron dinitrosyl complex of the g = 2.03 family that bears an imidazole ligand, $Fe(NO)_2$(1-methylimidazole)$_2$,[120] formed from the rapid reaction of $Fe(NO)_2(CO)_2$ with an excess of 1-methylimidazole in diethyl ether, is shown in Figure 2.41. The rapid reaction again suggests the presence of a 17 electron iron radical intermediate that facilitates carbonyl substitution by 1-methylimidazole. EPR studies and Mossbauer spectroscopy support the existence of 17-electron intermediate $[Fe(NO)_2(1\text{-MeIm})_2]^+$ whose EPR signal disappears upon formation of the green crystal $[Fe(NO)_2(1\text{-MeIM})_2]$. The linear nitrosyl groups (167.5(3)° and 170.1(3)°) are symmetrically tilted with the two oxygen atoms oriented toward each other in an attracto conformation. The nitrosyl stretching frequencies shifted from 1810 and 1767 cm^{-1} for $Fe(NO)_2(CO)_2$ to 1673 and 1616 cm^{-1} upon addition of the 1-MeIm ligands which act as good σ donors and decrease the NO stretching frequencies as rationalized by molecular orbital calculations.

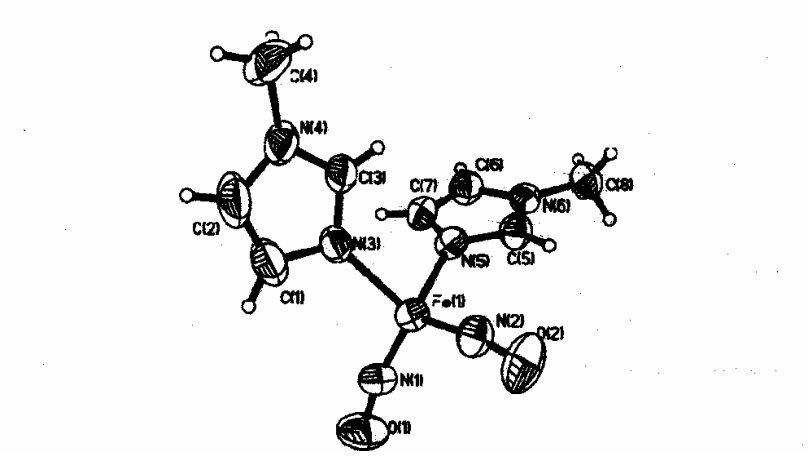

Figure 2.41 – X-ray Structure of $Fe(NO)_2$(I-MeIm)$_2$
showing the atomic numbering scheme. Anisotropic thermal displacement ellipsoids are shown at the 50% probability level. Selected bond distances and angles: Fe-Ni/Fe-N2 = 1.648(3)/1.650(3) Å;Fe-N3/Fe-N5 = 2.044(3)/2.048(3) Å; N1-O1/N2-O2 = 1.189(3)/1.188(4) Å; N1-Fe-N2 = 116.57(14)º; N3-Fe-N5 = 91.20(11)º; N1-Fe-N3/N1-Fe-N5 = 111.28(13)/112.76(12)º; N2-Fe-N3/N2-Fe-N5 = 114.43(13)/107.78(13)º. (Reprinted with permission from *J. Am. Chem. Soc*., **1999**, *121*, 10217-10218. Copyright 1999 American Chemical Society. 118)

2.5. BIMETALLIC NITROSYLS

Lower oxidation state bimetallic Fe and Ni organometallic complexes are of interest as models for Fe/Ni/S hydrogenase enzymes. Many syntheses have been directed toward hydrogenase active site modeling. The dinitrosyl diiron complex $[Fe_2(Et\text{-}HPTB)(O_2CPh)(NO)_2](BF_4)_2$[121] (Et-HPTB = *N*,*N*,*N*′,*N*′-tetrakis(*N*-ethyl-2-benzimidazolyl-methyl)-2-hydroxy-1,3-diaminopropane) formed upon addition of NO to $[Fe_2(Et\text{-}HPTB)(O_2CPh)](BF_4)_2$. The crystal structure (Figure 2.42) shows equivalent and slightly bent (166.6(7) and 168.3(7)°) Fe-NO groups. The $\{FeNO\}^7$ complex was characterized by magnetic susceptibility, Mossbauer, optical, and IR spectroscopies. Extended Huckel molecular orbital calculations on a model complex, $[Fe_2(NO)_2(NH_3)_6(OH)(O_2CH)]^{2+}$, indicate that the 167° Fe-N-O bond angle is dictated by the Fe-N π-bonding orbitals rather than by the π-antibonding HOMO.

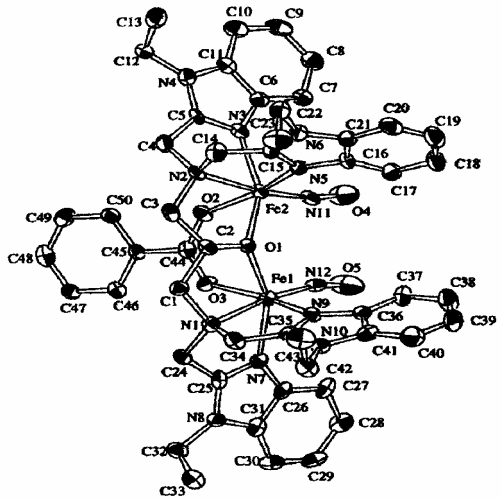

Figure 2.42 – ORTEP Representation of the Cation $[Fe_2(Et\text{-}HPTB)(O_2CPh)(NO)_2](BF_4)_2$
(40% probability ellipsoids) with hydrogen atoms removed for clarity (Reprinted with permission from *Inorg. Chem.*, **1996**, *35*, 6892-6898. Copyright 1996 American Chemical Society. 119)

Knox[122] and co-workers prepared two di-iron nitrosyl complexes by using $Fe_2(CO)_9$ to induce homolytic cleavage of the X-NO bond of nitrosoamines. Specifically, R_2NNO (R = methyl or ethyl) reacted with $Fe_2(CO)_6$ to form $(OC)_4Fe(\mu\text{-}CNR_2)Fe(CO)_2NO$. A crystal structure of the ethyl derivative exhibited a linear nitrosyl group. Both complexes were characterized by IR spectroscopy. In the same study $Fe(CO)_2(NO)_2$ was synthesized from the reaction between ethyl nitrite and $Fe_2(CO)_9$ as well as from the reaction between silver nitrite and $Fe(CO)_4I_2$.

Glidewell and co-workers[123] formed $[Fe(SMe)_2(NO)_4]$ by direct incorporation of the SMe fragment of methionine. In the presence of iron(II)sulfate and sodium nitrite, methionine produced $[Fe_2(SMe_2)(NO)_4]$. The product was characterized by IR, ^1H NMR, ^{13}C NMR, ^{15}N NMR, spectroscopies as well as by mass spectrometry. Ethionine, methionine ethyl ester, and S-methylcysteine reacted similarly. Control experiments using iron(II)chloride instead of iron(II) sulfate confirmed that the sulfur in the product originated from the methionine rather than from reduction of sulfate. This methodology[124] was extended to form similar dinuclear complexes as well as tetranuclear $[Fe_4S_3(NO)_7]^-$ from iron(II), nitrite and the cysteine and penicillamine derivatives shown in Figure 2.43 Thiols 1-6, 12 and 13 only yielded $Na[Fe_4S_3(NO)_7]$ under autoclave conditions; however, at reflux under nitrogen, thiols 2, 4, 6, 12 and 13 formed dinuclear complexes $[Fe_2(SR)_2(NO)_4]$ in addition to $[Fe_4S_3(NO)_7]^-$. Lanthionine formed the tetranuclear complex only in the presence of ascorbate. In contrast to 12 and 13, *S*-nitroso-*N*-acetylpenicillamine (SNAP) 14 acted as an NO source rather than as a sulfur source.

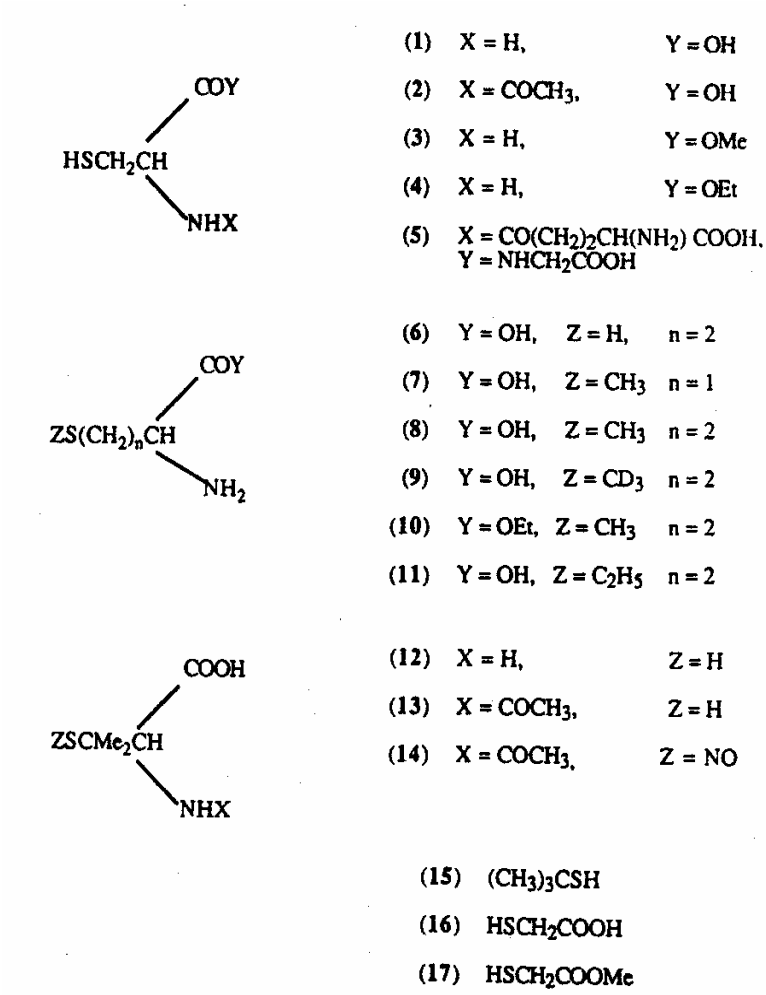

Figure 2.43 – Methionine, Cysteine, and Penicillamine Derivatives
(Reprinted from *Polyhedron*, 11, Anthony R. Butler, Christopher Glidewell* and Sheila M. Glidewell, "Formation of Bismethanthiolatobis(Dinitrosyliron) [$Fe_2(SMe)_2(NO)_4$] By Capture of Methanethiol Groups From Methionine and Its Derivatives in Reactions With Iron(II) And Nitrite", 591-596, 1992, with permission form Elsevier. 122)

Osterloh and co-workers[125] synthesized the heterobinuclear $[Ni(\mu\text{-}SR)_2Fe(NO)_2]$ complex via the reaction depicted in Figure 2.44. Two carbonyls of $Fe(CO)_2(NO)_2$ are displaced by a square planar N_2S_2 complex of Ni^{II}. The crystal structure is shown in figure 2.45. The small Ni-Fe distance of 279.7(1) pm, compared to that for the binuclear complex of the active center of NiFe Hydrogenase at 290 pm is partially explained by the low coordination number of the iron center. While infrared data does not mimic the absorption pattern for NiFe hydrogenase, the authors do not rule out the possibility that a nitrosyl ligand is at the active center of NiFe hydrogenase because ligand effects may cause the variation.

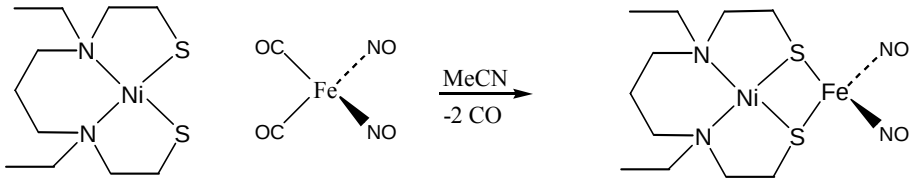

Figure 2.44 – Formation of $Ni(\mu\text{-}SR)_2Fe(NO)_2$
(*J. Chem. Soc., Chem. Commun*. **1997**, 979-980 reproduced by permission of the Royal Society of Chemistry 123)

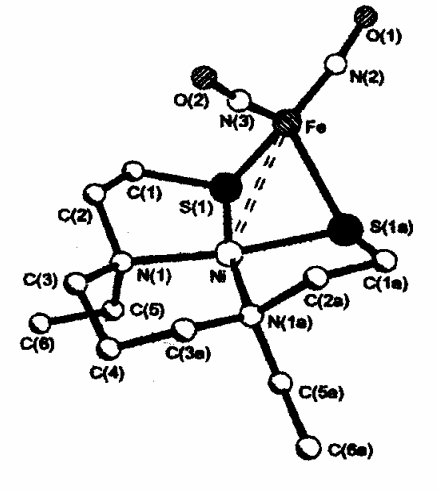

Figure 2.45 – Molecular Structure of $Ni(\mu SR)_2Fe(NO)_2$
Molecular Structure of $Ni(\mu SR)_2Fe(NO)_2$ with atom labeling scheme: $Ni(\mu SR)_2Fe(NO)_2$ exhibits crystallographic mirror symmetry; H atoms have been omitted. (*J. Chem. Soc. Chem. Commun*. **1997**, 979-980 – Reproduced by permission of The Royal Society of Chemistry. 123)

Liaw and co-workers[126] prepared analogues of Osterloh's N_2S_2 complex. Coordination of other S donating ligands to $[Fe(NO)_2(CO)]$ and $[Fe(NO)_2]$ generated the series of monomeric and homodimetallic derivatives of the $Fe(NO)_2$ fragments shown in figure Figure 2.48. The crystal structure of the dinitrosyl iron complex $[Fe(NO)_2[(PhSe)_2]^-$, formally $Fe(^-I)$ with two NO^+ ligands, is displayed in figure 2.46. The $[Fe(NO)_2[(PhSe)_2]^-$ complex is a precursor to the neutral heterobimetallic $[(ON)Ni(\mu\text{-}S(CH_2)S(CH_2)_2S)Fe(NO)_2]$ which exhibits linear nitrosyls as shown in Figure 2.47.

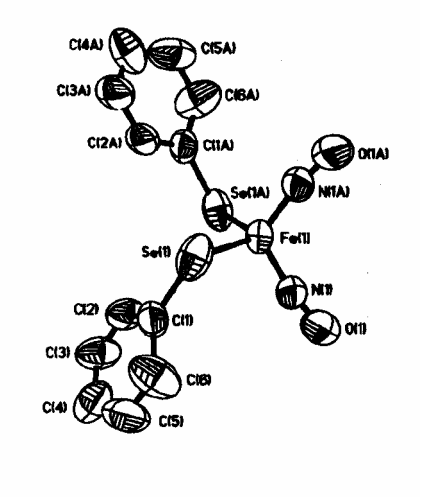

Figure 2.46 – Labeling Scheme for $[Fe(NO)_2(SePh)_2]^-$
with thermal ellipsoids drawn at the 50% probability level. Fe-Se, 2.395(1); Fe-N(1), 1.669(4); N(1)-O(1), 1.162(5). Se-Fe-Se(a), 114.08(5); Se-Fe-N(1), 107.88(13); Se-Fe-N(1a), 105.06(13); N(1)-Fe-N(1a), 117.20(19); Fe-N(1)-O(1), 169.2(4). (Reprinted with permission from *Inorg. Chem*., **2000**, *39*, 480-484. Copyright 2000 American Chemical Society. 124)

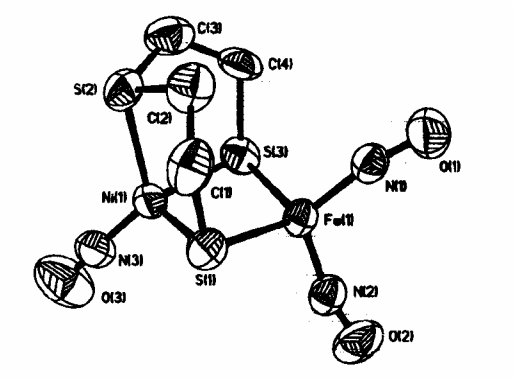

Figure 2.47 – [(ON)Ni(μ–S$(CH_2)_2$S$(CH_2)_2$S)Fe$(NO)_2$]
Labeling scheme for [(ON)Ni(μ-S$(CH_2)_2$S$(CH_2)_2$S)Fe$(NO)_2$] with thermal ellipsoids drawn at the 50% probability level. Fe-S(1), 2.2907(9); Fe-S(3), 2.3039(9); Fe-N(1), 1.670(2); Fe-N(2), 1.674(3); N(1)-O(1), 1.163(3); N(2)-O(2), 1.159(3); Ni-S(3), 2.2931(9); Ni-N(3), 1.644(2); N(3)-O(2), 1.119(3); Ni-Fe, 2.8001(6). S(1)-Fe-S(3), 103.73(3); S(1)-Fe-N(1), 114.88(9); S(1)-Fe-N(2), 106.03(9); N(1)-Fe-N(2), 115.06(12); S(1)-Ni-S(2), 91.67(3); S(1)-Ni-S(3), 103.94(3); S(1)-Ni-N(3), 120.53(10); S(2)-Ni-S(3), 92.31(4); S(2)-Ni-N(3), 126.69(9); S(3)-Ni-N(3), 115.83(10); Fe-S(1)-Ni, 75.28(3); Fe-S(3)-Ni, 75.05(3); Fe-N(1)-O(1), 1.66.21(23); Fe-N(2)-O(2), 167.3(3); Ni-N(3)-O(3), 175.1(3). (Reprinted with permission from *Inorg. Chem*., **2000**, *39*, 480-484. Copyright 2000 American Chemical Society. 124)

Compound	Compound	ν(NO), cm^{-1} [ν(CO), cm^{-1}]	∠N-Fe-N, deg [∠L-Fe-L]	∠Fe-N-O, deg
1		1697, 1741[a]	117.20(19) [114.08(5)]	169.2(4)
1a	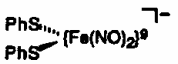	1709, 1744[b]	117.36(9) [109.73(2)]	168.5(2) 169.4(2)
2	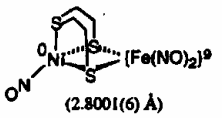 (2.8001(6) Å)	1725, 1767[a]	115.06(12) [103.73(3)]	166.21(23) 167.3(3)
3[20]	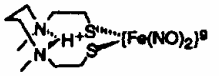	1695, 1740[c]	118.09(12) [109.15(3)]	169.8(3) 169.8(3)
4[4]	 (2.797(1) Å)	1624, 1663[c] 1630, 1675[d]	118.2(3) [74.10(6)]	167.0(5) 174.6(5)
5	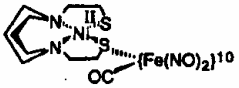	1691, 1733[e] [2006]		
6		1630, 1677[d]		
7[21]	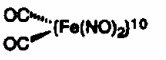	1756, 1810[f] [2034, 2087]	114(6) [110(3)]	ca. 180
8[22]		1722, 1764[g] [2009]	114.4(4)[h] [103.9(4)]	177.9(6)[h]
9[22]		1678, 1724[g]	123.8(4) [111.9(1)]	178.2(7)
10[27]	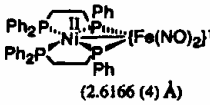 (2.6166 (4) Å)	1710, 1760[e]	120.8(1) [101.11(3)]	173.1(3) 171.4(3)

[a] Dichloromethane. [b] CsI. [c] KBr. [d] Acetonitrile. [e] THF. [f] Cyclohexane. [g] Tetrachloroethylene. [h] Shown are average values.

Figure 2.48 – Selected Structure and Infrared Data for Dichalcogenide {Fe(NO)$_2$}^{9,10}
Based on Enemark–Feltham Notation (Reprinted with permission from *Inorg. Chem.*, **2000**, *39*, 480-484. Copyright 2000 American Chemical Society. 124)

Nitrosprussides, $[Fe(CN)_5NO]^{2-}$ are of interest because of their unusual magnetic and electronic behavior and because of their inhibitory effect on superoxide dismutase.[127,128] Two excited metastable states for sodium nitrosprusside, $[Na_2Fe(CN)_5NO]$, have been observed; several of their vibrational modes have been assigned.[129] The wavenumbers and isotopic shifts for majority of the 33 vibrational modes of normal and ^{54}Fe ^{13}C and $^{15}N(O)$ enriched sodium nitrosprusside dihydrate have also been obtained by FTIR and NIR Raman spectrscopies.[130] Heterobinuclear complexes, in which the nitrosprusside ion is bridged via cyanide to other metal sites, have been prepared.

Tang and co-workers[131] reported the X-ray crystal structure and magnetic properties of polymeric $[Cu_2(oxpn)Fe(CN)_5(NO)]_n$ (oxpn = dianion of *N*, *N*′ - bis(3-aminopropyl)oxamide) (Figure 2.49). The authors suggest that a very weak antiferromagnetic exchange in this *trans*-oxamidato-bridged compound, compared with that in other trans-oxamidato bridged compounds, may be due to the trigonal bipyramidal character of the Cu^{II} ion, which renders the two magnetic orbitals in the Cu^{II} dinuclear unit unable to interact from each side of the oxamidate bridge.

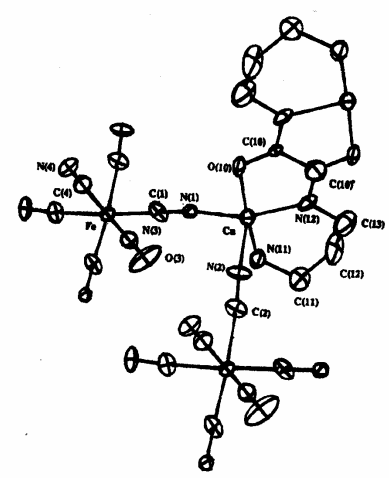

Figure 2.49 – Perspective View of $[Cu_2(oxpn)Fe(CN)_5(NO)]_n$
(Reprinted with permission from *Inorg. Chem.*, **1995**, *34*, 2255-2257. Copyright 1995, American Chemical Society. 125)

Shyu and co-workers[132] prepared the discrete double complex $[Ni(bpy)_3][Fe(CN)_5(NO)]\bullet 3H_2O$ shown in Figure 2.50 and the dimensional polymeric complex $[Ni(en)_2Fe(CN)_5(NO)]\bullet H_2O$, shown in Figure 2.51. Both nitrosyl groups are nearly linear with $\bar{\nu}_{NO}$ = 1911 and 1933 cm^{-1} respectively. The outer-sphere bpy complex exhibits classical paramagnetic behavior, while the ethylenediamine complex exhibits a very weak antiferromagnetic interaction between the two adjacent Ni(II) ions, possibly through the $[Fe(CN)_5(NO)]^{2-}$ group.

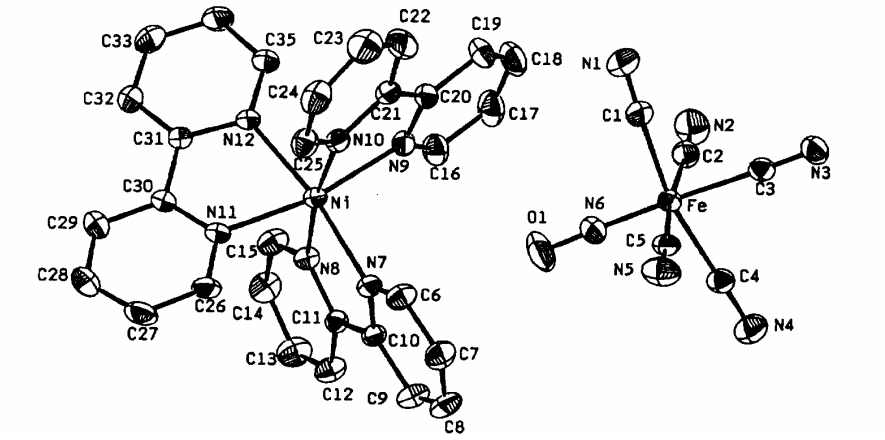

Figure 2.50 – ORTEP Stereoview of $[Ni(bpy)_3][Fe(CN)_5(NO)]$
Shown without H_2O, 30% probability thermal ellipsoids. (Reprinted from *Inorg. Chim. Acta*, 258, Huey Lih Shyu, Ho Hsiang Wei, Yu Wang, "Preparation, characterization and crystal structure of $[Ni(bpy)_3][Fe(CN)_5(NO)]\bullet 3H_2O$ and one dimensional cyanobridged $[Ni(en)_2Fe(CN)_5(NO)]\bullet H_2O$", 81-86, Copyright 1997, with permission from Elsevier. 126)

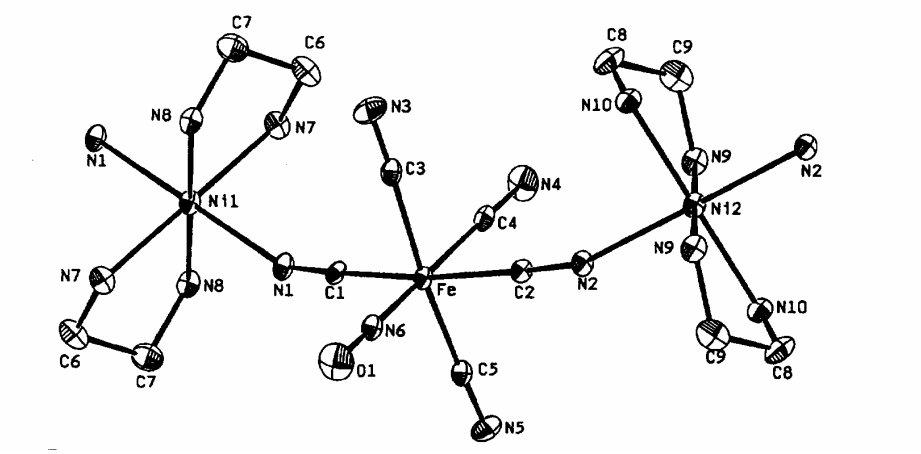

Figure 2.51 – ORTEP Stereoview of $[Ni(en)_2Fe(CN)_5(CO)]$
Shown without H_2O; 30% probability thermal ellipsoids. (Reprinted from *Inorg. Chim. Acta*, 258, Huey Lih Shyu, Ho Hsiang Wei, Yu Wang, "Preparation, characterization and crystal structure of $[Ni(bpy)_3][Fe(CN)_5(NO)]$ $3H_2O$ and one dimensional cyanobridged $[Ni(en)_2Fe(CN)_5(NO)]\bullet H_2O$", 81-86, Copyright 1997, with permission from Elsevier. 126)

To investigate the correlation between magnetic properties and structure in nitroprusside bridged complexes, Liao[133] prepared a new one-dimensional chain complex $[Cu(en)_2Fe(CN)_5(NO)]$, obtained its crystal structure, and determined its magnetic properties. The crystal structure shown in Figure 2.52 consists of alternating $Cu(en)^{2+}$ and $[Fe(CN)_5(NO)]^{2-}$ fragments connected in cis configuration by two cyanide ligands of the $[Fe(CN)_5(NO)]^{2-}$ fragment. The bridging cyanides are bent; longer axial distances Cu-N are attributed to the Jahn–Teller effect for the d^9 configuration of this distorted octahedral Cu^{II} ion. Magnetic measurements reveal a drop in the effective magnetic moment (μ_{eff}) at low temperatures, which indicates a weak antiferromagnetic coupling between copper ions. The weak interaction is rationalized by considering the large nearest Cu-Cu distance and the weakened Jahn–Teller distorted axial Cu-N contacts. The calculated J value for $[Cu(en)_2Fe(CN)_5(NO)]$ is over twice that for $[Ni(en)_2Fe(CN)_5(NO)]$. The authors propose that the lower energy of the magnetically active 3d orbitals of Cu(II) compared to those of nickel(II) moves the 3d orbitals of Cu(II) closer in energy to the symmetry-adapted-highest occupied molecular orbitals of $[Fe(CN)_5(NO)]^{2-}$.

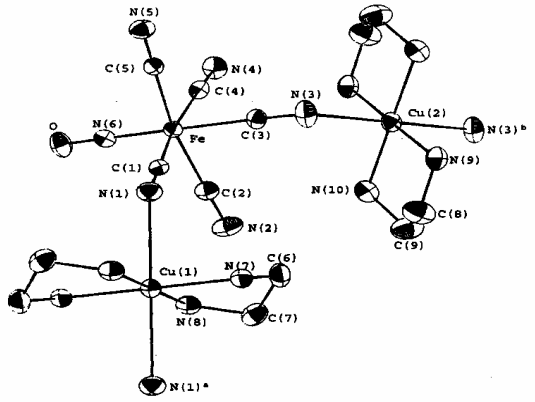

Figure 2.52 – ORTEP Drawing of $Cu(en)_2Fe(CN)_5(NO)$
Shows thermal ellipsoids at the 30% probability level. (Reprinted From *Aust. J. Chem*., 51, Hui-Zhong Kou, Hong-Mei Wang, Dai-Zheng Liao, Peng Cheng, Zong-Hui Jiang, Shi-Ping Yan, Xiao-Ying Huang and Geng-Lin Wang, "A New One-Dimensional Bimetallic Complex: $Cu(en)_2Fe(CN)_5(NO)$. Synthesis, Crystal Structure and Magnetic Behavior, 661-665, Copyright 1998, with permission from CSIRO publishing, 129).

Liao[127] and co-workers also synthesized relatively insoluble $[Cu(bpy)][Fe(CN)_5(NO)]\bullet 2H_2O$ which upon dissolving in a hot acetyl acetone and pyridine mixture formed the mixed metal complex $[Cu(acac)(bpy)](py)]_2[Fe(CN)_5(NO)]$ for which the crystal structure shown in Figure 2.53 was obtained. The crystal structure comprises two $[Cu(acac)(bpy)](py)]^+$ cations and one $[Fe(CN)_5(NO)]^{2-}$ anion. The nitrosyl ligand, assigned as NO^+, is indistinguishable from the CN ligand trans to it. The iron center is considered Fe^{II} as it is in the sodium nitrosprusside analogue. The authors propose that the weak magnetic interactions detected by EPR and magnetic studies may be attributed to π-stacking contacts between coordinated bpy ligands.

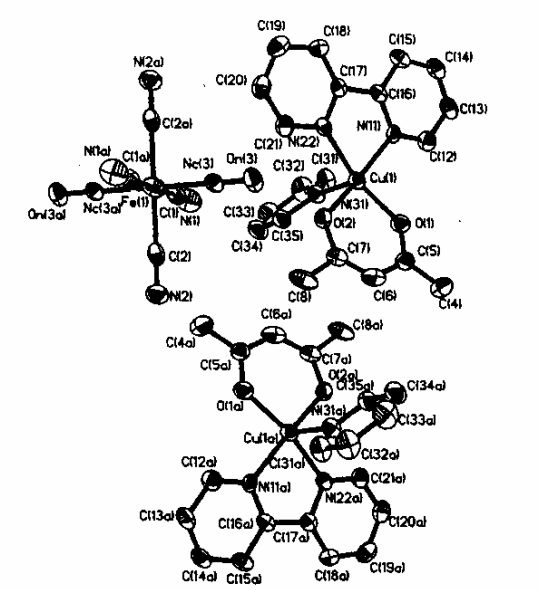

Figure 2.53 – ORTEP Drawing of $[Cu(acac)(bpy)(py)]_2[Fe(CN)_5(NO)]$
Shows 30% probability ellipsoids and the atomic labeling scheme. (Reprinted from *Acta Chem. Scandinavica*, *53*, **1999**, Hui-Zhong Kou, En-Qing Goa, Dai-Zheng Liao, Peng Cheng, Zong-Hui Jian, Shi-Ping Yan, Geng-Lin Wang, Zin-Kan Yao, Hong-Gen Wang and J. P. Tuchagues, "A new Copper(II)Iron(II) Complex $[Cu(acac)(bpy)(py)]_2[Fe(CN)_5(NO)]$ based on Nitroprusside: Synthesis, Structure and Spectroscopic Studies", 542-546, with permission form Blackwell Publishing. Ltd.)

Smekal[128] and co-workers obtained the crystal structure of the dimeric $[Cu(H_2NCH_2CH(NH_2)CH_3)_2Fe(CN)_5NO]\bullet 2H_2O$, which is analogous to the polymeric $[Cu(en)Fe(CN)_5NO]$. The authors propose that methyl groups on the propane-1,2-diamine interfere with polymer formation. The crystal structure, presented in figure 2.54 illustrates that the copper(II) ion is coordinated by five nitrogen atoms, four from two propane-1,2-diamine ligands and one from a bridging cyanide ligand in a distorted tetragonal pyramid. The linear nitrosyl group in the distorted octahedrally coordinated $[Fe(CN)_5NO]^{2-}$ fragment is cis to the bridging cyanide group. In the same study four other new bimetallic complexes were prepared and characterized by IR and UV-vis spectroscopies in addition to magnetic measurements. The

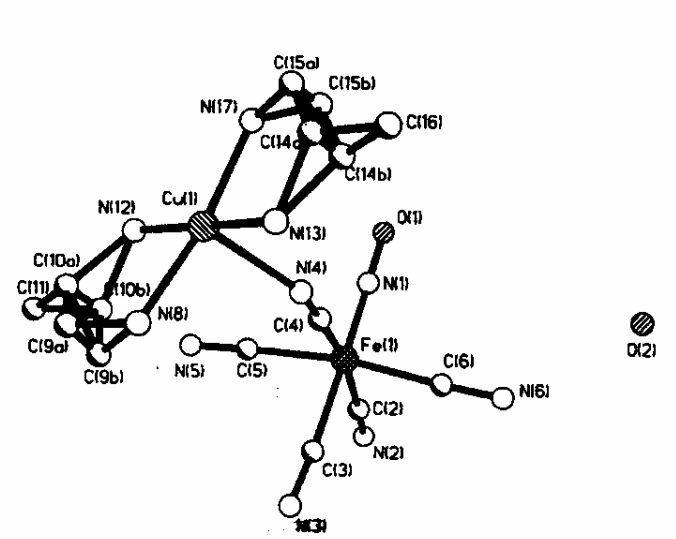

Figure 2.54 – Molecular Structure of $[Cu(1,2\text{-pn})_2Fe(CN)_5NO]\bullet H_2O$
Shown with the atom numbering scheme. Hydrogen atoms are omitted for the sake of clarity. (Reprinted from *Aust. J. Chem.*, 53, Zdenék Smékal*, Zdenék Trávniček, Jarmir Marek and Milan Nádvornik, "Cyano-Bridged Bimetallic Complexes of Copper(II) with Nitroprusside. Crystal Structure of $[Cu(H_2NCH_2CH(NH_2)CH_3)_2Fe(CN)_5NO]\bullet H_2O$", 225-228, Copyright 2000, with permission form CSIRO Publishing, (131))

four other new complexes, $[Cu(L)Fe(CN)_5NO]\bullet xH_2O$ (L = tmen (*N*,*N*,*N*′,*N*′ - tetramethylethane-1,2-diamine), x = 0.5; L = trimeen (*N*,*N*,*N*′-trimethylethane-1,2-diamine), x = 1; L = dien (*N*-(2-aminoethyl)ethane-1,2-diamine), x = 0; L = medpt (*N*-(3-aminopropyl)-*N*-methylpropane-1,3-diamine), x = 2) were obtained from the reaction between $Cu(ClO_4)_2\bullet 6H_2O$ or $CuCl_2\bullet 2H_2O$, $Na_2[Fe(CN)_5NO]\bullet 2H_2O$, and the amine in water.

To clarify the correlation between structure and magnetic properties of dinuclear complexes with the $[Fe(CN)_5(NO)]^{2-}$ anion, Mitra[134] and co-workers prepared and characterized two new cyano-bridged heterometallic complexes $[Cu(dmen)_2Fe(CN)_5(NO)]$ (dmen = 2-dimethylaminoethylamime) and $[Cu(dmpn)_2Fe(CN)_5(NO)]$ (dmpn = 1-dimethylamino-2-propylamine). In both structures the distorted octahedral Fe^{II} center connects to the distorted square pyramidal Cu^{II} ion through a bent cyano bridge. In agreement with molecular orbital

theory the NO^+ is linear. There is no magnetic interaction between Cu^{II} and Fe^{II} in either complex.

To verify the existence of an interaction between two metallic centers through a different metal center Gerbase et al.[135] prepared the formally d^{10} Co(⁻I) and Fe(⁻II) complexes $[(dppf)(CoNO)_2][SbF_6]$ (dppf = 1,1′ -bis(diphenylphosphino)ferrocene), $[(dppf)Fe(NO)_2]$ as well as $[(dppf)(FeCO)_3]$. The crystal structure of $[(dppf)(CoNO)_2][SbF_6]$ shown in figure 2.55 reveals two linear nitrosyl groups which absorb at 1850 and at 1789 cm^{-1}. The dppf chelates to the cobalt nitrosyl moiety in a distorted tetrahedral fashion. The complex may be considered formally Co(⁻I) with two NO^+ ligands. Mossbauer data revealed a weak interaction between the two metal atoms through the dppf ligand. Mossbauer parameters also show that electronic effects of powerful π acceptors, such as CO and NO^+ are very different from those observed for σ and π donors. For the halide series, the distortion of the ferrocenyl moiety had been attributed to coordination geometry of the metal rather than to the nature if the ligands. For example, in Mossbauer studies of a series of dppf metal halide and carbonyl complexes, Houlton et al.[136] reported that tetrahedral complexes produce the highest IS (0.55-0.58 mm s^{-1}) and the highest QS (2.29-2.36 mm s^{-1}), octahedral complexes ($dppfM(CO)_4$, M = Pd, Pt, Cd) had intermediate IS (0.52-0.54 mm s^{-1}) and QS (2.23-2.27 mm s^{-1}) values, and that square planar complexes ($dppfMCl_2$, M = Pd, Pt, Cd) had the lowest IS (0.50-0.51 mm s^{-1}) and QS (2.14-2.29 mm s^{-1}) parameters. Thus it was concluded that the geometry of the metal, rather than the ligand electronic character that influences the hyperfine interactions of the ferrocenyl iron atom. However, the Mossbauer parameters of ferrocenyl iron in the tetrahedral complexes $dppfFe(NO)_2$ (IS = 0.52 mm s^{-1}, QS = 2.34 mm s^{-1}) and $[dppfCo(NO)_2][SbF_6]$ (IS = 0.52 mm s^{-1}, QS = 2.30 mm s^{-1}) do not fit the coordination geometry-based trend suggested by Houlton et

al.[136] On the contrary, in addition to the steric component, there is an electronic contribution to the effect of the MLn moiety on the Mossbauer parameters of the ferrocenyl Fe atom. Electrochemical studies indicate that, in solution, MLn coordination hinders iron dppf oxidation and can change the oxidation mechanism.

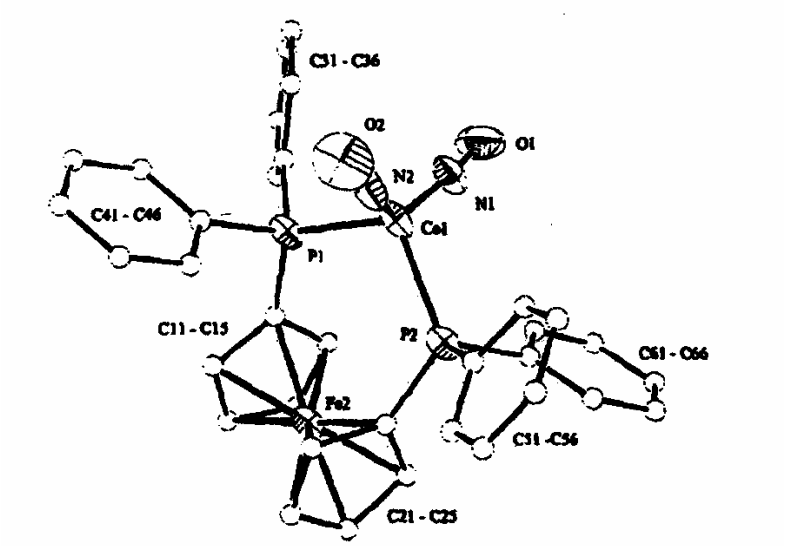

Figure 2.55 – ORTEP Plot of [dppfCo(NO)$_2$][SbF$_6$] Cation
Displacement of ellipsoids at the 50% level; H atoms omitted for clarity. (Reprinted from *Inorg. Chim. Acta*, *266*, Annelise E. Gerbase, Eduardo, J. S. Vichi, Edison Stein, Livio Amaral, Adalberto Vasquez, Manfredo Hörner, Cäcilia Maichle-Mössmer, "Preparation, characterization and electrochemical studies of 1,1-bis(diphenylphosphine) ferrocene (dppf) derivatives. Crystal structure of [dppfCo(NO)$_2$][SbF$_6$]", 19-27, Copyright 1997, by permission from Elsevier. 127)

2.6. CLUSTERS

Metal nitrosyl clusters are of interest to chemists in various branches of chemistry For example, organometallic chemists investigate metal nitrosyl clusters for catalytic applications.[137] Theoretical chemists are interested studying metal nitrosyl cluster frameworks. And biochemists are interested in clusters such as Roussin's salts and their which have potential applications to photodynamic therapy. [138-140]

Many derivatives [139-144] of Roussin's red salt, $Na_2[Fe_2S_2(NO)_4]$ and Roussin's black salt $NH_4[Fe_5S_4(NO)_7]$ have been reported since Roussin's salts were discovered in 1858;[145] however, until Dance and coworkers reported the synthesis of $[Fe_5S_4(NO)_8]^-$ and $[Fe_7S_6(NO)_{10}]^-$,[146] the only other known nitrosyl containing sulfide clusters were $[Fe_4S_4(NO)_4]^z$ (z = 0, -1)[147,148] and $[Fe_6S_6(NO)_6]^{2-}$.[149] The structures of $[Fe_2S_2(NO)_4]^{2-}$, $[Fe_5S_4(NO)_8]^-$, $[Fe_4S_4(NO)_4]^z$, $[Fe_6S_6(NO)_6]^{2-}$, proposed on the basis of density functional calculations, are illustrated in Figure 2.56.

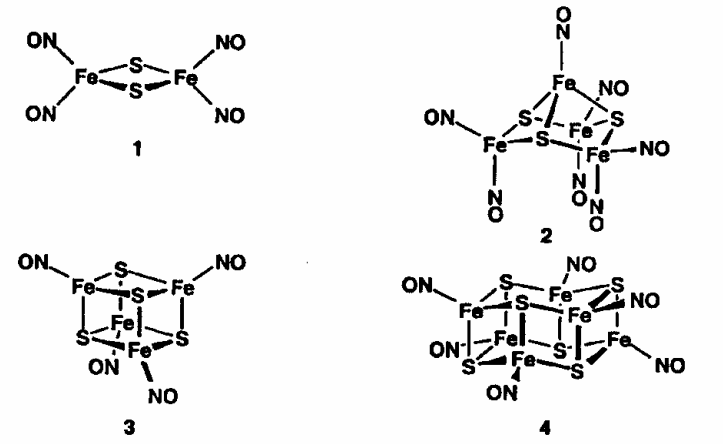

Figure 2.56 – $[Fe_2S_2(NO)_4]^{2-}$, $[Fe_4S_3(NO)_7]^z$, $[Fe_4S_4(NO)_4]^z$, z = 0, -1, and $[Fe_6S_6(NO)_6]^{2-}$
$[Fe_2S_2(NO)_4]^{2-}$ (**1**), $[Fe_4S_3(NO)_7]^z$ (**2**), $[Fe_4S_4(NO)_4]^z$ (**3**), z = 0, -1, and $[Fe_6S_6(NO)_6]^{2-}$ (**4**) (*Chem. Commun.*, **2000**, 947-948 - Reproduced by permission of the Royal Society of Chemistry. 142)

Relatively rapid formation of $[Fe_5S_4(NO)_8]^-$ and $[Fe_7S_6(NO)_{10}]^-$ occurs under negative ion electrospray mass spectrometry conditions from a solution of $Na_2[Fe_2S_2(NO)_4]$ in methanol or in acetonitrile. The lack of observable intermediates, suggests a facile associative mechanism which involves collisions of $[Fe_2S_2(NO)_4]^{2-}$ complexes, followed by simple connectivity changes between the starting materials and the products.

Scott and Holm studied the following tetranuclear iron sulfur clusters with linear NO^+ nitrosyl ligands: $[Fe_4S_3(NO)_7]^-$, $[Fe_4S_4(NO)_4]$, $[Fe_4S_4(NO)_4]^-$, $[Fe_4S_3(NO)_4(PPh_3)_3]$, $[Fe_4S_3(NO)_4(PPh_3)_3]^+$, $[Fe_6S_6(NO)_6]^{2-}$ [149] Crystal structures were obtained for $[Fe_4S_3(NO)_4(PPh_3)_3]$, $[Fe_4S_3(NO)_4(PPh_3)_3]^+$, and $[Fe_6S_6(NO)_6]^{2-}$. The $[Fe_6S_6(NO)_6]^{2-}$ complex was isolated as $[Fe(dmf)_6][Fe_6S_6(NO)_6]$ and as $[Et_4N]_2[Fe_6S_6(NO)_6]$. The cluster $[Fe_6S_6(NO)_6]^{2-}$ whose crystal structure is displayed in figure 2.57 is the first example of a structure, for Fe(NO)(S)L, systems with a bridging ligand with $L \neq RS^-$, RO^- or halide. The X-ray crystal structures of $[Fe_4S_3(NO)_4(PPh_3)_3]$ and $[Fe_4S_3(NO)_4(PPh_3)_3]^+$ shown in figures 2.58 and 2.59 exhibit a cuboidal Fe_4S_3 core. Holm[150] later extended his study of $[Fe_4S_3(NO)_4(PR_3)_3]$ clusters to include phosphines of larger cone angle and higher basicity, where R = Et, Pr^i, and Cy and found that the cuboidal core is maintained.

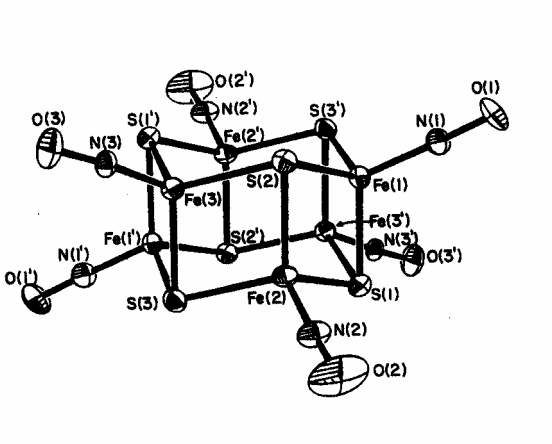

Figure 2.57 – Crystal Structure of $[Fe_6S_6(NO)_6]^{2-}$ as its Et_4N^+ Salt
Shows 30% probability ellipsoids; Selected interatomic distances [pm] and angles [º]: Fe(1)-Fe(2) 266.3(2). Fe(1)-Fe(3)′ 265.6(2). Fe(2)-Fe(3) 265.9(2). mean Fe-S 222.1(5). mean Fe-N 166(1). Mean Fe-N-O 176(1); within the Fe3S3 cyclohexane-type ring mean values are S-Fe-S 113.2(9), Fe-S-Fe 111.9(8): within the Fe2S2 rhombuses mean values are S-Fe-S 106.3(2) and Fe-S-Fe 73.6(2). Primed and unprimed atoms are related by an inversion center. (Reprinted with permission from *Angew. Chem. Int. Ed., Engl*., **1993**, *32*, 564-566. Copyright 1993, John Wiley & Sons.)

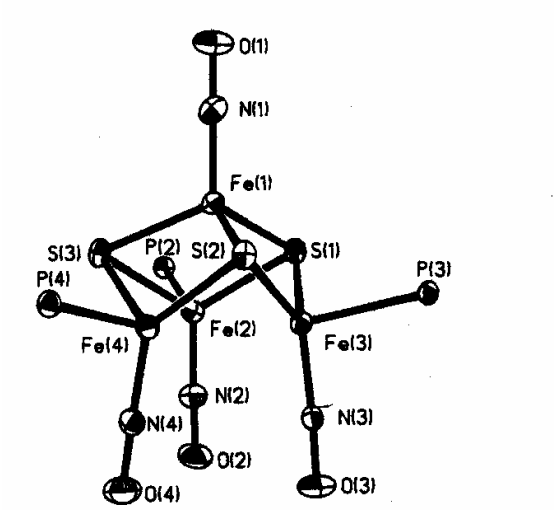

Figure 2.58 – The Structure of $[Fe_4S_3(NO)_4(PPh_3)_3]$
Phenyl groups omitted, 30% probability ellipsoids. Selected interatomic distances [pm] and angles [º]: Fe(1)-Fe(2) 257.1(2), Fe(1)-Fe(3) 261.4(2), Fe(1)-Fe(4) 262.8(2), Fe(2)-Fe(3) 277.1(2), Fe(2)-Fe(4) 278.0(2), Fe(3)-Fe(4) 267.8(2), Fe(1)-S 224.3(17), Feb-S 221.4(7), Fe-P 224.8(5), S-Fe(1)-S 105.5(16), S-Fe(1)-N(1) 113.2(7), Fe(1)-S-Feb 71.5(7), Feb-S-Feb 76.6(18), S-Feb-S 107.5(14), S-Feb-N 124(6), S-Feb-P 95.7(20), N-Feb-P 98.1(5). Fe(1)-N(1)-O(1) 177.9(7), Feb-N-O 177.0(6). Except for the unique angle, data involving P, S, and N atoms are mean values under idealized trigonal symmetry (Feb = Fe(2)-Fe(4)). (Reprinted with permission from *Angew. Chem. Int. Ed. Engl*., **1993**, *32*, 564-566. Copyright 1993 John Wiley & Sons, Inc.)

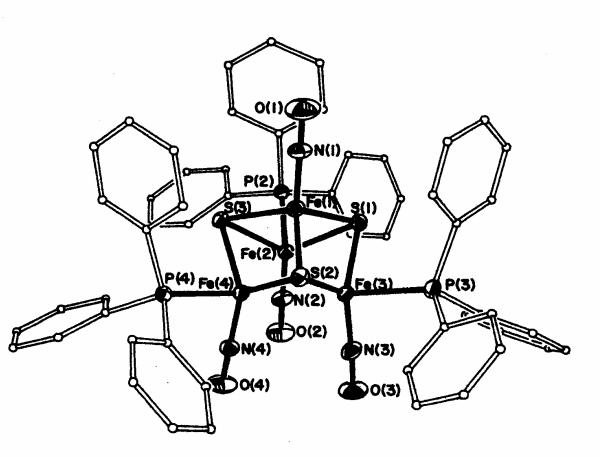

Figure 2.59 – Structure of $[Fe_4S_3(NO)_4(PPh_3)_3]^+$
From the solvated $[Fe_4S_3(NO)_4(PPh_3)_3]^+[Fe_4S_3(NO)_7]^-$ salt (30% probability ellipsoids). Selected interatomic distances [pm] and angles [º]: Fe(1)-Fe(2) 258.8(2), Fe(1)-Fe(3) 260.6(2), Fe(1)-Fe(4) 258.7(2), Fe(2)-Fe(3) 260.6(2), Fe(2)-Fe(4) 262.2(2), Fe(3)-Fe(4) 259.0(2), Fe(1)-S 224.0(9), Feb-S 220.6(9), Fe-P 228.0(6), S-Fe(1)-S 103(2), S-Fe(1)-N(1) 113.6(3), Fe(1)-S-Fe_b 71.4(4), Fe_b-S-Fe_b 72.4(7), S-Fe_b-S 107.4(9), S-Fe_b-N 125.4(17), S-Fe_b-P 92.3(4), N-Fe_b-P 98(3). Data involving P, S, and N atoms are mean values under idealized trigonal symmetry (Fe_b = Fe(2)-Fe(4)). Phenyl group orientations in this cluster and $[Fe_4S_3(NO)_4(PPh_3)_3]$ are similar. The structure of $[Fe_4S_3(NO)_4(PPh_3)_3]^+$ in this compound as in the PF_6^- salt are essentially identical. (Reprinted with permission from *Angew. Chem. Int. Ed. Engl*., **1993**, *32*, 564-566. Copyright 1993 John Wiley & Sons, Inc.)

Figure 2.60 presents the reactions through which the phosphine-ligated cuboidal clusters were formed. Reaction **1** involves reductive desulfurization of the cubane core of $[Fe_4S_4(NO)_4]$ accompanied by binding of phosphine. In reaction **2** PPh_3 is replaced by a more basic phosphine.

$$[Fe_4S_4(NO)_4] + 4R_3P \rightarrow [Fe_4S_3(NO)_4(PR_3)_3] + R_3PS \quad (1)$$

$$[Fe_4S_3(NO)_4(PPh_3)_3] + xPR_3 \rightleftarrows [Fe_4S_3(NO)_4(PPh_3)_{3-x}(PR_3)_x] \quad (2)$$

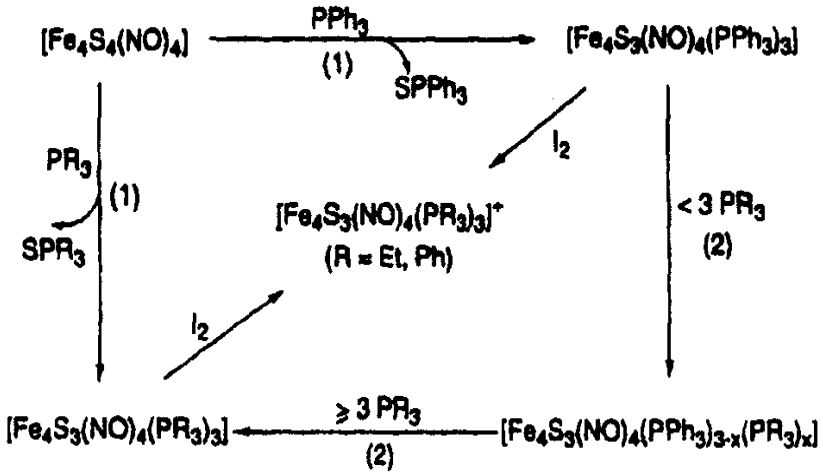

Figure 2.60 – Synthesis of $[Fe_4S_3(NO)_4(PR_3)_3]^{0,1}$ (R = Ph, Et, Pr^i, Cy)
Synthesis of cuboidal clusters $[Fe_4S_3(NO)_4(PR_3)_3]0,1$ (R = Ph, Et, Pr^i, Cy) (Reprinted from *Inorg. Chim. Acta, 270*, Synthesis and structures of the cuboidal iron-sulfur-phosphine clusters $[Fe_4S_3(NO)_4(PR_3)_3]0,1$ (R = Et, Pr^i, C_6H_{11}", 46-54, Copyright 1998, with permission form Elsevier 146).

Geiser and Williams prepared the analogous bis(tetra-*n*-butylammonium) hexa-μ_3-sulfido-hexakis(nitrosoiron), $(TBA)_2[Fe_6S_6(NO)_6]$, shown in figure 2.61, by substituting tetra-*n*-butyl ammonium hydroxide for ammonium hydroxide in synthesis of Roussin's salt.[151] The crystal structure shown in Figure 2.62 reveals that the $(TBA)_2[Fe_6S_6(NO)_6]$ complex is composed of two fused rings bearing terminal Fe bound nitrosyl groups. Bond lengths and angles are consistent with those reported by Scott and Holm[149].

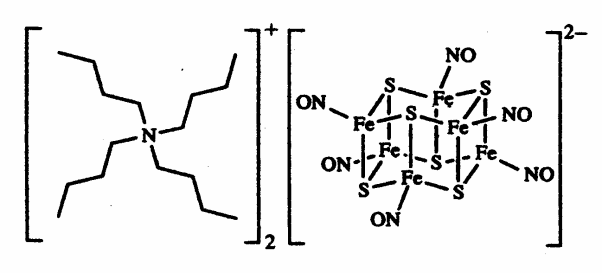

Figure 2.61 – $[N(C_4H_9)_4]_2[Fe_6S_6(NO)_6]$
Bis(tetra-*n*-butylammonium) Hexa-μ_3-sulfido-hexakis(nitrosoiron). (Reprinted from Acta Cryst., C54, Urs Geiser and Jack M. Williams, "Bis(tetra-*n*-butylammonium) Hexa-μ_3-sulfido-hexakis(nitrosoiron)", 292-293, Copyright 1998 with permission from the International Union of Crystallography).

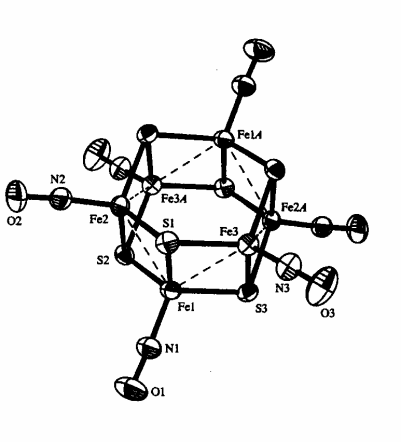

Figure 2.62 – The Anion in $(TBA)_2[Fe_6S_6(NO)_6]$
Shown with the anion in $(TBA)_2[Fe_6S_6(NO)_6]$ and with atomic labels. Selected inversion-symmetry-generated Fe atoms are indicated with a suffix A in the atomic label. The atomic displacement ellipsoids are drawn at the 50% probability level. Short Fe---Fe contacts of ca 2.6 Å are drawn as dashed lines. (Reprinted from *Acta Cryst*., C54, Urs Geiser and Jack M. Williams, "Bis(tetra-*n*-butylammonium) Hexa-μ_3-sulfido-hexakis(nitrosoiron)", 292-293, Copyright 1998 with permission from the International Union of Crystallography).

Longoni and co-workers completed electrochemical and chemical investigations of the redox behavior of the black Roussinate $[Fe_4(\mu_3\text{-}S)_3(NO)_7]^-$ monoanion.[144] They have compared the two forms of the redox couple $[Fe_4(\mu_3\text{-}S)_3(NO)_7]^{-\,/\,2\,-}$ as their tetraethylammonium salts (Figure 2.63), and made the spectroscopic assignments for the $[Fe_4(\mu_3\text{-}S)_3(NO)_7]^{-\,/\,2\,-\,/\,3-}$ series of compounds. Extended Huckel molecular orbital calculations revealed a doubly degenerate LUMO; the two orbitals, which are antibonding with respect to the Fe-Fe, Fe-S, and Fe-NO interactions, are derived mainly from the four iron atoms and either one of the remaining nitrosyl ligands. Structural evidence supports the theoretical conclusions.

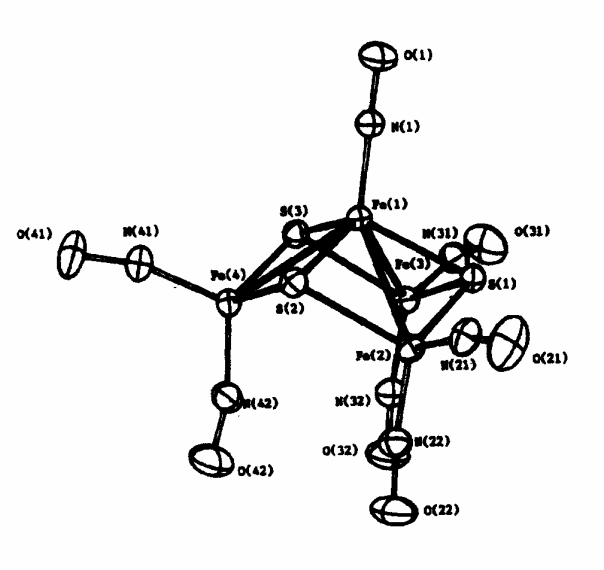

Figure 2.63 – ORTEP Drawing of $[Fe_4(\mu_3\text{-}S)_3(NO)_7]^-$ Monoanion
Also representative of that of the corresponding $[Fe_4(\mu_3\text{-}S)(NO)_7]^{2-}$ (Reprinted with permission from *Inorg. Chem.*, **1993**, *32*, 1153-1160. Copyright 1993 American Chemical Society.141)

Curtis and co-workers[152] synthesized a series of heterobimetallic iron sulfido nitrosyl clusters via the reactions shown in Figure 2.64 In the first reaction, two equivalents of $Na[Fe(CO)_3NO]$ along with $[Cp^{Et}{}_2Mo_2S_4]^{2+}$ ($Cp^{Et} = C_5Me_4Et$) in THF yield

$Cp^{Et}_2Mo_2Fe_2S_4(NO)_2$; in the second and third reactions, $Cp^{Et}_2Mo_2S_4$ and $Cp_2Mo_2(S)_2(\mu\text{-}SH)_2$ react with $Fe(NO)_2(CO)_2$ at reflux in toluene to produce the $Cp^{Et}_2Mo_2Fe_2S_4(NO)_2$ and $Cp_2Mo_2Fe_2S_4(NO)_2$ clusters, respectively. Another substrate, $Cp^*_2W_2S_4$, was used to prepare the tungsten Cp* analogue of the complexes shown in Scheme 2.64. $Cp^*_2W_2S_4$ reacted with 2.5 equivalents of $Fe(NO)_2(CO)_2$ at reflux in toluene for two hours to yield $Cp^*_2W_2Fe_2S_4(NO)_2$ (Figure 2.65). Crystal structures for $Cp^{Et}_2Mo_2Fe_2S_4(NO)_2$ and for $Cp^*_2W_2Fe_2S_4(NO)_2$ can be seen in Figures 2.66 and 2.67.

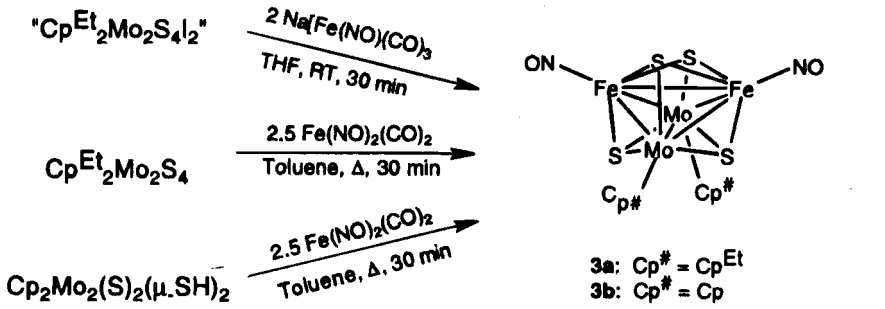

Figure 2.64 – Synthesis of Sulfido Nitrosyl Clusters
(Reprinted with permission from *Organometallics*, **1997**, *16*, 275-284. Copyright 1997 American Chemical Society 148).

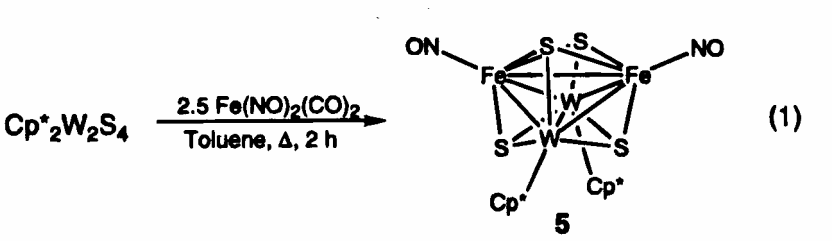

Figure 2.65 – Synthesis of the Cp* Analogue
(Reprinted with permission form *Organometallics*, **1997**, *16*, 275-284. Copyright 1997, American Chemical Society. 148).

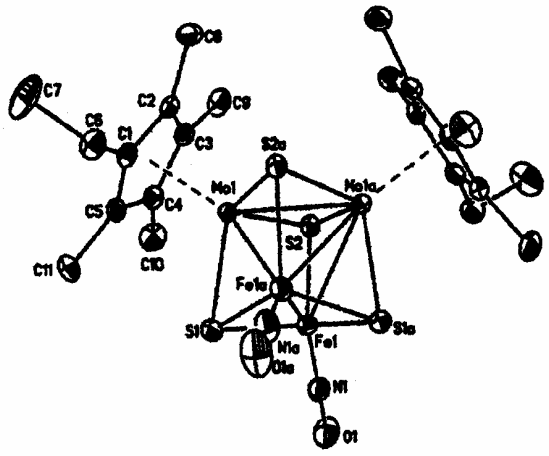

Figure 2.66 – ORTEP Plot of $Cp^{Et}_2MoFe_2S_4(NO)_2$
Shown with the atomic numbering scheme. Thermal ellipsoids are drawn at the 50% probability level. (Reprinted with permission form *Organometallics*, **1997**, *16*, 275-284. Copyright 1997, American Chemical Society 148).

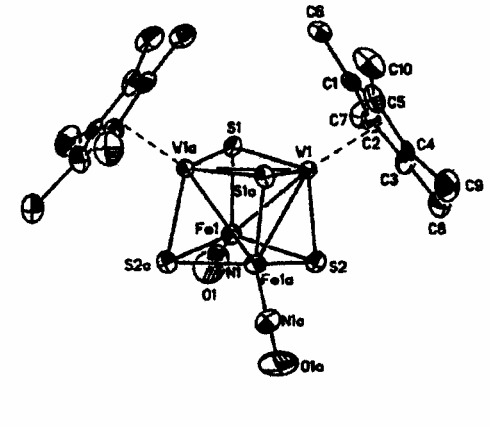

Figure 2.67 – ORTEP Plot of $Cp^*_2W_2Fe_2S_4(NO)_2$
Shown with the atomic numbering scheme. Thermal ellipsoids are drawn at the 50% probability level. (Reprinted with permission form *Organometallics*, **1997**, *16*, 275-284. Copyright 1997, American Chemical Society 148).

Core geometries are consistent with theoretical bonding schemes for clusters that follow the 18 electron rule. Electrochemical analysis reveals multiple stable oxidation states and lower energy HOMOs for these nitrosyl complexes in comparison to isostructural carbonyl complexes. This is consistent with better stabilization of the π electrons by NO^+ than CO.

Rossell and Seco et al.[153] were interested in using nitrosyl containing clusters as precursors to nitrido clusters via hydrogenation, electrophilic attack and deoxygenation. The ruthenium analogue of the target complex, $[Ru_6C\{AuPPh_3\}(CO)_{15}(NO)]$[154] had been synthesized by reacting $[Ru_6C(CO)_{15}(NO)]^-$ with $ClAuPPh_3$. This method was unsuccessful with $[Fe_6C(CO)_{15}(NO)]^-$ due to the poor nucleophilicity of the iron derivative in comparison to that of the ruthenium derivative. Another route, which involved the reaction between $(NEt_4)[Fe_6C\{\mu_3\text{-}AuPPh_3\}(CO)_{16}]$ with $NOBF_4$, yielded $[Fe_6C\{AuPPh_3\}(CO)_{15}(NO)]$; the same reaction with excess $NOBF_4$ produced $[Fe_4C\{AuPPh_3\}(CO)_{11}(NO)]$. $[Fe_4C\{AuPPh_3\}(CO)_{11}(NO)]$ was characterized by X-ray crystallography and elemental analysis. Among eleven linear CO groups, the NO group could not be identified conclusively from the X-ray crystal data; however, other experimental evidence indirectly confirms its presence.

Pergola, Manassero, and co-workers[155] reported an unusual reaction between $[Fe_4N(CO)_{12}]^-$ and $Mo(CO)_3(EtCN)_3$ which produces the $[Fe_6N(CO)_{15}]^{3-}$ and a small amount of the nitrido-nitrosyl iron cluster $[Fe_6N(CO)_{14}NO]^{2-}$ depicted in figure 2.68. The interstitial nitride is surrounded by the six iron atoms which define an octahedron. The linear nitrosyl group has an Fe-N-O angle of 176.4(3)° an Fe-N bond distance of 1.677(3) A, and absorbs in the infrared region at 1723 cm^{-1}. While it is clear that the NO ligand forms from oxidation of the exposed nitride, the oxygen source is uncertain. The authors propose that thermal activation of a carbonyl or molybdenum mediated splitting of a carbonyl may provide the oxygen.

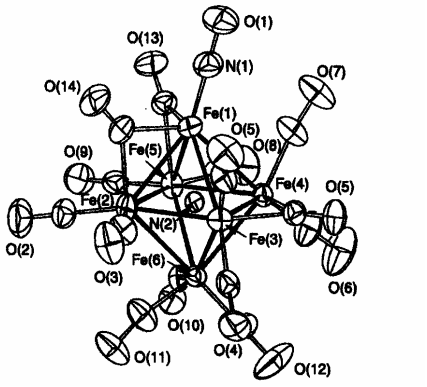

Figure 2.68 – The Solid State Structure of $[Fe_6N(CO)_{14}NO]^{2-}$
Carbon atoms are labeled as the oxygen to which they are attached. Relevant bond lengths and angles: Fe(1)-N(1) 1.677(3) Å, N(1)-O(1) 1.175(4) Å; Fe(1)-N((1)-O(1) 176.4(3)º. (*J. Chem. Soc. Dalton Trans*., **2001**, 2179-2183 - Reproduced by permission of The Royal Society of Chemistry. 151)

2.7. NON-HEME NITROSYL COMPLEXES

Many metalloproteins including deoxyhemerythrin,[154] ribonucleotide reductase,[156] and isopenicillin N synthase,[157] possess non-heme ferrous centers which reversibly bind NO to form EPR active S = 3/2 $\{FeNO\}^7$ centers. Two complexes, [Fe(EDTA)(NO)] and $Fe[Me_3TACN](NO)(N_3)_2]$ (Me_3TACN = N, N′, N″-trimethyl-1,4,7-triazacylcononane) are classic models of these complexes.[158-160] Wieghardt and co-workers[158] characterized the following octahedral nitrosyl iron complexes by UV-vis, EPR and Mossbauer spectroscopies: *trans*-[(cyclam)Fe(NO)Cl])ClO_4 ($\{FeNO\}^7$, (S = ½)), *cis*-[(cyclam)Fe(NO)I]I ($\{FeNO\}^7$, (S = 3/2)), *trans*-$[(cyclam)Fe(NO)Cl]^{2+}$ ($\{FeNO\}^6$, (S = 0)), and *trans*-$[(cyclam)Fe(NO)I]^0$ ($\{FeNO\}^8$, (S = 0)) where cyclam = 1,4,8,11 – tetraazacyclotetradecane.

Aminocarboxylates have also been investigated for potential use as an NO scavengers in sepsis.[161-163] Ward and Shepherd[164] studied the interaction of Ni^{II}, Cu^{II}, Zn^{II} and Fe^{II} complexes of *N*,*N*′-bis(pyridylmethyl)ethylenediamine-*N*,*N*-diacetate ($edampda^{2-}$) with NO. See Figure 2.69 for the structure of $edampa^{2-}$. [Fe^{II} $edampda^{2-}$], shown in Figure 2.70, readily and reversibly binds NO with a formation constant $K_f(NO) = 1.3 \times 10^4\ M^{-1}$. Its lack of charge and its greater resistance to oxidation compared to $[Fe^{II}(edta)]^{2-}$ make $[Fe^{II}(edampda^{2-})]$ a promising antisepsis agent and suggest that it may also be a better scavenger than $[Fe^{II}(edta)]^{2-}$ in some industrial applications. The $edampda^{2-}$ ligand accommodates a variety of coordination geometries as demanded by the d^n configuration as well.

In addition to their biological applications, Fe^{II} aminocarboxylate complexes are involved in a key step in the reduction of NO in denitrification processes in aqueous solution.[165,166] Aminocarboxylato complexes, such as $[Fe^{II}(edta)(H_2O)]$[166-169] are known for their propensity to bind rapidly and readily to NO.[170,171]

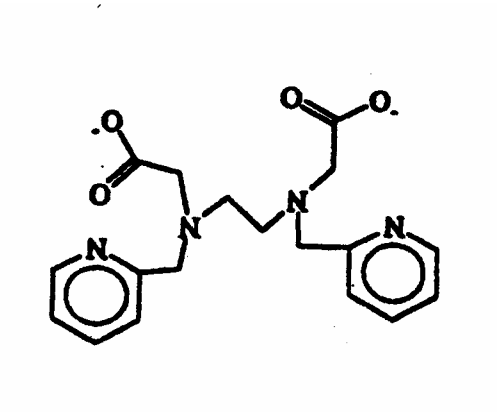

Figure 2.69 – *N,N′*- bis(pyridylmethyl)ethylenediamine - *N,N′*- diacetate (edampda^{2-})
(Reprinted from *Inorg. Chim*. Acta, 286, Matthew S. Ward, Rex E. Shepherd*, "A reversible NO Complex of [Fe^{II}(edampda)] and the Ni^{II}(edampda) analogue (edampda^{2-} = *N*, *N′*- bis(pyridylmethyl) ethylenediamine – *N*, *N′* - diacetate)" 197-206, Copyright 1999, with permission from Elsevier. 160)

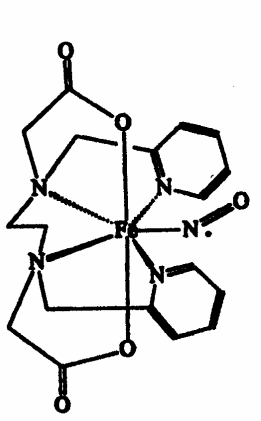

Figure 2.70 – [Fe^{II}(edampda^{2-})]
(Reprinted from *Inorg. Chim. Acta*, 286, Matthew S. Ward, Rex E. Shepherd*, "A reversible NO Complex of [Fe^{II}(edampda)] and the Ni^{II}(edampda) analogue (edampda^{2-} = N, N′- bis(pyridylmethyl) ethylenediamine – N, N′ - diacetate)" 197-206, Copyright 1999, with permission from Elsevier. 160)

Since aminocarboxylates are inexpensive, they are used in industry to remove NO from exhaust gases.[61,165,171] Consequently several studies have focused on NO binding to chelate complexes of Fe^{II}.[164,167] EDTA complexes are the most well studied because they offer many possibilities for variation. Detailed kinetic and thermodynamic data[170-174] as well as spectral data[62,159,170,171,175,176] are available for $[Fe^{II}(EDTA)(H_2O)]^{2-}$ complexes. For example Stochel and van Eldik *et al*.[177,178] have used ATR-IR,[171] UV-vis spectroscopy and other techniques to study the factors influencing the efficiency and reversibility of the NO binding process for the EDTA derivatives and other chelates shown in Figures 2.71, 2.72, 2.73, and 2.74.

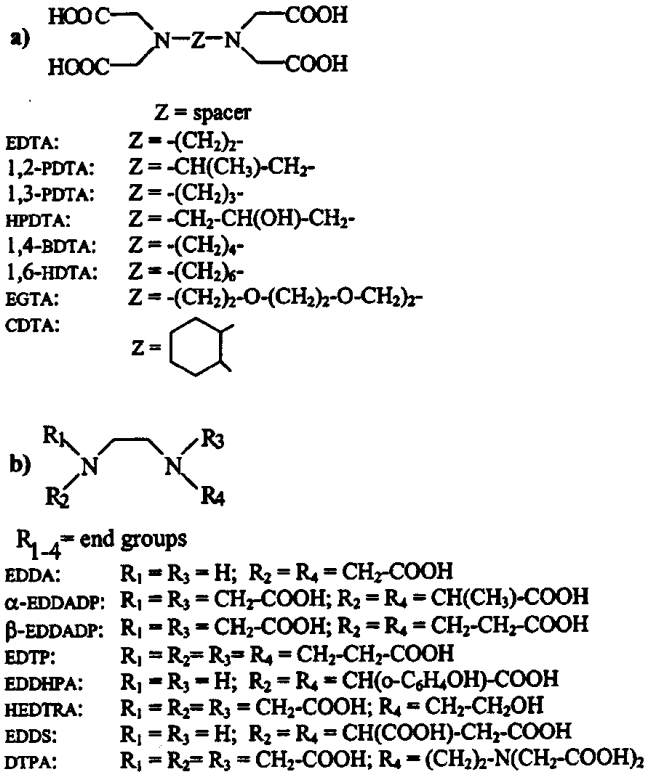

Figure 2.71 – EDTA Derivatives
(Reprinted with permission from *Eur. J. Inorg. Chem*. **2001**, 491-501. Copyright 2001, John Wiley & Sons 174).

Methyliminodiacetic acid (MIDA) derivatives (Figure 2.72) were studied to determine the effect of reducing chelate size on NO binding. The MIDA methyl group was replaced by a non-coordinating group, a coordinating group or a heteroatom.

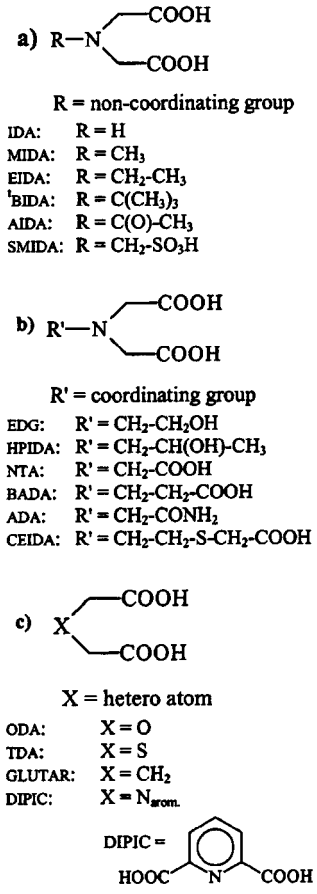

Figure 2.72 – MIDA Derivatives
(Reprinted with permission from *Eur. J. Inorg. Chem.*, **2001**, 491-501. Copyright 2001, John Wiley & Sons 174).

The third main group of multidentate ligands, unrelated to EDTA and MIDA, is shown in Figure 2.73.

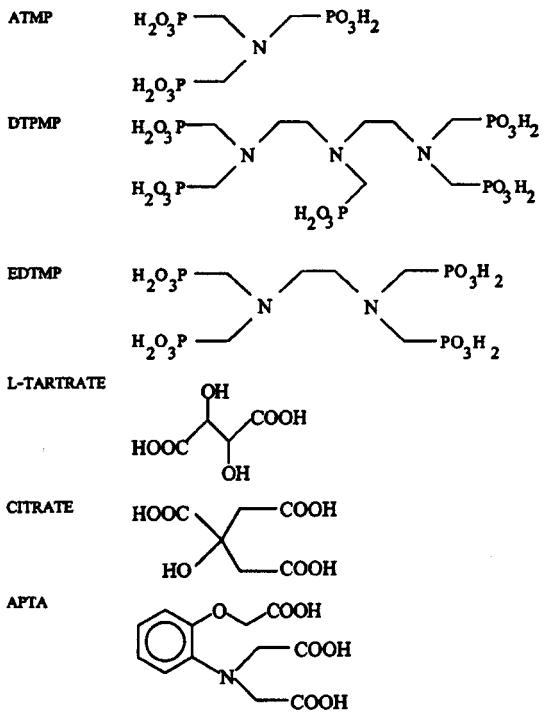

Figure 2.73 – Non - EDTA Chelating Ligands
(Reprinted with permission from *Eur. J. Inorg. Chem.*, **2001**, 491-501. Copyright 2001, John Wiley & Sons 174).

Stronger coordination was observed for chelate ligands bearing donor groups. Donor groups also accelerated oxidation of Fe^{II} to Fe^{III} by dioxygen as a result of their tendency to transfer electron density from iron to substrates such as dioxygen and nitric oxide. Finally, the binding constant for NO was found to increase as the inductive effect of the chelate increased. Oxygen sensitivity correlated with the decreasing ability of the $Fe^{II}(L)NO$ complex to release NO and with the tendency of the $Fe^{II}(L)NO$ to exist in solution as $Fe^{III}(L)NO^{-}$ before decomposing to $Fe^{III}(L)$ and N_2O. Van Eldik and co-workers continued their work with mechanistic studies of selected Fe^{II} complexes with the ligands shown in Figure 2.74.

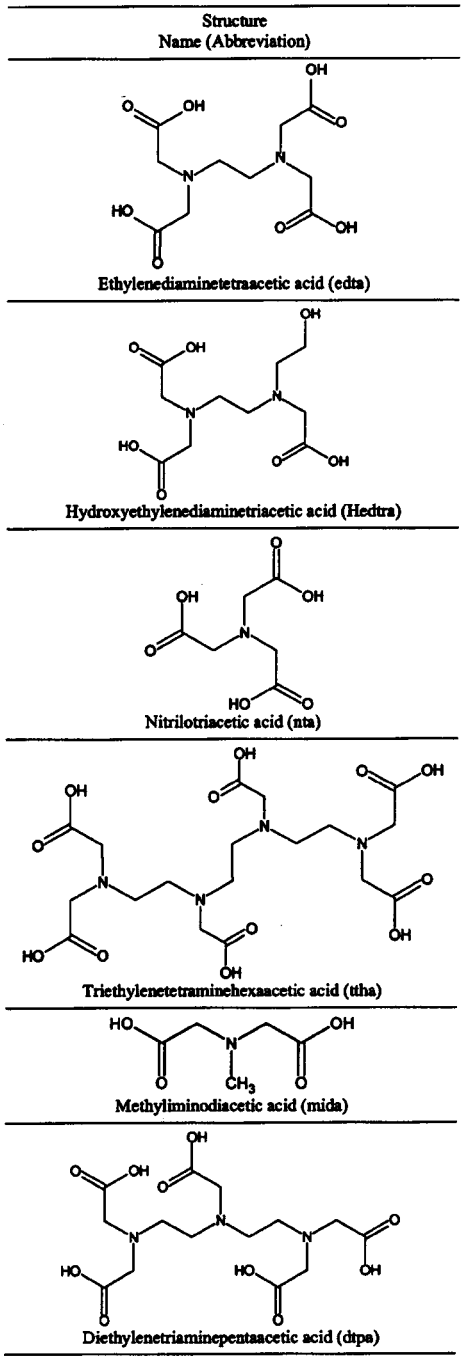

Figure 2.74 – Other Chelating Ligands
(Reprinted with permission from *Eur. J. Inorg. Chem*. **2001,** 2317-2325. Copyright 2001, John Wiley & Sons. 173)

The Fe^{II}mida complex was insensitive to oxygen, had a low binding affinity for NO and almost completely released NO under inert gas. Fe^{II}edta is very oxygen sensitive, had a high binding affinity for NO and released NO slowly and incompletely under inert gas. The oxygen sensitivity of the Fe^{II} complex suggests that the Fe(L)NO complex is stabilized in the form of $Fe^{III}(L)(NO^{-})$ similar to $Fe^{III}(L)O_2^{-}$, as demonstrated by Solomon et al.[159] Complementary stopped-flow, temperature jump, flash photolysis, and pulse radiolysis techniques were use to complete kinetic studies of the formation and dissociation of Fe(L)NO. The experimental data, combined with a variety of previously available kinetic data, illustrates the strong influence of the aminocarboxylato chelates on the rate constant and on the overall equilibrium constant. However, there appears to be no clear correlation between the constants and the donor groups or the charge on the iron (II) complexes. The binding of NO must be related to the lability of coordinated water to the iron(II) center; however, the dissociation reaction must be influenced by whether the metal center is Fe^{II}-NO or Fe^{III}-NO^{-} or Fe^{I}-NO^{+}, which should be related to the donor properties of the chelate. Since the rate constant of formation is likely to be controlled by the lability of coordinated water, the rate constant and activation parameters for solvent exchange reactions in the absence of a ligand were studied.[61]

The reversible binding of NO with aquated iron salts has been studied since 1906.[179-182] The brown ring test, in which the interaction of aquated Fe^{2+} with NO is used as a spot test for nitrite, is a familiar introductory chemistry lab experiment. Tarte[183] has reviewed studies on the decomposition products of the brown ring compounds in acidic, neutral, and alkaline solutions.[184-188] Early magnetic susceptibility, ESR, IR, Mossbauer, and other techniques led to the conclusion that the product of the iron ring test was appropriately considered as $[Fe^{I}(H_2O)_5(NO^{+})]^{2+}$.[189-193] However, more recent evidence from studies on non-heme iron

nitrosyl centers in inorganic complexes[11-13,121,159,160] and in proteins[154,156,157] along with data from EXAFS, XAS, Fe-edge measurements, resonance Raman spectroscopy, EPR, absorption spectroscopy, MCD spectroscopy, and applied field Mossbauer studies on a series of isostructural complexes containing the $\{FeNO\}^{6/7/8}$ unit indicated that the $\{FeNO\}^{7}$ unit is best described as $[Fe^{III}(H_2O)_5(NO^{-})]^{2+}$. The UV-vis, IR, Mossbauer and EPR evidence described by Stochel and van Eldik[178] confirms that the brown ring product is also most appropriately formulated as $[Fe^{III}(H_2O)_5(NO^{-})]^{2+}$, not as $[Fe^{I}(H_2O)_5(NO^{+})]^{2+}$ as previously believed. Activation values suggest that the nitrosylation occurs via a dissociative interchange mechanism in which NO acts as a nucleophile to displace coordinated water. The rate determining step is followed by rapid intramolecular charge redistribution to produce the final $[Fe^{III}(H_2O)(NO^{-})]^{2+}$. Overall, as NO displaces coordinated water, Fe^{II} is oxidized to Fe^{III} and NO is reduced to NO^{-}. Complete kinetic data is also reported for the reverse reaction, the release of NO to form $[Fe^{II}(H_2O)_6]^{2+}$. This water "assisted" homolysis reaction involves electron transfer followed by simultaneous displacement of NO by water.

There are relatively few well characterized $\{FeNO\}^{6}$ non-heme nitrosyl complexes.[158,194] Of the few $\{FeNO\}^{6}$ non-heme nitrosyl complexes that have been studied, a few have thiolates in their coordination sphere.[194,195] Artaud and co-workers[194] prepared the first five coordinate $\{FeNO\}^{6}$ complex with a mixed carboxamido nitrogen and thiolato sulfur donor set to study as a model for nitrile hydratase (NHase), an enzyme which binds NO at an Fe^{III} center N-coordinated to two peptide amides and S-coordinated to three cysteines. The model complex is short by one RS^{-} donor compared to the enzyme. The crystal structure of the diamagnetic square pyramidal Fe^{III}, S = 3/2 complex, depicted in Figure 2.75, reveals a linear NO group. The authors consider the Mossbauer data ($\delta = {}^{-}0.171$ mm s^{-1}) and low ν_{NO} of 1780 cm^{-1} as consistent with (Fe^{IV} NO^{-}).

They also acknowledge that ($Fe^{II}NO^{+}$) is a major contributor. When they prepared a related dithiolene $Fe(NO)L_2$ complex with four anionic RS^{-} donors, the analogous nitrosyl had properties attributed to ($Fe^{II}NO^{+}$) only.

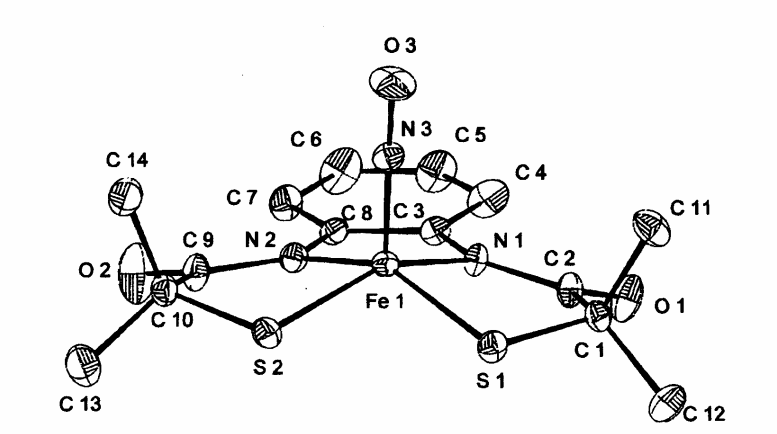

Figure 2.75 – X-ray Structure of $[Fe(N_2S_2)NO]^{-}$
Cameron projection of the X-ray structure of the nitrosyl complex 2 without H atom labeling (anionic part). Reprinted from *Inorg. Chim. Acta*, *336*, Sandrine Chatel, Anne-Sophie Chauvin, Jean-Pierre Tuchagues, Philippe Leduc, Echardt Bill, Jean Claude Chottard, Daniel Masuy, Idabelle Artaud, "Structural and spectroscopic characterization of a five coordinate $\{FeNO\}^6$ complex derived from an iron complex with carboxamido N and thiolato S donors," 19-28, Copyright 2002 with permission from Elsevier 175.

Initially, the Enemark–Feltham system, which has been used to predict bent or linear nitrosyls, was applied to strong field ligand sets that were available at the time of their work. Enemark and Feltham's rules do not explain cases for bent NO^{+} arrangements described by Hoffman or account for weak field metal nitrosyls. Current investigation into metal-nitrosyl ligand field effects have appeared to fill the void of the Enemark and Feltham assignments. Shepherd and co-workers[167] studied [$Fe^{II}L$] and $Fe^{II}L(NO)$ complexes of polyaminocarboxylates and pyridylmethylamines as models for $\{FeNO\}^7$ nitrosylated nonheme proteins which adopt

the unusual S = 3/2 spin state. The series of ligands studied, included nitrilotriacetate (nta^{3-}), *N*,*N*-ethylenediaminediacetate ($uedda^{2-}$), 2-pyridylmethyliminodiacetate ($pida^{2-}$), tris(2-pyridylmethyl)amine (tpa), and *N*, *N*, *N*′, *N*′-tetrakis(2-pyridylmethyl)ethylenediamine (tpen), illustrated in Figure 2.76, was chosen to demonstrate the effects of increasing ligand field strength or molecular orbital filling patterns. The complexes were investigated with differential pulse polarography (DPP), cyclic voltammetry (CV), and electron paramagnetic resonance spectroscopy (EPR). Of the $[Fe^{II}L]$ complexes studied, $[Fe^{II}(uedda)(H_2O)_2]$ had the lowest effective stability constant and was not studied further. Formation of the $Fe^{II}L(NO)$ complexes of the ligands nta^{3-}, $pida^{2-}$, and tpa was indicated by the appearance of yellow-green solutions upon admission of NO to the respective $Fe^{II}L$ complexes. Formation of the $Fe^{II}L(NO)$ complexes was confirmed by CV and DPP analysis. As depicted in Figure 2.77, EPR investigations show that, similar to the $[Fe(edta)NO]^{2-}$ control, which is known to be an S = 3/2 ground state with resonances

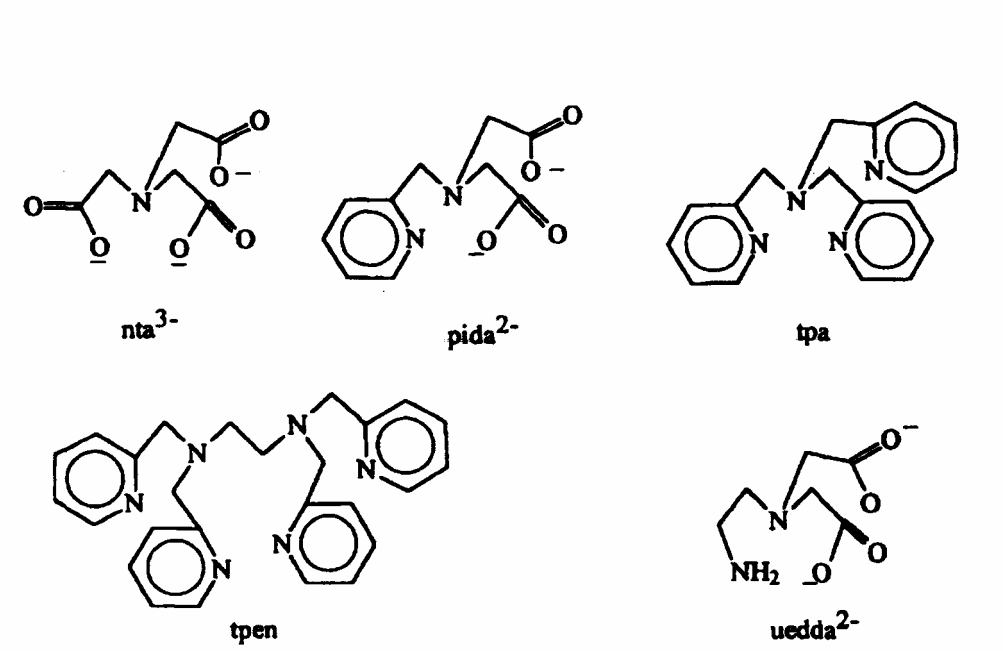

Figure 2.76 – Polyaminocarboxylate and Pyridylmethylamine Complexes
(Reprinted form *J. Inorg. Biochem*., Rex E. Shepherd*, Michael A. Sweetland, Diane E. Junker, 65, "Ligand field factors promoting S = 3/2 $\{FeNO\}^7$ nitrosyls", 1-14, Copyright 1997 with permission from Elsevier. 163)

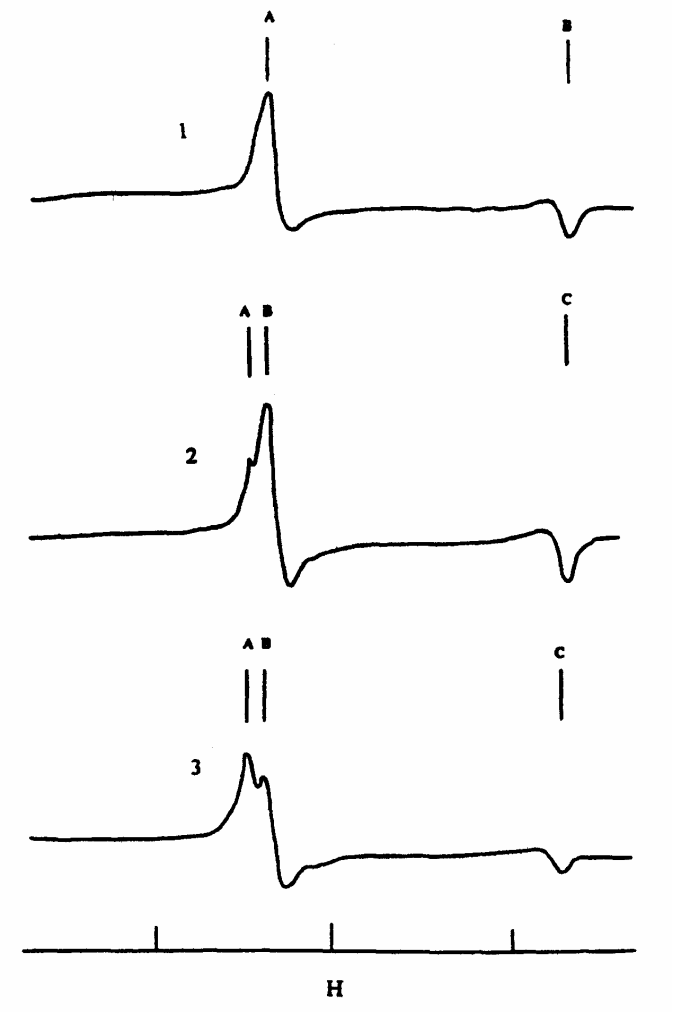

Figure 2.77 – EPR Spectra of [FeL(NO)] Complexes
At 77 K in 0;01 M frozen NaCl. $[Fe^{II}L] \approx 5.0 \times 10^{-3}$ M, Ar/NO gas passed for 3-5 min. before freezing in liquid N_2: (1) $[Fe(pida)(H_2O)NO]$, field markers; A, B: g = 4.02 and 2.00: (2) $[Fe(nta)(NO)(H_2O)]^-$, field markers: A, B, C: g = 4.36, 4.02, and 2.00: (3) $[Fe(edta)NO]^{2-}$ (control), field markers: A, B, C: g = 4.28, 4.02, and 2.00. (Reprinted form *J. Inorg. Biochem*., Rex E. Shepherd*, Michael A. Sweetland, Diane E. Junker, 65, "Ligand field factors promoting S = 3/2 $\{FeNO\}^7$ nitrosyls", 1-14, Copyright 1997 with permission from Elsevier. 163)

at g = 4.1, 3.9, and 2.0, $[Fe(nta)NO(H_2O)]^-$ and [Fe(pida)(H_2O)(NO)] exhibit resonances near g = 4.0 and 2.0 which also indicate an S = 3/2 ground state. A nearly axial EPR spectrum with peak and trough features at g = 4.00 and 3.48 indicate a ground state S = 3/2 nitrosyl for $[Fe(tpa)Cl(NO)]^+$ as well. In contrast, EPR studies of $[Fe(tpen)NO]^{2+}$ reveal signals at g = 2.032, 1.973, and 1.960. Since the starting complex, $[Fe(tpen)]^{2+}$, is known to be six coordinate, NO addition must occur either with loss of a pyridyl donor or with expansion of the coordination number to seven. Since a seven coordinate pentagonal bipyramidal moiety would reduce ring strain for all pyridyl donors, and since no N-*shf* structure appears in the EPR spectrum, coordination most likey occurs with the expansion of coordination number. EPR and electrochemical data suggest a HOMO with an almost purely metal centered character.

The EPR and electrochemical results, and the fact that CO fails to coordinate to $[Fe^{II}(nta)]$, $[Fe^{II}(pida)]$ and $[Fe^{II}(tpa)$ fragments are explained by the ligand field splitting diagrams of six coordinate complexes shown in figure 2.78. In the absence of a strong ligand field, metal d orbitals lie above the ligand based bonding molecular orbitals and below the π^*_{xy} levels of NO. The approximate C_{4v} symmetry is split into C_s symmetry, which is more correct for asymmetric six coordinate complexes. The molecular orbital diagram for free NO and free Fe(II) in D_5h symmetry, illustrated to the left in Figure 2.78, is ensured by failure of NO to oxidize Fe(II) in the absence of coordination. The second molecular orbital diagram in Figure 2.78 shows that the $(e\pi^*_{xy})^1$ orbitals of the NO ligand split as the FeNO moiety bends upon NO coordination in the presence of weak field donors, such as the nitrogen and the oxygen donors of nta^{3-}, $pida^{2-}$, or tpa (Figure 2.76). The ligand based π^* orbitals remain at higher energy, albeit close to the energy of the d orbitals. As a result, spin pairing of the $1a''_{yz}$ orbital is removed and an electron transfers to the NO π^* orbital, spin parallel with the original π^* electron of free NO. The presence of

electrons in the $2a''_{xz}$ and $1a''_{yz}$ with simultaneous filling of the $a\pi^*_{x(NO)}$, $a\pi^*_{y(NO)}$ levels requires the spin opposed arrangement in order for electrons to share the same region of space since the π^* based molecular orbitals of NO are spatially overlapping with the a_{yz} and a_{xy} orbitals.

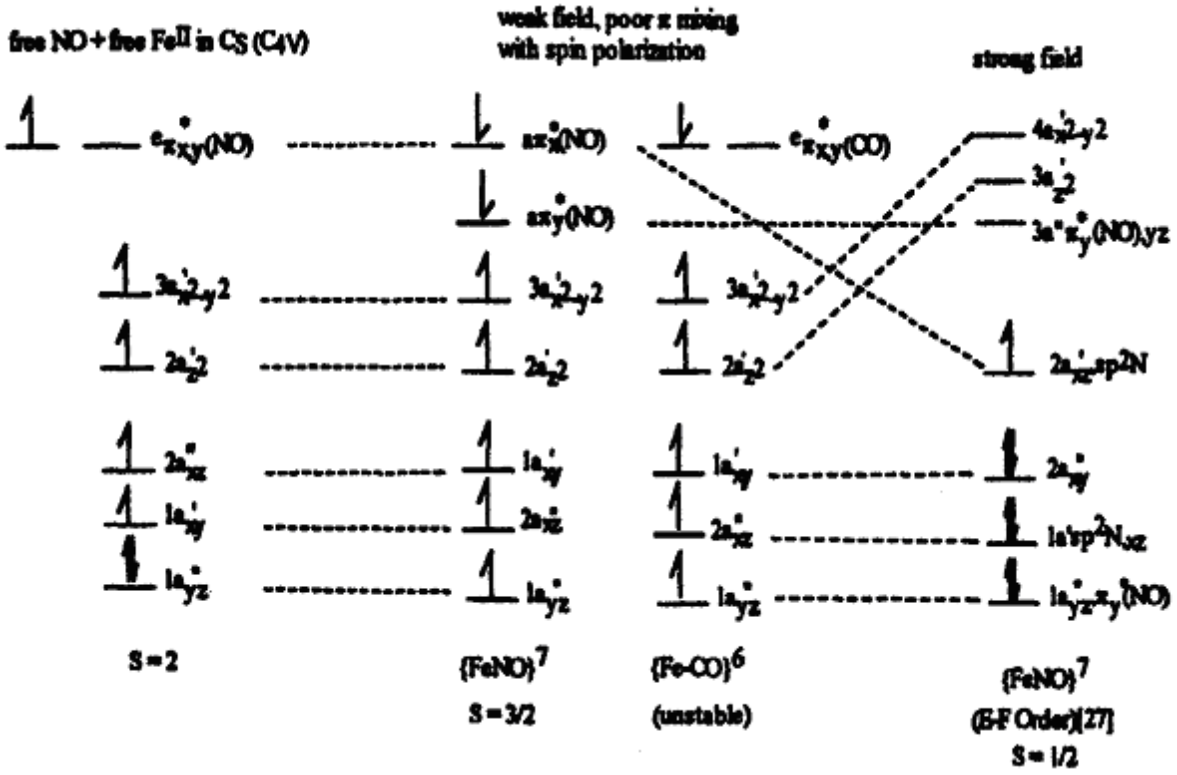

Figure 2.78 – Six-coordinate Complexes before Jahn-Teller Effects
Note: The spacing between MO levels is actually increased in the strong field case, promoting spin pairing. The figure does not mean to imply equal spacing energetically. (Reprinted form *J. Inorg. Biochem*., Rex E. Shepherd*, Michael A. Sweetland, Diane E. Junker, 65, "Ligand field factors promoting S = 3/2 $\{FeNO\}^7$ nitrosyls", 1-14, Copyright 1997 with permission from Elsevier. 163)

Solomon[196] had previously presented the same argument to explain the similar influence in $[Fe(edta)NO]^{2-}$. Spin polarization stabilizes the system and produces a net S = 3/2 ground state for $[Fe(nta)NO]^{-}$, $[Fe^{II}(pida)NO(H_2O)]$ and $[Fe^{II}(tpa)NO(X)]^{+}$ (X = Cl^{-}, $CH_3CO_2^{-}$, $H_2PO_4^{-}$, etc.). Spin polarization also substantially stabilizes metal ligand bonds when π bonding is poor. The existence of a weak field six coordinate $\{FeNO\}^7$ species, then, is largely due to the stabilization conferred by spin polarization. The weak field molecular orbital diagram for NO coordination yields formal electron counting assignments of $\{Fe^{III}$, S = 5/2), NO^{-} (S = 1)}; however, the coordination number of six ultimately influences the percentage of NO based character. In contrast with the molecular orbital diagram for the weak ligand field case, in the presence of a strong ligand field the energy of the $d_{x^2-y^2}$ levels is higher than that of the π^* levels of NO, a situation that favors π mixing between the d_{xz} orbital and the π^*_x orbital of NO. The π^*_x and the π^*_y orbitals of NO split to give σ based sp^2 type orbital and an energetically increased $2a'_{(xzsp^2_N)}$ level. As a result the strong field order reverts to the one predicted by the Enemark–Feltham rules.

Except for approximate D_{5h} symmetry, characteristic of a pentagonal bipyramid, the analysis for seven coordinate complexes is similar to that for six coordinate complexes (pseudo-C_{4v} symmetry). Column 2 of Figure 2.79 shows the molecular orbitals of seven coordinate weak-field complexes such as $[Fe(edta)NO]^{2-}$. The seven coordinate complexes establish spin polarization to yield an Fe^{III} (S = 5/2), NO^{-} (S = 1) electronic arrangement with a net spin of 3/2 in the ground state. Column 3 in figure 2.79 illustrates the molecular orbital order for seven coordinate strong field complexes such as $[Fe(tpen)NO]^{2+}$. Stabilization is enhanced by mixing the $e_{xz,yz}$ with two orbitals of suitable π* symmetry from ligands such as the pyridyl donors of

tpen. After the appropriate Jahn–Teller distortion, column 4 in figure 2.79 shows that the highest energy electron resides in purely metal based orbital parented largely by d_{xy}. As a consequence, the EPR spectral lines should lack *shf* coupling from the coordinated NO group, as is observed experimentally. Thus, the formal electron assignment for strong field six or seven coordinate complexes is best designated as {Fe(I)(S=1/2), NO^+ (S =0)} for a net S = ½ ground state for the tpen complex.

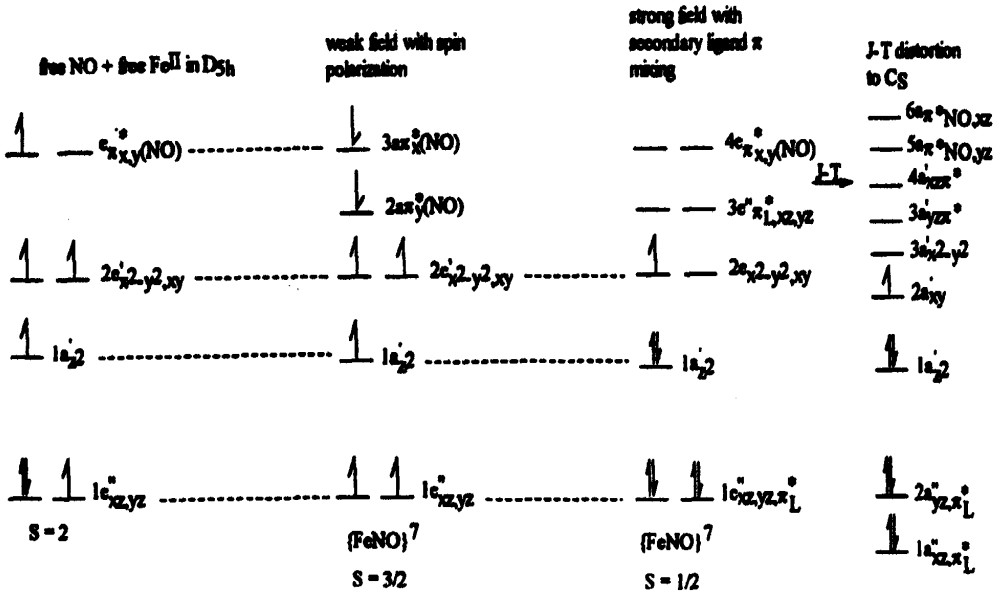

Figure 2.79 – Ligand Field Splitting Diagram for Seven Coordinate Complexes
(Reprinted form *J. Inorg. Biochem*., Rex E. Shepherd*, Michael A. Sweetland, Diane E. Junker, 65, "Ligand field factors promoting S = 3/2 $\{FeNO\}^7$ nitrosyls", 1-14, Copyright 1997 with permission from Elsevier. 163)

In contrast with the highest occupied molecular orbital for seven coordinate $\{FeNO\}^7$ complexes, the HOMO for six coordinate $\{FeNO\}^7$ complexes retain nitrogen-based as well as d_{xz} character, as shown in Figure 2.79. Hence, strong-field six-coordinate $\{FeNO\}^7$ complexes should exhibit *shf* coupling. This EPR spectral outcome was observed with the strong field macrocyclic 2,3,9,10-tetramethyl-1,4,8,11-tetraazacyclododeca-1,3,8,10-tetraene (TIM) ligand (Figure 2.80) which produces low-spin Fe^{II} complexes. $[Fe(TIM)(CH_3CN)(NO)]^{2+}$ exhibits N-*shf* coupling from the axial NO group and an S = ½ ground state.

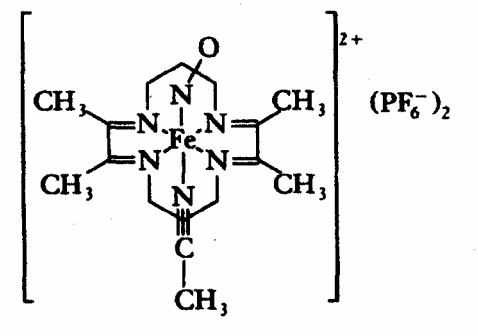

Figure 2.80 – TIM Ligand
(Reprinted form *J. Inorg. Biochem*., Rex E. Shepherd*, Michael A. Sweetland, Diane E. Junker, 65, "Ligand field factors promoting S = 3/2 $\{FeNO\}^7$ nitrosyls", 1-14, Copyright 1997 with permission from Elsevier. 163)

2.8. CONCLUSION

In conclusion, iron porphyrin nitrosyl complexes, non-heme iron nitrosyl complexes, iron nitrosyl cluster complexes, and the other iron nitrosyl complexes discussed in this paper are important in many biological processes (Appendix B). Their importance stems from their role as nitric oxide carriers and from the range of structural forms they exhibit. For example, upon coordination with NO, a change in the geometry of an iron heme in guanylate cyclase induces a conformational change that opens an active site to guanosine triphosphate. Guanosine triphosphate is then converted to cyclic guanosine monophosphate which helps regulate blood pressure. In order to develop iron nitrosyl complexes for medicinal purposes, it is crucial to understand the nature, origin and effect of such structural changes.

Structural features of iron nitrosyl complexes are controlled by several factors. The dominant factors seem to be the number of electrons within the MNO moiety (n in $\{MNO\}^n$) and the coordination number. Within a given $\{MNO\}^n$ and coordination number system, subtle changes of the ligand donors alter the placement of NO π^* orbitals relative to the d orbitals within a certain geometry. Population of antibonding orbitals in these systems leads to a bent nitrosyl group. The recent identification of many Fe spin state coupled with NO spin state combinations, expands MNO characterization well beyond the standard classifications for linear NO^+ or bent NO^- systems. For example, deviations from linearity for $\{MNO\}^6$ systems, have been observed. Refinement of early classifications to account for such deviations is made possible by the many analytical techniques available today. Together, Cyclic voltammetry, EPR, magnetic susceptibility, NMR, and X-ray crystallography, Mossbauer spectroscopy, and UV-vis spectroscopy are used to establish and verify the geometry of NO, as well as the oxidation state,

and spin state assignments within the MNO unit. These techniques provide a more complete picture of iron nitrosyl complexes than was ever possible. The trend toward merging biological and chemical knowledge about iron nitrosyl complexes provides a more balanced perspective on what mechanisms control the behavior of the various physiologically important iron nitrosyl complexes. All of these factors combine to accelerate advances in iron nitrosyl chemistry and in transition metal nitrosyl chemistry.

APPENDIX A

NITRIC OXIDE SYNTHASE

Lincoln *et al*.[27] have summarized the evolution of the nomenclature that describes the isoforms of nitric oxide synthase. Initially nitric oxide synthases were classified in terms of whether their activity was calcium dependent, (cNOS) or calcium independent (iNOS). At the time it was accepted that, in general, cNOS is constitutive (ever present under normal conditions; activation doesn't require new enzyme protein synthesis) while iNOS is inducible (only expressed under activation; new enzyme protein synthesis occurs in response to certain stimuli).[197] Constitutive NOS enzymes are responsible for mediating rapid events such as neurotransmission and blood vessel dilation. For example, within seconds a glutamate induced increase in Ca^{2+} levels activates neuronal NOS via calmodulin; similarly, the endothelial form of NOS is activated by an increase in intracellular Ca^{2+} which facilitates binding of calmodulin. The increase in intracellular Ca^{2+} is caused by activation of the phosphoiniside cycle by action of acetylcholine or bradykinen on endothelial muscarinic or bradykinen receptors. The function of calmodulin will be discussed in more detail later. An example of an inducible NOS is the NOS that is induced in macrophages by the presence γ-interferon and lipopolysaccharide to destroy tumors.[197]

As experimental evidence accumulated, it became apparent that some inducible NOS enzymes are also constitutive, and that constitutive NOS enzymes could be induced.[197] So another classification was developed based upon whether the cells of NOS origin were endothelial (eNOS) or neuronal (nNOS). When the three isoforms were finally purified and cloned, another designation was required because, while the first isoform (Type I NOS) is

constitutive and found in neurons in rat and porcine cerebellum, it is also present in skeletal muscle, endometrium, and neutrophils, among other tissues and cells. The second isoform (Type II NOS), which is inducible, was cloned from murine macrophages, and is also inducible in cells from neurons and from endothelial cells. The isoform (Type III NOS) that was cloned from bovine vascular endothelial cells is also present in neurons. Since a family of three genes has been identified to encode for the three forms of NOS, Nathan and Xie[198] have proposed to combine the findings on the NOS genes with an earlier numerical classification to define the isoforms in a way that is independent of the cells of origin or of whether they are inducible or constitutive, but that expresses the dependence of their activity on Ca^{2+}. Their suggested nomenclature is shown in Figure A.1. Another classification is based upon the physiological roles played by NO. These are as follows, inducible NOS (iNOS, immune system), neuronal NOS (nNOS) and endothelial NOS (eNOS cardiovascular system).[18]

Preferred Designation			
Numerical[a]	Descriptive	Definition	Chromosomal Localization (Human)
I	ncNOS	NOS whose activity depends on elevated Ca^{2+},[b] of the type first identified in neurons	12q24.2
II	iNOS	NOS whose activity is independent of elevated Ca^{2+},[b]	17cen-q12
III	ecNOS	NOS whose activity depends on elevated Ca^{2+},[b]7 of the type first identified in endothelial cells	q35-36

[a] Simplified from Schmidt et al (1991).
[b] Above the level in resting cells

Figure A.1 – NOS Nomenclature
(Reproduced from *Cell*, Carl Nathan and Qioa Wen Xie, "Nitric Oxide Synthases: Roles, Tolls and Controls", 915- 918, Copyright 1994 with permission from Elsevier. 196)

Once the NOS isoforms were cloned, the structures of the three isoforms were elucidated. As shown in Figure A.2, nitric oxide synthases all seem to include an oxygenase and a reductase domain between which the Ca^{2+} dependent binding protein, calmodulin, resides.[26,27,197] The reductase domain is homologous with that of cytochrome P450 reductase, which is also shown in

Figure A.2. Cytochrome P-450 reductase is the only other mammalian enzyme that exhibits recognition sites for nicotinamide adenine dinucleotide phosphate, (NADPH) flavin mononucleotide (FMN), and flavin adenine dinucleotide (FAD)[197,199] (Figure A.3).

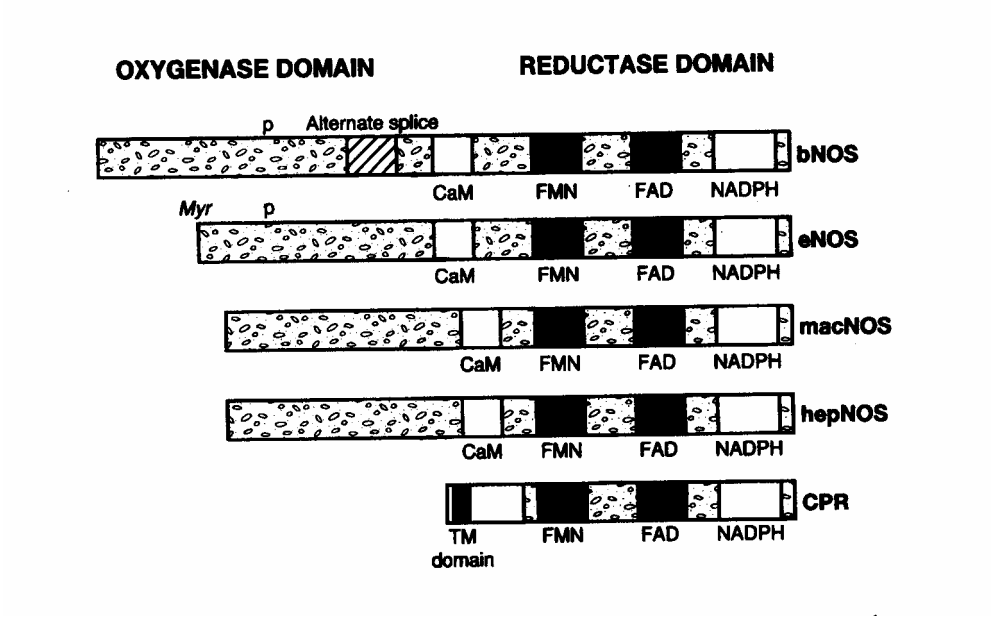

Figure A.2 – NOS Isoforms and NADPH-Cytochrome P450 Reductase
"Diagram displaying the structural relationship between the NOS isoforms and NADPH-cytochrome P450 reductase (CPR). The cloned NOS isoforms from brain (bNOS), endothelium (eNOS), macrophage (macNOS), and hepatocytes (hepNOS) are all comprised of an oxygenase and reductase domain, with a binding domain for calmodulin between them. The reductase domain contains binding sites for NADPH, FAD, and FMN, and is homologous with the dual flavin enzyme NADPH-cytochrome p450 reductase. The oxygenase domain on bNOS and eNOS contain phosphorylation sites (P). Also noted are a myristoylation site near the N terminus of eNOS, a hydrophobic transmembrane anchoring domain in CPR." (Reprinted from *Nitric Oxide Principles and Actions*, "The Intracellular Reactions of Nitric oxide in the Immune System and Its Enzymatic Synthesis", Jack Lancaster, Jr. and Dennis J. Stuehr, p.153, Copyright 1996, with permission from Elsevier.)

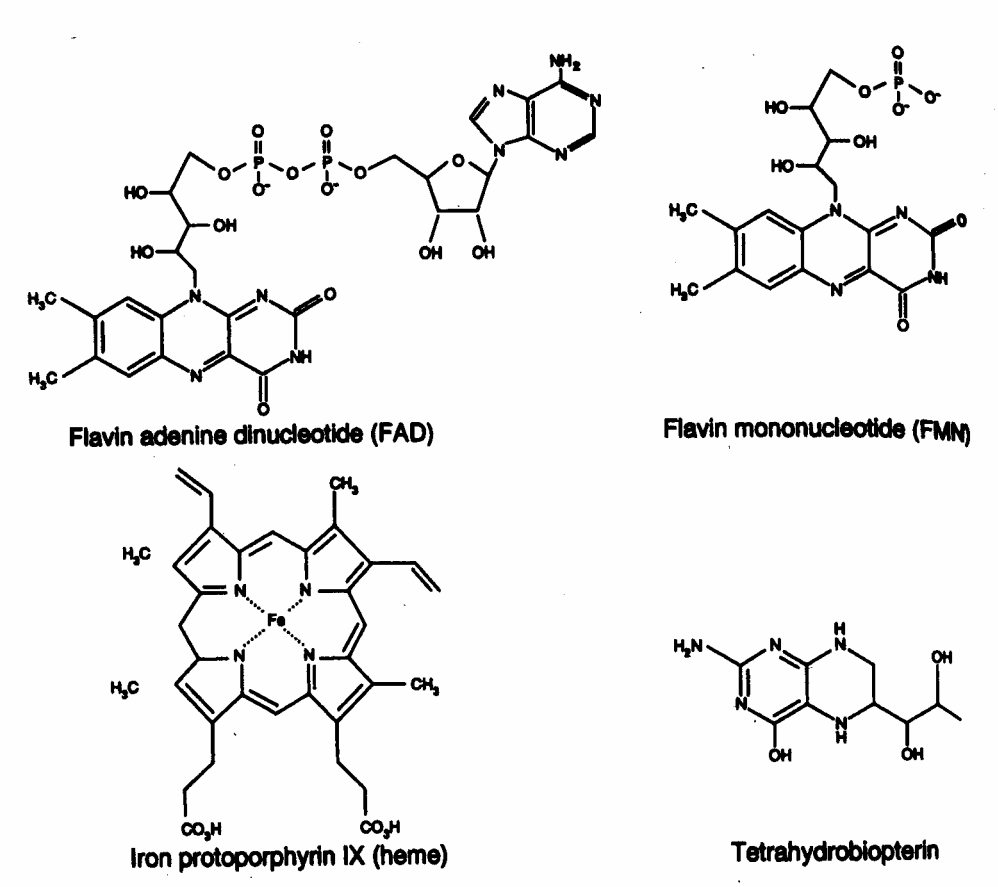

Figure A.3 – Prosthetic Groups Contained within NOS
"Prosthetic groups contained within NOS. Nitric Oxide synthases are isolated containing approximately one molecule each of heme, FAD, and FMN per subunit, and also contain variable quantities of tetrahydrobiopterin (0.1 to 1 molecule per subunit)" (Reprinted from *Nitric Oxide Principles and Actions*, "The Intracellular Reactions of Nitric oxide in the Immune System and Its Enzymatic Synthesis", Jack Lancaster, Jr. and Dennis J. Stuehr, p.152, Copyright 1996, with permission from Elsevier.)

The Combination of NADPH, FMN and FAD in NOS suggests that, as in cytochrome P450 reductase, the NOS flavins store NADPH derived electrons prior to transferring them to a catalytic center in the NOS oxygenase domain. The heme unit and the tetrahydrobiopterin are presumed to bind in the oxygenase domain. A highly conserved 320-amino-acid region exists in all NOS oxygenase domains. Modeling studies have shown that within this sequence is a

cysteine residue which may be involved in heme iron ligation.[200,201] The heme unit reacts with CO to form a species which absorbs at 445 nm. CO also inhibits purified NOS. These observation also suggest the involvement of a cytochromeP-450 type heme which is coordinated to a cysteine ligand.[28,200,202,203] However, as Figure A.4 shows, there is no significant homology between the cytochrome P-450 and NOS, even at the N-terminus where the heme is located. See figure A.2. This lack of homology is expected since the P-450's act on hydrophobic substrates while NOS acts on L-arginine which is hydrophilic. So, while NOS uses the P-450 chromophore, NOS itself doesn't fit the category of P-450 enzyme.[204]

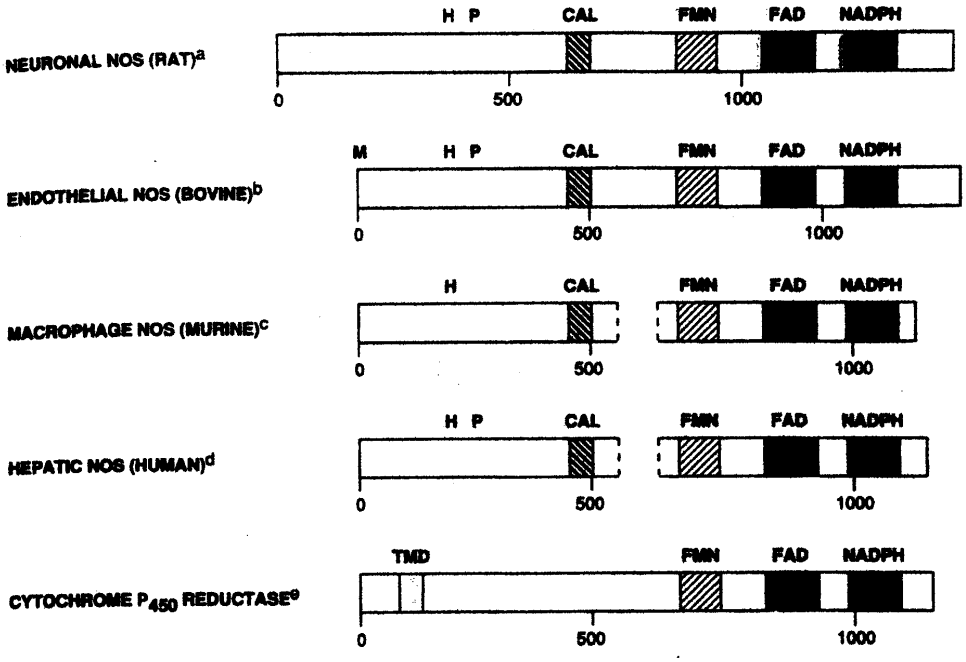

Figure A.4 – Sequence Homologies of Molecular Isoforms of NOS
"Sequence homologies of molecular isoforms of NOS. All NOS enzymes cloned thus far have homologous regions to cytochrome P450 reductase and substrate binding sites that reflect the oxidative mechanism of NO biosynthesis. Consensus binding sites for FAD, FMN, NADPH, and calmodulin are conserved for all NOS enzymes cloned. Protein kinase A phosphorylation sites (labeled P). Abbreviations: P, consensus sequence for phosphorylation by cAMP-dependent protein kinase; CAL, calmodulin binding site; FMN, flavin mononucleotide; FAD, flavin adenine dinucleotide; H, heme binding site; NADPH, reduced form of nicotinamide adenine dinucleotide phosphate; TMD, transmembrane domain, M, myristoylation site. (Reprinted with permission from *J. Neurosci*., **1994**, 14, 5147-5159. Copyright 1994 Society for Neuroscience. 195)

The peptide that connects the heme and the flavin domains is the peptide that binds calmodulin in the presence of Ca^{2+}. Binding to calmodulin[16,22,205] induces a structural change that permits electrons to flow from the flavin to the heme domain Figure A.5.

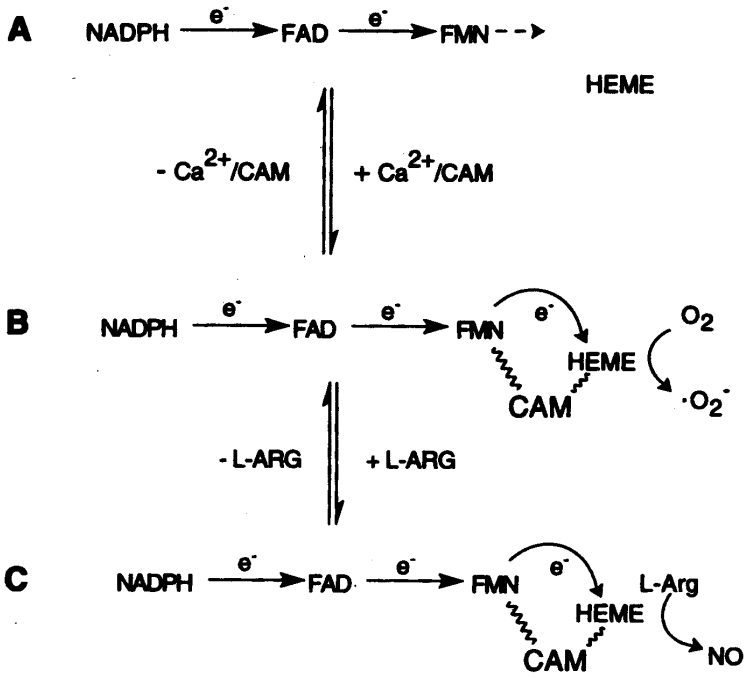

Figure A.5 – Role for Calmodulin in Control of Heme Reduction in NOS
"Role for calmodulin in control of heme reduction in NOS. (A) In the absence of bound calmodulin, electrons derived from NADPH can load into the flavins but cannot be transferred onto the heme iron. (B) On calmodulin binding, electrons transfer from the flavins onto the heme. In the absence of bound L-arginine, heme reduction generates superoxide (C), whereas in the presence of L-arginine, heme **reduction** can lead to NO synthesis." **(**Reprinted from *Nitric Oxide Principles and Actions*, "The Intracellular Reactions of Nitric oxide in the Immune System and Its Enzymatic Synthesis", Jack Lancaster, Jr. and Dennis J. Stuehr, p.161, Copyright 1996, with permission from Elsevier.)

In the presence of L-arginine, electron transfer to the heme generates NO. Calmodulin and Ca^{2+} control the activity of the constitutive NOS forms, so, it was not surprising that calmodulin sequences were found in all constitutive isoforms. It was surprising, however, that the inducible forms of NOS also exhibited calmodulin recognition sequences. The discrepancy was resolved when the iNOS derived from murine macrophages was purified with calmodulin subnunit bound so tightly that it rendered the NOS virtually insensitive to changes in Ca^{2+} concentration.[204,206] This keeps iNOS in its active state.[206] The affinity of that particular iNOS for calmodulin is sufficiently high that only negligible amounts of Ca^{2+} are required for activation. Other inducible isoforms are somewhat inhibited upon exposure to Ca^{2+}chelating agents, CaM antagonists, or both. The propensity of constitutive and inducible isoforms to bind calmodulin is depicted in Figure A.6.

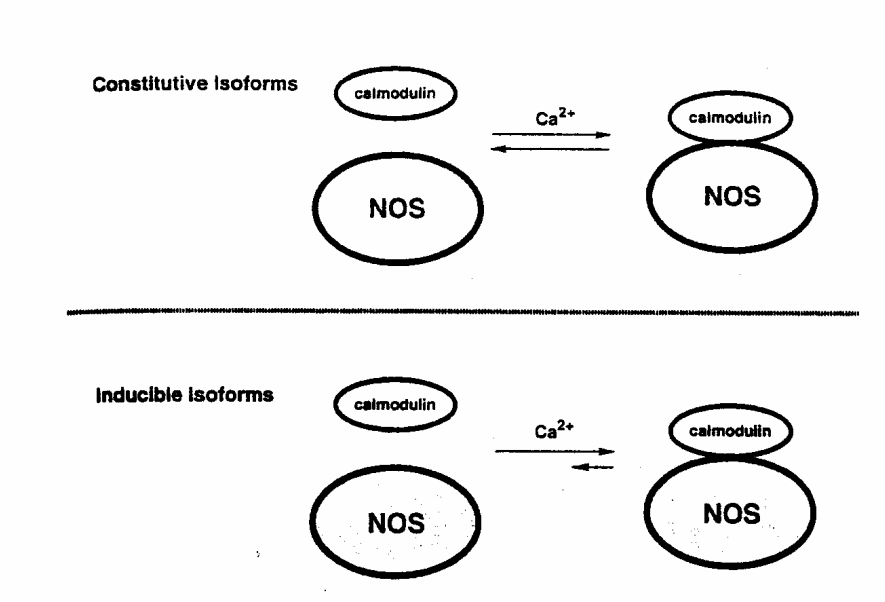

Figure A.6 – Calmodulin Binding
Calmodulin Binding by Constitutive and Inducible NOS Isoforms (Reprinted from *Cell* **78**, Michael Marletta, "Nitric Oxide Synthases: Aspects Concerning Structure and Catalysis, 927-930, Copyright 1994, with permission from Elsevier.)

Although the exact role of tetrahydrobiopterin, a redox active cofactor,[207-210] is unclear, it may facilitate L-arginine binding by stabilizing the enzyme.[29,211,212] Whether tetrahydrobiopterin is redox active in NOS is not known conclusively. It is known that tetrahydrobiopterin deficient NOS displays a diminished capacity to generate NO via electron flow from NADPH.[207,211,213] Instead of producing NO, the tetrahydrobiopterin deficient NOS transfers electrons from NADPH to oxygen to create superoxide.[213] So, tetrahydrobiopterin seems to be involved in connecting NOS NADPH oxidation with NO synthesis. Tetrahydrobiopterin also may have a catalytic role in NO synthesis. Brain and macrophage NOS isoforms exist as homodimers.[202,214,215] A mixture of monomeric and dimeric forms of macrophage NOS has been isolated.[216] In the monomeric form macrophage NOS has FAD, FMN, and calmodulin and lacks bound heme and tetrahydrobiopterin. Without heme and tetrahydrobiopterin, the monomeric form of macrophage NOS only acts as an NADPH-dependent reductase toward acceptors such as cytochrome *c* or ferricyanide.[26,216] This finding strongly suggests that tetrahydrobiopterin functions as a reductase. The crystal structure of the heme domain of endothelial NOS in tetrahydrobiopterin free and bound forms was obtained Poulos and co-workers;[217] their conclusions also support the theory that tetrahydrobiopterin acts as an electron transfer agent. Reassociation of the monomeric forms to form their active dimeric forms is required for NO production. Reassociation of the monomeric forms to form their active dimeric forms requires the presence of tetrahydrobiopterin, L-arginine, and stoichiometric amounts of heme.[26,216] L-arginine, tetrahydrobiopterin and heme appear to cooperatively interact to facilitate dimerization. However, the precise mechanism is unclear. Figure A.7 illustrates the proposed role played by tetrahydrobiopterin in nitric oxide synthesis.[26] Regardless of its exact role, tetrahydrobiopterin is

known to be involved in the first step of the reaction sequence that leads to N-hydroxylation and ultimately to NO production.

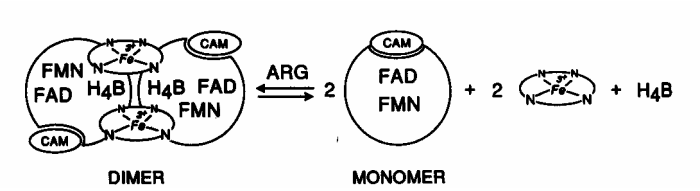

Activated Inactive

Figure A.7 – Role for Heme H4biopterin and L-arginine
"Role for heme H4biopterin, and L-arginine in subunit assembly of macrophage NOS. Assembly of NOS from its isolated subunits in vitro requires that subunits be coincubated with heme, L-arginine and H4biopterin, Tetrahydrobiopterin and heme become bound within the dimer during its assembly and enable NOS to catalyze NO synthesis. Dissociation of dimeric NOS leads to loss of its bound heme and H4biopterin, and it generates subunits which are inactive regarding NO synthesis." (Reprinted from *Nitric Oxide Principles and Actions*, "The Intracellular Reactions of Nitric oxide in the Immune System and Its Enzymatic Synthesis", Jack Lancaster, Jr. and Dennis J. Stuehr, p.164, Copyright 1996, with permission from Elsevier.)

APPENDIX B

ADDITIONAL BIOLOGICAL ROLES OF IRON NITROSYL COMPLEXES

The more that is understood about the nature of heme and non-heme iron heme nitrosyl complexes, the more likely it is that nitric oxide based therapies can be developed to treat illnesses at their origin. Thus, much research is devoted to the study of the role of iron heme nitrosyl complexes in biology. Iron nitrosyl complexes, whether they are heme, non-heme, cluster or bimetallic complexes, are important agents in nitric oxide synthesis and regulation as well as in other physiological functions. This section reviews some of the research directed toward the physiological roles of nitric oxide and iron nitrosyl complexes.

Bastian et al. provided EPR evidence that inducible nitric oxide synthase is activated in the cell-mediated immune response to syngenic tumors and that the resulting nitric oxide diffuses from cytokine activated macrophages to tumor cells within which it interacts with iron containing molecules to form complexes of the general formula $[Fe(SR)_2(NO)_2]$, as well as five and six coordinate heme-nitrsosyl complexes. Bastian's study illustrates the existences of iron sulfur and iron heme containing nitric oxide targets in murine cancers.[33] NOS expressing vascular cells can also participate in defense against tumors.[218]

EPR analysis of liver tissue obtained from mice exhibiting chronic inflammation induced by infection with *Cornybacterium parvum* after treatment with lipopolysaccharide revealed a cytochrome P420 nitrosyl complex as well as non-heme nitrosyl complexes.[219,220] Detection of nitrosylated heme and nonheme iron containing proteins during rejection of rat heart allograft (by EPR measurements) suggest that destruction of iron-containing protein function is crucial in the rejection response.[34]

In 1969 it was reported that aquacobalamin does not bind NO.[38] However, recent evidence suggests that aquacobalamin does bind NO.[39-45] Van Eldik and co-workers investigated the discrepancy and demonstrated that cobalamin, vitamin B_{12}, doesn't bind with NO but with nitrite impurities in aqueous solution.[46] (A side implication of this finding is that, because NO in aqueous solutions readily reacts with dissolved oxygen to form other nitrogen oxide species, great care must be taken when running experiments with NO in water.[46,221]) It was shown, however, that the reduced form of cobalamin, which is present under physiological conditions[35-37] does react with nitric oxide to form a Co^{II}-NO complex.[222] The binding of NO to reduced cobalamin may be responsible for the inactivation of some cobalamin-dependent enzymes as well as inhibition of NO actions *in vivo*. Van Eldik and co-workers completed a kinetic and mechanistic study of the binding of NO to reduced cobalamin.[223] The reactivity of nitrite ions with reduced cobalamin was also studied. Spectroscopic and laser flash photolysis results support a proposed dissociative interchange mechanism. Reduced cobalamin reacts with nitrite impurities several much more slowly than with NO therefore, the kinetic results were unaffected by the presence of nitrite impurities. The authors have also completed a similar study on the reaction of NO with metmyglobin.[47] Metmyoglobin reacts with NO in a manner analogous to that of water-soluble Fe^{III} porphyrin model systems.[224] Kinetic studies support a dissociative mechanism.

The X-ray crystal structure of the nitric oxide of the ferrous nitric oxide form of native sperm whale myoglobin exhibits a bent nitrosyl.[225] Just as nitric oxide binds to metmyoglobin and met hemoglobin, so does nitrite. Binding proceeds by a dissociative mechanism. Nitrite binding is much slower than NO binding therefore kinetic studies of NO binding to metmyoglobin and methemoglobin are also unaffected by trace nitrite impurities.[226]

Hendrich and co-workers carried out Mossbauer and EPR studies of the NO adduct of hydroxylamine oxidoreductase.[227] Hydroxylamine oxidoreductase, derived from the autotrophic nitrifying bacterium, *Nitrosomonas europaea*, contains eight hemes per subunit. These hemes are active in catalysis of the oxidation of hydroxylamine to nitrite and in electron transport.

Mechanistic studies of the reductive nitrosylation of ferricytochrome (Cyt^{III}), metmyoglobin (Mb^{III}), and methemoglobin (Hb^{III}) reveal that after the initial formation of the nitrosyl ferrihemeprotein adduct, the rate limiting nucleophilic attack by OH^- to produces the ferrohemeproteins plus nitrite. Rate constants k_{OH} are in the order $Hb^{III} > Cyt^{III} > Mb^{III}$.[228]

Kagan[48,49] and coworkers demonstrated that nitrosylation of hemoglobin-heme and of non-heme iron centers formed complexes that interact with t-BuOOH to prevent cytotoxicity. Nitric oxide is proposed to protect cells against oxidative damage by decreasing catalytic heme- and non-heme iron sites and by direct chemical interaction with hydrogen peroxide induced free radicals such as oxyferryl and alkoxy radicals. The first pathway may operate after long term cell exposure to NO. The second pathway is a faster reaction that responds to acute and intense oxidative stress. Several investigations suggest that NO acts as an antioxidant by directly scavenging radicals or by binding to and hindering metal centers that participate in Fenton-type catalysis in oxidation.[50-52] Another possible interpretation is that, in addition to reducing oxoferryl to ferri-hemoproteins, NO directly quenches t-BuOOH derived radicals, and protein radicals.[229]

Nitric oxide binds to deoxyhemerythrin which is a derivative of the oxygen transporting non-heme protein found in marine invertebrates.[17,230] Nitric oxide adducts have been proposed as analogues of a semi-methemerythrin superoxide intermediate in oxygenation.[159,231,232]

Rodriguez and co-workers completed Mossbauer spectroscopic studies and density functional theory investigations of the nitrosyl derivatives of deoxyhemerythrin.[154]

As a radical, nitric oxide has a high affinity toward ferric and ferrous proteins. But, as NO^+, nitric oxide forms S-nitrosothiols. Reichenbach and co-workers demonstrated that it is possible to obtain nitrosothiols from metmyoglobin under physiological pH conditions.[53] Nitrosothiols are important because they are vasodilators, because they inhibit platelet aggregation, and are associated with signal transduction.[233-235] Albumin, hemoglobin, and glyceraldehyde-3-phosphate dehydrogenase are all examples *S*-nitrosylated proteins. It had been assumed that NO diffused passively into smooth muscle tissue and reacted with proteins that cause vasodilation and increased blood flow. However, given nitric oxide's high affinity for ferro and ferric proteins, hemoglobin in particular, random diffusion is insufficient to explain how NO reaches blood vessels. Blood would immediately consume the nitric oxide. Pawloski and co-workers demonstrated that NO movement is more complicated than simple diffusion. They propose that much of the previously considered irreversibly hemoglobin consumed NO actually returns to the blood vessel wall as an S-nitrosothiol molecule. Thus the NO is protected from reaction with hemoglobin by a thiol. Some of the NO bound by Fe^{2+} hemoglobin is transferred intramolecularly to a conserved thiol group to produce S-nitroso-hemoglobin. The authors propose that the nitrosothiol might then transfer the NO group to other thiol containing molecules, which carry the NO from the hemoglobin. This process would be most likely to occur in oxygen depleted tissues. Hemoglobin changes conformation upon loss of oxygen from the R (relaxed form) to the deoxygenated T (tense) structure. This system provides an NO delivery system to oxygen poor tissues. Increased NO concentration causes vasodilation and increased blood flow which allows the needed influx of oxygen. Pawloski and co-workers

suggest that the anion exchange protein AE1 which anchors a subpopulation of hemoglobin molecules to red blood cell membranes, may have evolved specifically for the transfer of NO groups.[233,234]

It is noteworthy that glutathione (GSH) will react with nitric oxide in the presence of ferrimyoglobin at physiological pH to form nitrosoglutathione.[53] *S*-nitrosoglutathione also forms *in vivo* from alkylnitrites catalyzed by glutathione transferase.[236] So, alkyl nitrites act as nitrosating agents *in vivo.*[237] Ethyl nitrite formed upon intake of ethanol may be absorbed by the stomach and transported to the duodenum and small intestine.[238]

Given the importance *S*-nitrosothiols in particular and of nitrosyl complexes in general, Loscalzo and co-workers have developed a method of detecting biologically important S-nitrosothiols and other nitric oxide derivatives using photolysis-chemiluminescence spectrometry.[239] Photolysis homolytically cleaves the NO radical from its parent compound. The NO radical is transported by helium to an ozone chamber in which it is oxidized to the electronically excited NO_2* which exhibits chemiluminescence upon decay to the ground state. Cold traps collect all nonvolatile parent compounds and derivatives. Although this method, by itself, cannot distinguish between different S-nitrosothiols or other NO derivatives, when used in conjunction with HPLC or other separation systems, characterization is possible.

Gas phase NO has been detected in exhaled breath of animals and humans. Asthmatic patients exhibit increased exhaled NO levels[240-244] while cystic fibrosis patients have been reported to exhibit decreased exhaled NO levels [244-246] as well as unchanged NO levels as compared to healthy subjects.[242,243,247-251] Denitrifying bacteria consume nitrogen oxides via assimilatory and dissimilatory pathways. For example, *Psuedomonas aeruginosa* carries nitric oxide reductase which consumes NO and produces NH_4^+. Denitrifying bacteria may be

responsible for disrupting nitrogen balance in the airway of cystic fibrosis patients.[252] Therefore, there is a potential clinical role for the measurement of exhaled NO as a noninvasive biological[247] marker in the study and treatment of disease. Previous methods depended on the use of anaesthetized mechanically ventilated animals for NO measurement. However, the effects of the anesthetic on NO measurements were unclear. Mehta and co-workers developed a noninvasive method for measuring exhaled NO in a spontaneously breathing mouse.[253]

In the respiratory system NOS is found in airway epithelial cells, vascular endothelial cells, macrophages, neutrophils, fibroblasts, and neuronal synapses. Since NOS from any of these cells can contribute to exhaled NO, lower respiratory tract NO can come from bronchial or alveolar sources. Patients with liver cirrhosis and with asthma exhibit an increased output of exhaled NO. Multiple flow rate analysis allows the increase NO from a bronchial source to be differentiated from that from an alveolar source.[254] While cirrhosis of the liver causes an increase in NO output from alveolar sources and can participate in arterial hypoxemia, asthma causes an increase in NO output from the bronchial tree. That alveolar NO production in liver cirrhosis increases suggests that either there is a local increase in alveolar NO production along with an impairment of diffusion through the alveolar capillary wall, or that there is increased NO excretion from pulmonary circulation into the alveolar region. New anesthetic independent methods for measuring exhaled NO are being developed.

Cluster compounds are important in biology. For example, nitrogenase catalyzes the reduction of N_2 to ammonia. Nitrogenase from *Azobacter vinelandii* has two protein components, a homodimeric iron protein and a molybdenum iron protein. The homodimeric iron component has one ferredoxin-like center that acts as a bridge between it and the molybdenum-iron component. The iron protein catalytically transfers an electron from reduced carriers to the

molybdenum-iron component. The metals in this component are found in chemically distinct clusters. Understanding the role of these clusters is important for elucidating the enzymology of *Azobacter vinelandii* nitrogenase. Mortenson and co-workers carried out kinetic and spectroscopic studies of the inactivating effects of nitric oxide on the two components of *Azobacter vinelandii*.[31]

BIBLIOGRAPHY

(1) Ignarro, L. J. *Nitric Oxide Biology and Pathobiology*; Academic Press: New York, 2000.

(2) Maxwell, A. J. *NITRIC OXIDE* **2002**, *6*, 101-124.

(3) Ring, A.; Depnering, C.; Pohl, J.; Nizet, V.; Shenep, J. L.; Stremmel, W. *J. Infect. Dis.* **2002**, *186*, 1518-1521.

(4) Fiorucci, S.; Antonelli, E.; Burgaud, J. L.; Morelli, A. *Drug Safety* **2001**, *24*, 801-811.

(5) Schmidt, H. H.; Walter, U. *Cell* **1994**, *78*, 919-925.

(6) Ford, P. C.; Lorkovic, I. M. *Chem. Rev.* **2002**, *102*, 993-1017.

(7) Fuji, S.; Yoshimura, T. *Coord. Chem. Rev.* **2000**, *198*, 89-99.

(8) Mingos, D. M. P.; Sherman, D. J. In *Advances in Inorganic Chemistry*; Sykes, A. G., Ed.; Harcourt, Brace and Jovanovich: London, 1989; Vol. 34, pp 293-377.

(9) Hayton, T. W.; Legzdins, P.; Sharp, W. B. *Chem. Rev.* **2002**, *102*, 935-991.

(10) Coppens, P.; Novozhilova, I.; Kovalevsky, A. *Chem. Rev.* **2002**, *102*, 861-884.

(11) Enemark, J. H.; Feltham, R. D. *Coord. Chem. Rev.* **1974**, *13*, 339-406.

(12) Feltham, R. D.; Enemark, J. H. In *Topics in Inorganic and Organometallic Stereochemistry*; Geoffroy, G., Ed.; John Wiley & Sons: New York, 1981; Vol. 12, pp 155-215.

(13) Westcott, B. L.; Enemark, J. H. In *Inorganic Electronic Spectroscopy*; Solomon, E. I., Lever, A. B. P., Eds.; John Wiley & Sons, Inc.: New York, 1999; Vol. II, pp 403-450.

(14) Connelly, N. G. *Inorganica Chimica Acta* **1972**, 47-89.

(15) Coe, B. J.; Glenwright, S. J. *Coord. Chem. Rev.* **2000**, *203*, 5-80.

(16) Crivici, A.; Ikura, M. *Ann. Rev. Biophys. Biomol. Struct.* **1995**, *24*, 85-116.

(17) Feig, A. L.; Lippard, S. J. *Chem. Rev.* **1994**, *94*, 759-805.

(18) Poulos, T. L. In *The Porphyrin Handbook*; Kadish, K. M., Smith, K. M., Guilard, R., Eds.; Academic Press: New York, 2000; Vol. 4.

(19) Marletta, M. A. *J. Biol. Chem.* **1993**, *268*, 12231-12234.

(20) Schmidt, H. H.; Lohmann, S. M.; Walter, U. *Biochim. Bipohys. Acta* **1993**, *1178*, 153-175.

(21) Stamler, J. S.; Meissner, G. *Physiol. Rev.* **2001**, *81*, 209-237.

(22) Weinstein, H.; Mehler, E. L. *Ann. Rev. Physiol.* **1994**, *56*, 213-236.

(23) Ye, R. W.; Averill, B. A.; Tiedje, J. M. *Appl. Environ. Microbiol.* **1994**, *60*, 1053-1058.

(24) Koppenol, W. H. *NITRIC OXIDE* **2002**, *6*, 96-98.

(25) Richter-Addo, G. B.; Legzdins, P. *Metal Nitrosyls*; Oxford University Press, 1992.

(26) Lancaster, J. R., Jr.; Stuehr, D. J. *Nitric Oxide Principles and Actions*; Academic Press: San Diego, 1996.

(27) Lincoln, J.; Hoyle, C. H. V.; Burnstock, G. In *Biomedical Research Topics*; Cambridge University Press: Cambridge, 1997; Vol. 1.

(28) White, K. A.; Marletta, M. A. *Biochem.* **1992**, *31*, 6627-6631.

(29) Pufahl, R. A.; Marletta, M. A. *Biochem. Biophys. Res. Commun.* **1993**, *193*, 963-970.

(30) Pufahl, R. A.; Wishnok, J. S.; Marletta, M. A. *Biochem.* **1995**, *34*, 1930-1941.

(31) Hyman, M. R.; Seefeldt, L. C.; Morgan, T. V.; Arp, D. J.; Mortensen, L. E. *Biochem.* **1992**, *31*, 2947-2955.

(32) Pant, K.; Bilwes, A. M.; Adak, S.; Stuehr, D. J.; Crane, B. R. *Biochem.* **2002**, *41*, 11071-11079.

(33) Bastian, N. R.; Yim, C. Y.; Hibbs, J. B.; Samlowski, W. E. *J. Biol. Chem.* **1994**, *269*, 5127-5131.

(34) Lancaster, J. R.; Langrehr, J. M.; Bergonia, H. A.; Murase, N.; Simmons, R. L.; Hoffman, R. A. *J. Biol. Chem.* **1992**, *267*, 10994-10998.

(35) Pezacka, E. H. *Biochim. Bipohys. Acta* **1993**, *1157*, 167-177.

(36) Watanabe, F.; Saido, H.; Yamaji, R.; Miyatake, K.; Isegawa, Y.; Ito, A.; T., Y.; Rosenblatt, D. S.; Nakano, Y. *J. Nutr.* **1996**, *126*, 2947-2951.

(37) Watanabe, F. *Bitamin* **1992**, *66*, 617-625.

(38) Firth, R. A.; Hill, H. A. O.; Pratt, J. M.; Thorp, R. G.; Williams, R. J. P. *J. Chem. Soc. A* **1969**, *3*, 381-386.

(39) Rochelle, L. G.; Morana, S., J.; Kruszyna, H.; Russel, M. A.; Wilcox, D. E.; Smith, R. P. *J. Pharmacol. Exper. Ther.* **1995**, *275*, 48-52.

(40) Brouwer, M.; Chalmulitrat, W.; Ferruzzi, G.; Sauls, D. L.; Weinberg, J. B. *Blood* **1996**, *88*, 1857-1864.

(41) Greenberg, S. S.; Xie, J.; Zatarain, J. M.; Kapusta, D. R.; Miller, M. J. S. *J. Pharmacol. Exper. Ther.* **1995**, *273*, 257-265.

(42) Rajanayagam, M. A. S.; Li, C. G.; Rand, M. J. *Brit. J. Pharmacol.* **1993**, *108*, 3-5.

(43) Li, C. G.; Rand, M. J. *Clin. Exp. Pharmacol. Physiol.* **1993**, *20*, 633-640.

(44) Jenkinson, K. M.; Reid, J. J.; Rand, M. J. *Eur. J. Pharmacol.* **1995**, *275*, 145-152.

(45) Bauer, J. A. *Anti-Cancer Drugs* **1998**, *9*, 239-244.

(46) Wolak, M.; Stochel, G.; Hamza, M.; van Eldik, R. *Inorg. Chem.* **2000**, *39*, 2018-2019.

(47) Laverman, L. E.; Wanat, A.; Oszajca, J.; Stochel, G.; Ford, P. C.; van Eldik, R. *J. Am. Chem. Soc.* **2001**, *123*, 285-293.

(48) Gorbunov, N. V.; Yalowich, J. C.; Gaddam, A.; Thampatty, P.; Ritov, V. B.; Kisin, E. R.; Elsayed, N. M.; Kagan, V. E. *J. Biol. Chem.* **1997**, *272*, 12328-12341.

(49) Yalowich, J. C.; Gorbunov, N. V.; Kozlov, A. V.; Allan, W.; Kagan, V. E. *Biochem.* **1999**, *38*, 10691-10698.

(50) Wink, D. A.; Hanbauer, I.; Krishna, M. C.; DeGraff, W.; Gamson, J.; Mitchell, J. B. *Proc. Natl. Acad. Sci. USA* **1993**, *90*, 9813-9817.

(51) Wink, D. A.; Cook, J. A.; Krishna, M. C.; Hanbauer, I.; DeGraff, W.; Gamson, J.; Mitchell, J. B. *Arch. Biochem. Biophys.* **1995**, *319*, 402-407.

(52) Juckett, M. B.; Weber, M.; Balla, J.; Jacob, H. S.; Vercellotti, G. M. *Free Rad. Biol. Med.* **1996**, *1996*, 63-73.

(53) Reichenbach, G.; Sabatini, S.; Palombari, R.; Palmerini, C. A. *NITRIC OXIDE* **2001**, *5*, 395-401.

(54) Greenwood, N. N.; Earnshaw, A. *Chemistry of the Elements*; Second ed.; Butterworth-Heinemann: Oxford, 1997.

(55) Caulton, K. G. *Coord. Chem. Rev.* **1975**, *14*, 317-355.

(56) Ungermann, C. B.; Caulton, K. G. *J. Am. Chem. Soc.* **1976**, *13*, 3863-3868.
(57) Haines, R. J.; DuPreez, A. L.; Marais, I. L. *J. Organomet. Chem.* **1971**, *28*, 404-413.

(58) Schumann, H. *J. Organomet. Chem.* **1985**, *293*, 75-91.

(59) King, J. E.; Simpson, S. J. *J. Organomet. Chem.* **1985**, *424*, 57-63.

(60) Sellmann, D.; Blum, N.; Heinemann, F. W.; Hess, B. A. *Chem. Eur. J.* **2001**, *7*, 1874-1880.

(61) Wanat, A.; Schneppensieper, T.; Stochel, G.; van Eldick, R.; Eckhard, B.; Wieghardt, K. *Inorg. Chem.* **2002**, *41*, 4-10.

(62) Chiou, Y. M.; Que, L., Jr. *Inog. Chem.* **1995**, *34*, 3270-3278.

(63) Fletcher, J. M.; Jenkins, I. L.; Lever, F. M.; Martin, F. S.; Powell, A. R.; Todd, R. *J. Inorg. Nuc. Chem.* **1955**, *1*, 378-401.

(64) Bhattacharyya, R. G.; Mallik, M.; Ghosh, P. M. *Inorg. Chim. Acta* **1990**, *168*, 141-143.

(65) Choi, I. K.; Liu, Y.; Wei, Z.; Ryan, M. D. *Inorg. Chem.* **1997**, *36*, 3113-3118.

(66) Davies, S. C.; Evans, D. J.; Highes, D. L.; Konkol, M.; Richards, R. L.; Roger, S. J.; Sobota, P. *J. Chem. Soc., Dalton. Trans.* **2002**, 2473-2582.

(67) Sidgwick, N. V.; Bailey, R. W. *Proc. Roy. Soc. London* **1934**, *A144*, 521-537.

(68) Hodgson, D. J. I., James A. *Inorg. Chem.* **1968**, *7*, 2345-2352.

(69) Guida, J. A.; Ramos, M. A.; Piro, O. E.; Aymonino, P. J. *J. Molec. Struct.* **2002**, *609*, 39-46.

(70) Fielder, A.; Iwata, S. *J. Phys. Chem. A* **1998**, *102*, 3618-3624.

(71) Nasri, H.; Haller, K. J.; Wang, Y.; Hahn, H. B.; Scheidt, W. R. *Inorg. Chem.* **1992**, *31*, 3459-3467.

(72) Cheng, L.; Powell, D. R.; Khan, M. A.; Richter-Addo, G. B. *J. Chem. Soc. Chem.Comm.* **2000**, 2301-2302.

(73) Yi, G. B.; Chen, L.; Khan, M. A.; Richter-Addo, G. B. *Inorg. Chem.* **1997**, *36*, 3876-3885.

(74) Lorkovic, I. M.; Ford, P. C. *Inorg. Chem.* **2000**, *39*, 632-633.

(75) Lorkovic, I. M.; Miranda, K. M.; Lee, B.; Bernhard, S.; Schoonover, J. R.; Ford, P. C. *J. Am. Chem. Soc.* **1998**, *120*, 11674-11683.

(76) Lorkovic, I. M.; Ford, P. C. *Inorg. Chem.* **1999**, *38*, 1467-1473.

(77) Lorkovic, I. M.; Ford, P. C. *J. Chem. Soc. Chem.Comm.* **1999**, 1225-1226.

(78) Nasri, H.; Ellison, M. K.; Chen, S.; Huynh, B. H.; Scheidt, W. R. *J. Am. Chem. Soc.* **1997**, *119*, 6274-6283.

(79) Scheidt, W. R.; Munro, W. Q. *Inorg. Chem.* **1998**, *37*, 2308-2316.

(80) Ellison, M. K.; Scheidt, W. R. *J. Am. Chem. Soc.* **1999**, *121*, 5210-5219.

(81) Ellison, M. K.; Scheidt, W. R. *J. Am. Chem. Soc.* **1997**, *119*, 7404-7405.

(82) Bohle, D. S.; Debrunner, P. G.; Fitzgerald, J. P.; Hansert, B.; Hung, C. H.; Thomson, A. J. *J. Chem. Soc., Chem. Comm.* **1997**, 91-92.

(83) Ellison, M. K.; Schulz, C. E.; Scheidt, W. R. *Inorg. Chem.* **2000**, *39*, 5102-5110.

(84) Ghosh, A.; Bocian, D. F. *J. Phys. Chem. A* **1996**, *100*, 6363-6367.

(85) Scheidt, W. R.; Duval, H. F.; Neal, T. J.; Ellsion, M. K. *J. Am. Chem. Soc.* **2000**, *122*, 4651-4659.

(86) Hoffman, R.; Chen, M. M. L.; Elian, M.; Rossi, A. R.; Mingos, D. M. P. *Inorg. Chem.* **1974**, *13*, 2666-2675.

(87) Richter-Addo, G. B.; Wheeler, R. A.; Hixson, C. A.; Chen, L.; Khan, M. A.; Ellison, M. K.; Schulz, C. E.; Scheidt, W. R. *J. Am. Chem. Soc.* **2001**, *123*, 6314-6326.

(88) Fomitchev, D. V.; Coppens, P.; Li, T.; Bagley, K. A.; Chen, L.; Richter-Addo, G. B. *J. Chem. Soc. Chem.Comm.* **1999**, 2013-2014.

(89) Cheng, L.; Novozhilova, I.; Kim, C.; Kovalevsky, A.; Bagley, K. A.; Coppens, P.; Richter-Addo, G. B. *J. Am. Chem. Soc.* **2000**, *122*, 7142-7143.

(90) Wondimagegn, T.; Ghosh, A. *J. Am. Chem. Soc.* **2001**, *123*, 5680-5683.

(91) Fomitchev, D. V.; Novozhilova, I.; Coppens, P. *Tetrahedron* **2000**, *56*, 6813-6820.

(92) Weichsel, A.; Andersen, J. F.; Roberts, S. A.; Montfort, W. R. *Nat. Struct. Biol.* **2000**, *7*, 551-554.

(93) Ding, X. D.; Weichsel, A.; Andersen, J. F.; Sokhireva, T. K.; Balfour, C.; Pierik, A. J.; Averill, B. A.; Montfort, W. R.; Walker, F. A. *J. Am. Chem. Soc.* **1999**, *121*, 128-138.

(94) Ozawa, S.; Sakamoto, E.; Ichikawa, T.; Watanabe, Y.; Morishima, I. *Inorg. Chem.* **1995**, 6362-6370.

(95) Younathan, J. N.; Wood, K. S.; Meyer, T. J. *Inorg. Chem.* **1992**, *31*, 3280-3285.

(96) Bedioui, F.; Trevin, S.; Albin, V.; Villegas, M. G. G.; Devynck, J. *Anal. Chim. Acta* **1997**, *341*, 177-185.

(97) Mimica, D.; Zagal, J. H.; Bedioui, F. *J. Electroanal. Chem.* **2001**, *497*, 106-113.

(98) Bedioui, F.; Bouhier, Y.; Sorel, C.; Devynck, J.; Coche-Guerente, L.; Deronzier, A.; Moutet, J. C. *Electrochim. Acta* **1993**, *38*, 2485-2491.

(99) Kim, C. H.; Hollocher, T. C. *J. Biol. Chem.* **1984**, *259*, 2092-2099.

(100) Ozawa, S.; Sakamoto, E.; Watanabe, Y.; Morishima, I. *J. Chem. Soc., Chem. Comm.* **1994**, 935-936.

(101) Fueloep, V.; Moir, J. W. B.; Ferguson, S. J.; Hajdu, J. *Cell* **1995**, *81*, 369-377.

(102) Liu, Y.; Ryan, M. D. *J. Electroanal. Chem.* **1994**, *368*, 209-219.

(103) Liu, Y.; DeSilva, C.; Ryan, M. D. *Inorg. Chim. Acta* **1997**, *258*, 247-255.

(104) Chen, J.; Ikeda, O. *Electroanal.* **2001**, *13*, 1076-1081.

(105) Baldwin, D. A.; Pfeiffer, R. M.; Reichgott, D. W.; Rose, N. J. *J. Am. Chem. Soc.* **1973**, *95*, 5152-5258.

(106) Chen, Y.; Sweetland, M. A.; Shepherd, R. E. *Inorg. Chim. Acta* **1997**, *260*, 163-172.

(107) Sugiura, Y.; Ishizu, K. *J. Inorg. Biochem.* **1979**, *11*, 171-180.

(108) Dickenson, L. C.; Chien, J. C. W. *J. Am. Chem. Soc.* **1971**, *93*, 5036-5040.

(109) Kon, H. *J. Biol. Chem.* **1968**, *243*, 4350-4357.

(110) Chien, J. C. W. *J. Chem. Phys.* **1969**, *51*, 4220-4227.

(111) Kon, H. *Biochim. Bipohys. Acta* **1975**, *379*, 103-113.

(112) Antonini, E.; Maurizio, B. *Hemoglobin and myoglobin in their reactions with ligands*; North Holland Publishing Company: Amsterdam, 1971.

(113) Kassner, R. J.; Romberg, R. W. *Biochem.* **1979**, *18*, 5387-5392.

(114) Rose, E. J.; Hoffman, B. M. *J. Am. Chem. Soc.* **1983**, *105*, 2866-2873.

(115) Mahler, H. R.; Cordes, E. H. *Biological Chemistry*; Harper & Row: New York, 1966.

(116) Gerbeleu, N. V.; Arion, V. B.; Simonov, Y. A.; Zavodnik, V. E.; Stavrov, S. S.; Turta, K. I.; Gradinaru, D. I.; Birca, M. S.; Pasynskii, A. A.; Ellert, O. *Inorg. Chim. Acta* **1992**, *202*, 173-181.

(117) Li, L.; Enright, G. D.; Preston, K. F. *Organomet.* **1994**, *13*, 4686-4688.

(118) Atkinson, F. L.; Blackwell, H. E.; Brown, N. C.; Connelly, N. G.; Crossley, J. G.; Orpen, G. A.; Rieger, P. H.; Rieger, A. L. *J. Chem. Soc., Dalton. Trans.* **1996**, *17*, 3491-3502.

(119) Horsken, A.; Zheng, G.; Stradiotto, M.; McCrory, C. T. C.; Li, L. *J. Organomet. Chem.* **1998**, *558*, 1-9.

(120) Reginato, N.; McCrory, C. T. C.; Pervitsky, D.; Lijuan, L. *J. Am. Chem. Soc.* **1999**, *121*, 10217-10217.

(121) Feig, A. L.; Bautista, M. T.; Lippard, S. J. *Inorg. Chem.* **1996**, *35*, 6892-6898.

(122) Bladon, P.; Dekker, M.; Knox, G. R.; Willison, D.; Jaffari, G.; Doedens, R. J.; Muir, K. W. *Organomet.* **1993**, *2*, 1725-1741.

(123) Butler, A. R.; Glidewell, C.; Glidewell, S. M. *J. Chem. Soc., Chem. Comm.* **1992**, *2*, 141-142.

(124) Butler, A. R.; Glidewell, C.; Glidewell, S. M. *Polyhedron* **1992**, *11*, 591-596.

(125) Osterloh, F.; Saak, W.; Haase, D.; Pohl, S. *J. Chem. Soc. Chem.Comm.* **1997**, 979-980.

(126) Liaw, W. F.; Chiang, C. Y.; Lee, G. H.; Peng, S. M.; Lai, C. H.; Darensbourg, M. Y. *Inorg. Chem.* **2000**, *39*, 480-484.

(127) Kou, H. Z.; Gao, E. Q.; Liao, D. Z.; Cheng, P.; Jiang, Z. H.; Yan, S. P.; Wang, G. L.; Yao, X. K.; Wang, H. G.; Tuchagues, J. P. *Acta Chim. Scan.* **1999**, *53*, 542-546.

(128) Smekal, Z.; Travnicek, Z.; Marek, J.; Nadvornik, M. *Aust. J. Chem.* **2000**, *53*, 225-228.

(129) Guida, J. A.; Aymonino, P. J.; Piro, O. E.; Castellano, E. E. *Spectrochim. Acta* **1993**, *49A*, 535-542.

(130) Villalba, M. E. C.; Varetti, E. L.; Aymonino, P. J. *Vib. Spect.* **1997**, *14*, 275-286.

(131) Chen, Z. N.; Wang, J. L.; Jun, Q.; Miao, F. M.; Tang, W. X. *Inorg. Chem.* **1995**, *34*, 2255-2257.

(132) Shyu, H. L.; Wei, H. H.; Wang, Y. *Inorg. Chim. Acta* **1997**, *258*, 81-86.

(133) Kou, H. Z.; Wang, H. M.; Liao, D. Z.; Cheng, P.; Jiang, Z. H.; Yan, S. P.; Huang, X. Y.; Wang, G. L. *Aust. J. Chem.* **1998**, *51*, 661-665.

(134) Mondale, N.; Saha, M. K.; Mitra, S.; Gramlich, V.; El Fallah, M. S. *Polyhedron* **2000**, *19*, 1935-1939.

(135) Gerbase, A. E.; Vichi, E. J. S.; Stein, E.; Amaral, L.; Wasquez, A.; Horner, M.; Maichle-Mossmer, C. *Inorg. Chim. Acta* **1997**, *266*, 19-27.

(136) Houlton, A.; Ibrahim, S. K.; Dilworth, J. R.; Silver, J. *J. Chem. Soc. Dalton. Trans.* **1990**, 2421-2424.

(137) Gladfelter, W. L. In *Advances in Organometallic Chemistry*; Academic Press Inc., 1985; Vol. 24, pp 41-86.

(138) Bourassa, J.; DeGraff, W.; Kudo, S.; Wink, D. A.; Mitchell, J. B.; Ford, P. C. *J. Am. Chem. Soc.* **1997**, *119*, 2853-2860.

(139) Bourassa, J.; Lee, B.; Bernhard, S.; Schoonover, J.; Ford, P. C. *Inorg. Chem.* **1999**, *38*, 2947-2952.

(140) Ford, P. C.; Bourassa, J.; Miranda, B.; Lee, I.; Lorkovic, I. M.; Boggs, S.; Kudo, S.; Laverman, L. E. *Coord. Chem. Rev.* **1998**, *171*, 185-202.

(141) Butler, A. R.; Glidewell, C.; Hyde, A. R.; McGinnis, J. *Polyhedron* **1983**, *2*, 1399-1400.

(142) Butler, A. R.; Glidewell, C.; Li, M. *Adv. Inorg. Chem.* **1988**, *32*, 335-393.

(143) Butler, A. R.; Glidewell, C.; Glidewell, S. M. *Polyhedron* **1990**, *9*, 2399-2405.

(144) D'Addario, S.; Demartin, F.; Grossi, L.; Iapalucci, M. C.; Laschi, F.; Longoni, G.; Zanello, P. *Inorg. Chem.* **1993**, *32*, 1153-1160.

(145) Roussin, F. Z. *Ann. Chim. Phys.* **1858**, *52*, 285.

(146) Lewin, M.; Fisher, K.; Dance, I. *J.Chem. Soc., Chem. Comm.* **2000**, 947-948.

(147) Gall, R. S.; Chu, C. T. W.; Dahl, L. F. *J. Am. Chem. Soc.* **1974**, *96*, 4019-4023.

(148) Chu, C. T. W.; Lo, F. Y. K.; Dahl, L. F. *J. Am. Chem. Soc.* **1982**, *104*, 3409-3422.

(149) Scott, M. J.; Holm, R. H. *Angew. Chem. Int. Ed. Engl.* **1993**, *32*, 564-566.

(150) Goh, C.; Holm, R. H. *Inorg. Chim. Acta* **1998**, *270*, 46-54.

(151) Geiser, U.; Williams, J. M. *Acta Chryst., Sec. C* **1998**, *C54*, 292-293.

(152) Mansour, M. A.; Curtis, M. D.; Kampf, J. W. *Oganomet.* **1997**, *16*, 275-284.

(153) Rossel, O.; Seco, M.; Segales, G.; Alvarez, S.; Pellinghelli, M. A.; Tiripicchio, A.; deMontauzon, D. *Organomet.* **1997**, *16*, 236-245.

(154) Rodriguez, J. H.; Xia, Y. M.; Debrunner, P. G. *J. Am. Chem. Soc.* **1999**, *121*, 7846-7863.

(155) Della Pergola, R.; Garlaschelli, L.; Manassero, M.; Sansoni, M.; Strumolo, D.; de Biani, F. F.; Zanello, P. *J. Chem. Soc., Dalton. Trans.* **2001**, 2179-2183.

(156) Haskin, C. J.; Ravi, N.; Lynch, J. B.; Munck, E.; Que, L., Jr. *Biochem.* **1995**, *34*, 11090-11098.

(157) Orville, A. M.; Chen, V. J.; Kriauciunas, A.; Harpel, M. R.; Fox, B. G.; Munck, E.; Lipscomb, J. D. *Biochem.* **1992**, *31*, 4602.

(158) Hauser, C.; Glaser, T.; Bill, E.; Weyhermueller, T.; Wieghardt, K. *J. Am. Chem. Soc.* **2000**, *122*, 4352-4365.

(159) Brown, C. A.; Pavlovsky, M. A.; Westre, T. E.; Zhang, Y.; Hedman, B.; Hodgson, K. O.; Solomon, E. I. *J. Am. Chem. Soc.* **1995**, *117*, 715-732.

(160) Westre, T. E.; DiCicco, A.; Filipponi, A.; Natoli, C. R.; Hedman, B.; Solomon, E. I.; Hodgson, K. O. *J. Am. Chem. Soc.* **1994**, *116*, 6757-6768.

(161) Moncada, S.; Palmer, R. M.; Higgs, E. A. *Pharmacol. Rev.* **1991**, *43*, 109-142.

(162) Nathan, C. F. *FASEB J.* **1992**, *6*, 3051-3064.

(163) Fricker, S. P. *Plat. Met. Rev.* **1995**, *39*, 150-159.

(164) Ward, M. S.; Shepherd, R. E. *Inorg. Chim. Acta* **1999**, *286*, 197-206.

(165) Pham, E. K.; Chang, S. G. *Nature* **1994**, *369*, 139-141.

(166) Harriot, P.; Smith, K.; Benson, L. B. *Environ. Prog.* **1993**, *12*, 110-113.

(167) Shepherd, R. E.; Sweetland, M. A.; Junker, D. E. *J. Inorg. Biochem.* **1997**, *65*, 1-14.

(168) Mizuta, T.; Wang, J.; Miyosho, K. *Bull. Chem. Soc. Jpn.* **1993**, *66*, 2547-2551.

(169) Mizuta, T.; Wang, J.; Miyosho, K. *Inorg. Chim. Acta.* **1995**, *230*, 119-125.

(170) Demmink, J. F.; van Gils, I. C. F.; Beenackers, A. A. C. M. *Ind. Eng. Chem. Res.* **1997**, *36*, 4914-4927.

(171) Zang, V.; van Eldick, R. *Inorg. Chem.* **1990**, *29*, 4462-4468.

(172) Hoefle, J.; van Velzen, D.; Langenkamp, H.; Schaber, K. *Chem. Eng. Proc.* **1996**, *35*, 295-300.

(173) Nymoen, H.; van Velzen, D.; Langenkamp, H. *Chem. Eng. Proc.* **1993**, *32*, 9-12.

(174) Kustin, K.; Taub, I. A.; Weinstock, E. M. *Inorg. Chem.* **1966**, *5*, 1079-1082.

(175) Williams, R. J. P. *Chem. Soc. Rev.* **1996**, *2*, 77-85.

(176) Stamler, J. S.; Singel, D. J.; Loscalzo, J. *Science* **1992**, *258*, 1898-1902.

(177) Schneppensieper, T.; Wanat, A.; Stochel, G.; Goldstein, S.; Meyerstein, D.; van Eldik, R. *Eur. J. Inorg. Chem.* **2001**, 2317-2325.

(178) Schneppensieper, T.; Finkler, S.; Czap, A.; van Eldick, R.; Heus, M.; Niuewenhuizen, P.; Wreesmann, C.; Abma, W. *Eur. J. Inorg. Chem.* **2001**, 491-501.

(179) Manchot, W.; Zechenmtmayer, K. *Ann.* **1907**, *350*, 368-389.

(180) Manchot, W. *Ber. Dtsch. Chem. Ges.* **1914**, *47*, 1601-1614.

(181) Manchot, W.; Lehman, G. *Ann.* **1928**, *460*, 179-201.

(182) Schlesinger, H. I.; van Valkenberg, H. B. *J. Am. Chem. Soc.* **1929**, *51*, 1323-1331.

(183) Tarte, P. *Ind. Chim. Belge.* **1952**, *17*, 42-44.

(184) Dunstan; Symond *Ann.* **1887**, *350*, 368.

(185) Usher, F. L. *Prag. Z. Physik. Chem.* **1908**, *62*, 622-625.

(186) Divers; Hager, J. *J. Chem. Soc.* **1885**, *47*, 361.

(187) Huffner, Z. *Phys. Chem.* **1907**, *59*, 416.

(188) Kohlschutter, V.; Sazanoff, P. *Ber. Dtsch. Chem. Ges.* **1911**, *44*, 1423.

(189) Gray, H. B.; Bernal, I.; Billig, E. *J. Am. Chem. Soc.* **1962**, *84*, 3404-3405.

(190) Griffith, W. P.; Lewis, J.; Wilkinson, G. *J. Chem. Soc., Abs.* **1958**, 3393-3398.

(191) Ogura, K.; Watanabe, M. *Inorg. Nucl. Chem.* **1981**, *43*, 1239-1241.

(192) Burlamacchi, L.; Martini, G.; Tiezzi, E. *Inorg. Chem.* **1969**, *8*, 2021-2025.

(193) Mosbaek, H.; Poulsen, K. G. *Acta Chem. Scan.* **1971**, *25*, 2421-2427.

(194) Chatel, S.; Chauvin, A. S.; Tuchagues, J. P.; Leduc, P.; Bill, E.; Chottard, J. C.; Mansuy, D.; Artaud, I. *Inorg. Chim. Acta* **2002**, *336*, 19-28.

(195) Schweitzer, D.; Ellison, J. J.; Shoner, S. C.; Lovell, S.; Kovacs, J. A. *J. Am. Chem. Soc.* **1998**, *120*, 10996-10997.

(196) Zhang, Y.; Pavlovsky, M. A.; Brown, C. A.; Westre, T. E.; Hedman, B.; Hodgson, K. O.; Solomon, E. I. *J. Am. Chem. Soc.* **1992**, *114*, 9189-9191.

(197) Dawson, T. M.; Snyder, S. H. *J. Neurosci.* **1994**, *14*, 5147-5159.

(198) Nathan, C. F.; Xie, Q. W. *Cell* **1994**, *78*, 915-918.

(199) Bredt, D. S.; Hwang, P. M.; Glatt, C. E.; Lowenstein, C.; Reed, R. R.; Snyder, S. H. *Nature* **1991**, *351*, 714-718.

(200) McMillan, K.; Bredt, D. S.; Hirsch, D. J.; Snyder, S. H.; Clark, J. E.; Masters, B. S. S. *Proc. Natl. Acad. Sci. USA* **1992**, *89*, 11141-11145.

(201) Renaud, J. P.; Boucher, J. L.; Vadon, S.; Delaforge, M.; Mansuy, D. *Biochem. Biophys. Res.* **1993**, *192*, 53-60.

(202) Klatt, P.; Schmidt, K.; Mayer, B. *Biochem. J.* **1992**, *288*, 15-17.

(203) Stuehr, D. J.; Ikeda-Saito, M. *J. Biol. Chem.* **1992**, *267*, 20547-20550.

(204) Marletta, M. A. *Cell* **1994**, *78*, 927-930.

(205) Snedden, W. A.; Koustsia, N.; Baum, G.; Fromm, H. *J. Biol. Chem.* **1996**, *271*, 4148-4154.

(206) Cho, H. J.; Xie, Q. W.; Calacay, J.; Mumford, R. A.; Swiderek, K. M.; Lee, T. D.; Nathan, C. F. *J. Exp. Med.* **1992**, *176*, 599-604.

(207) Kwon, N. S.; Nathan, C. F.; Stuehr, D. J. *J. Biol. Chem.* **1989**, *264*, 20496-20501.

(208) Tayeh, M. A.; Marletta, M. A. *J. Biol. Chem.* **1989**, *264*, 19654-19658.

(209) Mayer, B.; John, M.; Heinzel, B.; Werner, E. R.; Wachter, H.; Schulz, G.; Bohme, E. *FEBS lett.* **1991**, *288*, 187-191.

(210) Bec, N.; Gorren, A. C. F.; Voelker, C.; Mayer, B.; Lange, R. *J. Biol. Chem.* **1998**, *273*, 13502-13508.

(211) Giovanelli, J.; Campos, K. L.; Kaufman, S. *Proc. Natl. Acad. Sci. USA* **1991**, *88*, 7091-7095.

(212) Hevel, J. M.; Marletta, M. A. *Biochem.* **1992**, *31*, 7160-7165.

(213) Heinzel, B.; John, M.; Bohme, E.; Mayer, B. *Biochem. J.* **1992**, *281*, 627-630.

(214) Stuehr, D. J.; Cho, H. J.; Kwon, N. S.; Weise, M. F.; Nathan, C. F. *Proc. Natl. Acad. Sci. USA* **1991**, *88*, 7773-7777.

(215) Hevel, J. M.; White, K. A.; Marletta, M. A. *J. Biol. Chem.* **1991**, *266*, 22789-22791.

(216) Baek, K. J.; Thiel, B. A.; Lucas, S.; Stuehr, D. J. *J. Biol. Chem.* **1993**, *268*, 21120-21129.

(217) Raman, C. S.; Li, H.; Martasek, P.; Kral, V.; Masters, B. S. S.; Poulos, T. L. *Cell* **1998**, *95*, 939-950.

(218) Geng, Y. J.; Hellstrand, K.; Wennmalm, A.; Hansson, G. K. *Canc. Res.* **1996**, *56*, 866-874.

(219) Chamulitrat, W.; Jordan, S. J.; Mason, R. P.; Litton, A. L.; Wilson, J. G.; Wood, E. R.; Wolberg, G.; Molina y Vedia, L. *Arch. Biochem. Biophys.* **1995**, 30-37.

(220) Stadler, J.; Bergonia, H. A.; Di Silvio, M.; Sweetland, M. A.; Billiar, T. R.; Simmons, R. L.; Lancaster, J. R. *Arch. Biochem. Biophys.* **1993**, *302*, 4-11.

(221) Ohkawa, T.; Hiramoto, K.; Kikugawa, K. *NITRIC OXIDE* **2001**, *6*, 515-524.

(222) Zheng, D.; Birke, R. L. *J. Am. Chem. Soc.* **2001**, *123*, 4637-4638.

(223) Wolak, M.; Zahl, A.; Schneppensieper, T.; Stochel, G.; van Eldik, R. *J. Am. Chem. Soc.* **2001**, *123*, 9780-9791.

(224) Laverman, L. E.; Hoshino, M.; Ford, P. C. *J. Am. Chem. Soc.* **1997**, *119*, 12663-12664.

(225) Brucker, E. A.; Olson, J. S.; Ikeda, S. M.; Phillips, G. N. *Proteins: Struct. Funct. Gen.* **1998**, *30*, 352-356.

(226) Wanat, A.; Gdula-Argasinska, J.; Rutkowski-Zbik, D.; Witko, M.; Stochel, G.; van Eldick, R. *JBIC* **2002**, *7*, 165-176.

(227) Hendrich, M. P.; Upadhyay, A. K.; Riga, J.; Arciero, D. M.; Hooper, A. B. *Biochem.* **2002**, *41*, 4603-4611.

(228) Hoshino, M.; Maeda, M.; Konishi, R.; Seki, H.; Ford, P. C. *J. Am. Chem. Soc.* **1996**, *118*, 5702-5707.

(229) Kanner, J.; Harel, S.; Granit, R. *Arch. Biochem. Biophys.* **1991**, *289*, 130-136.

(230) Kurz, D. M., Jr. *JBIC* **1997**, *2*, 159-167.

(231) Que, L., Jr.; True, A. E. *Prog. Inorg. Chem.* **1990**, *38*, 97-200.

(232) Nocek, J. M.; Kurz, D. M.; Sage, T. J.; Debrunner, P. G.; Maroney, M. J.; Lawrence, Q. *J. Am. Chem. Soc.* **1985**, *107*, 3382-3384.

(233) Pawloski, J. R.; Hess, D. T.; Stamler, J. S. *Nature* **2001**, *409*, 622-626.

(234) Gross, S. S. *Nature* **2001**, *409*, 577-578.

(235) Gow, A. J.; Stamler, J. S. *Nature* **1998**, *391*, 169-173.

(236) Akerboom, T. P. M.; Ji, Y.; Wagner, G.; Sies, H. *Biochem. Pharmacol.* **1997**, *53*, 117-120.

(237) Cederqvist, B.; Persson, M. G.; Gustofsson, L. E. *Biochem. Pharmacol.* **1994**, *47*, 1047-1053.

(238) Yoshimura, T.; Sugata, H. *NITRIC OXIDE* **2002**, *6*, 347-352.

(239) Alpert, C.; Ramdev, N.; George, D.; Loscalzo, J. *Anal. Biochem.* **1997**, *245*, 1-7.

(240) Alving, K.; Weitzberg, E.; Lundberg, J. M. *Eur. Respir. J.* **1993**, *6*, 1368-1370.

(241) Lundberg, J. O. N.; Weitzberg, E.; Lundberg, J. M.; Alving, K. *Eur. Respir. J.* **1996**, *9*, 2671-2680.

(242) Dotsch, J.; Demiracka, S.; Terback, H. G.; Huls, G.; Rachser, W.; Kuhl, P. G. *Eur. Resp. J.* **1996**, *9*, 2537-2540.

(243) Lundberg, J. O. N.; Nordvall, S. L.; Weitzberg, E.; Kollberg, H.; Alving, K. *Arch. Dis. Child.* **1996**, *75*, 323-326.

(244) Kroesbergen, A.; Jobsis, Q.; Bel, E. H.; Hop, W. C.; deJongste, J. C. *Eur. Resp. J.* **1999**, *14*, 871-875.

(245) Thomas, S. R.; Kharitonov, S. A.; Scott, S. F.; Hodson, M. E.; Barnes, P. J. *Chest* **2000**, *117*, 1085-1089.

(246) Grasemann, H.; Michler, E.; Wallot, M.; Ratjen, F. *Pediatr. Pulmonol.* **1997**, *24*, 173-177.

(247) Shin, H. W.; Rose-Gottron, C. M.; Sufi, R. S.; Perez, F.; Cooper, D. M.; Wilson, A. F.; George, S. C. *Am. J. Respir. Crit. Care Med.* **2002**, *165*, 349-357.

(248) Balfour-Lynn, I. M.; Laverty, A.; Dinwiddie, R. *Arch. Dis. Child.* **1996**, *75*, 319-322.

(249) Corradi, M.; Montuschi, P.; Donnelly, L. E.; Pesci, A.; Kharitonov, S. A.; Barnes, P. J. *Am. J. Respir. Crit. Care Med.* **2001**, *163*, 854-858.

(250) Ho, L. P.; Innes, J. A.; Greening, A. P. *Thorax* **1998**, *53*, 680-684.

(251) Ho, L. P.; Innes, J. A.; Greening, A. P. *Eur. Resp. J.* **1998**, *12*, 1290-1294.

(252) Gaston, B.; Ratjen, F.; Vaughan, J. W.; Malhotra, N. R.; Canaday, R. G.; Snyder, A. H.; Hunt, J. F.; Gaertig, S.; Goldberg, J. B. *Am. J. Respir. Crit. Care Med.* **2002**, 387-390.

(253) Weicker, S.; Karachi, T. A.; Scott, J. A.; McCormack, D. G.; Mehta, S. *Am. J. Respir. Crit. Care Med.* **2001**, *163*, 1113-1116.

(254) Delclaux, C.; Mahut, B.; Zerah-Lancner, F.; Delacourt, C.; Laoud, S.; Cherqui, D.; Duvous, C.; Mallat, A.; Harf, A. *Am. J. Respir. Crit. Care Med.* **2002**, *165*, 332-337.